

# **Characterisation of Laser Fabricated Graphene Materials and Their Application in Electrochemical Sensing**

Katie Griffiths

Thesis submitted to the Faculty of Medical Sciences, Newcastle University as part of the requirements for the degree of Doctor of Philosophy

Institute of Cellular Medicine

December 2016

## Abstract

Graphene has been publicised as the electrode material of the future due to its large surface area and excellent electrical properties. However when considering electrochemical sensors, true monolayer graphene is of limited use owing to its basal nature which results in electrochemical performance akin to basal plane pyrolytic graphite. The future of electrochemical sensing requires electrodes with performance superior to edge plane pyrolytic graphite the 'gold standard' of carbon electrodes. Such electrodes must not only be simple and cost effective to produce but also capable of high sensitivity and precision.

Here, two new materials are presented which demonstrate excellent electrochemical responses whilst being amenable to disposable point of care sensors, akin to the planar three electrode screen printed predecessors. Laser scribed graphene and laser induced graphene both rely on a simple laser reduction method to fabricate electrodes. Laser scribed graphene, utilises the laser within Lightscribe enabled DVD drives to thermally reduce graphene oxide to a multi-layered graphene material. The expanded surface area and low oxygen content of 6.5 % result in electrochemical performance surpassing that of edge plane pyrolytic graphite. Laser induced graphene employs a CO<sub>2</sub> laser to reduce Kapton to a highly porous graphene material. It also retains low levels of oxygen (10 %) making it an interesting prospect for electrochemical sensing. These materials have been extensively characterised physicochemically and electrochemically. Regarding electrochemistry both inner- and outer-sphere redox probes were used in comparative studies with conventional carbon based electrodes. Here the graphene electrodes demonstrated enhanced performance compared to other carbon electrodes. The heterogeneous electron transfer rate of laser scribed graphene was calculated as 0.02373 cm s<sup>-1</sup>, compared with edge plane pyrolytic graphite at 0.002601 cm s<sup>-1</sup> and basal plane pyrolytic graphite at 0.00033 cm s<sup>-1</sup>. Electrochemical performance of such materials is clearly influenced by small changes in the oxygen content of the material but most importantly by the morphology of the electrode surface.

Ability to detect biologically relevant molecules dopamine, ascorbic acid, uric acid and NADH was then investigated. Laser scribed graphene and laser induced graphene demonstrated successful simultaneous detection of dopamine, ascorbic acid and uric acid which was not achieved with edge plane pyrolytic graphite or glassy carbon electrodes. Detection limits of 0.17 μM were achieved for detection of dopamine with laser scribed

graphene electrodes comparing well with the literature. In conclusion both laser scribed graphene and laser induced graphene electrodes have demonstrated exceptional electrochemical behaviour with promise for future use in disposable point of care electrochemical sensors.

## **Acknowledgements**

I'd like to acknowledge my supervisors Neil Keegan and John Hedley and group members Carl Dale, Julia Spoors for their help throughout my project and for getting me started with electrochemistry. Particularly Carl for his help in introducing me to graphene and performing Raman Spectroscopy of samples for my analysis. I'd also like to thank the Nexus at Newcastle team; Anders Barlow, Jose Potoles and Naoko Sano for their help and guidance in performing XPS and providing training in the use of the SEM. Lastly, to acknowledge the contribution of Richard Kaner and his lab group at UCLA. Their work on laser scribed graphene as a supercapacitor and their knowledge of the production of high quality graphene oxide, initiated my investigation of laser scribed graphene materials for electrochemical sensors which led to the studies covered within this thesis.

## Contents

List of Tables .....	8
List of Figures .....	9
Glossary.....	12
Chapter 1. Introduction .....	13
1.1 Graphene.....	13
1.1.1 History.....	14
1.1.2 Properties.....	15
1.1.3 Manufacture .....	16
1.1.4 Characterisation .....	18
1.2 Graphene's potential in sensing applications.....	20
1.2.1 What does the future hold for graphene?.....	21
1.3 Graphene in electrochemical sensing.....	22
1.3.1 Basic graphene electrochemistry .....	23
1.3.2 Voltammetry and amperometry .....	26
1.4 Biosensors.....	27
1.4.1 Classes of Biosensor .....	33
1.4.2 Biological detection .....	35
1.5 Conclusions .....	37
1.6 References .....	38
Chapter 2. Laser-scribed graphene presents an opportunity to print a new generation of disposable electrochemical sensors .....	48
2.1 Introduction.....	48
2.2 Experimental.....	51
2.2.1 Materials.....	51
2.2.2 Manufacture of laser-scribed graphene.....	52
2.2.3 Laser-scribed graphene characterisation .....	52

2.2.4	Laser-scribed graphene electrodes .....	53
2.2.5	Electrochemistry.....	53
2.3	Results and Discussion .....	54
2.3.1	Physicochemical characterisation of laser-scribed graphene electrodes	54
2.3.2	Electrochemical sensing of inner- and outer-sphere redox probes using LSG electrodes .....	58
2.3.3	Electrochemical evaluation of a planar three-electrode LSG system ....	67
2.4	Conclusions .....	71
2.5	References .....	72
Chapter 3. Laser-induced graphene as an electrochemical sensor.....		75
3.1	Introduction.....	75
3.2	Experimental.....	79
3.2.1	Materials.....	79
3.2.2	Manufacture of laser-induced graphene.....	79
3.2.3	Calculation of sheet resistance .....	79
3.2.4	Physicochemical characterisation of laser-induced graphene.....	80
3.2.5	Electrochemical characterisation.....	80
3.3	Results and Discussion .....	81
3.3.1	Characterisation of laser-induced graphene.....	81
3.3.2	Electrochemical assessment of laser-induced graphene .....	87
3.4	Conclusions .....	109
3.5	References .....	111
Chapter 4. Electrochemical detection of biologically relevant molecules.....		114
4.1	Introduction.....	114
4.2	Experimental.....	117
4.2.1	Materials.....	117
4.2.2	Manufacture of electrodes.....	118

4.2.3	Electrode material characterisation .....	118
4.2.4	Electrochemistry.....	118
4.3	Results and discussion .....	119
4.3.1	Characterisation of electrode materials .....	119
4.3.2	Electrochemical detection of biologically relevant molecules .....	120
4.3.3	Simultaneous detection of dopamine, ascorbic acid and uric acid .....	124
4.4	Conclusions .....	131
4.5	References .....	132
Chapter 5.	General conclusions and future work.....	137
5.1	Conclusions and future work .....	137
5.2	References .....	140

## List of Tables

Table 1-1 Examples of biosensors with various transduction elements.....	33
Table 2-1 $\Delta E_p$ values for selected electrode materials.....	61
Table 2-2 Electrochemical parameters of four LSG electrodes.....	64
Table 3-1 $\Delta E_p$ values for selected electrode materials at $10 \text{ mV s}^{-1}$ .....	104
Table 3-2 $\Delta E_p$ values for selected electrode materials at $10 \text{ mV s}^{-1}$ .....	106
Table 4-1 Analytical parameters for dopamine detection by DPV .....	129

## List of Figures

Figure 1-1 Graphene can be visualised optically on silicon dioxide .....	14
Figure 1-2 Trend in publications in graphene research.....	15
Figure 1-3 Comparison of the Raman spectra of graphene and graphite .....	19
Figure 1-4 Raman spectroscopy of pristine (upper) and an edge (lower) of a monolayer graphene. ....	20
Figure 1-5 Redox reactions.....	23
Figure 1-6 Achieving edge- and basal-plane electrodes from highly ordered pyrolytic graphite .....	24
Figure 1-7 Basic structure of a biosensor .....	28
Figure 1-8 Human Chorionic Gonadotropin digital lateral flow test .....	34
Figure 1-9 Typical immunoassay methods. ....	36
Figure 2-1 The process of patterning LSG electrodes on a flexible PET substrate... ..	55
Figure 2-2 SEM images of GO and LSG.....	56
Figure 2-3 X-ray photoelectron spectroscopy data for GO and LSG. ....	57
Figure 2-4 Diagram and photograph of an LSG working electrode .....	58
Figure 2-5 Cyclic voltammograms of four carbon electrodes in 1,1'-ferrocene dimethanol .....	59
Figure 2-6 Raman spectra of CVD SLG.....	61
Figure 2-7 Cyclic voltammograms of four carbon based electrodes in potassium ferricyanide .....	62
Figure 2-8 Effect of scan rate on peak current and peak potential for LSG electrodes in 1,1'-ferrocene dimethanol.....	65
Figure 2-9 Patterned LSG planar three-electrode system.....	67
Figure 2-10 Comparing electrochemical performance of the disposable planar three electrode LSG system with EPPPG by CV .....	69
Figure 2-11 Comparing electrochemical performance of the disposable planar three electrode LSG system with the stand alone LSG working electrode by CV .....	70
Figure 3-1 Structure of polyimide (Kapton®) .....	77
Figure 3-2 Process of manufacturing LIG electrodes.....	82
Figure 3-3 Scanning electron microscope images of LIG cross-sections .....	82

Figure 3-4 Raman analysis of Kapton <sup>®</sup> and LIG produced from varying CO <sub>2</sub> laser powers .....	85
Figure 3-5 Survey scan XPS spectra of Kapton <sup>®</sup> (PI) and laser-induced graphene (30%).....	86
Figure 3-6 High resolution XPS spectra of the C1s peak with peak fitting of Kapton <sup>®</sup> (A) and LIG from 30% power (B) .....	87
Figure 3-7 Effect of incubation time on electrochemical response of LIG electrodes in 1,1'-ferrocene dimethanol .....	89
Figure 3-8 Effect of incubation time on electrochemical response of LIG electrodes in potassium ferricyanide .....	89
Figure 3-9 Peak potential separation in 1,1'-ferrocene dimethanol for LIG electrodes produced from various laser powers.....	91
Figure 3-10 Peak current of various LIG samples in 1,1'-ferrocene dimethanol plotted against square root of scan rate.....	93
Figure 3-11 Linearity of peak oxidation current vs square root of scan rate for various LIG samples in 1,1' ferrocene dimethanol .....	94
Figure 3-12 Peak current of various LIG samples in 1,1'-ferrocene dimethanol plotted against scan rate.....	95
Figure 3-13 Linearity of peak oxidation current vs scan rate for various LIG samples in 1,1' ferrocene dimethanol.....	96
Figure 3-14 Peak potential separation in potassium ferricyanide for LIG electrodes produced from various laser powers.....	97
Figure 3-15 Peak current of various LIG samples in potassium ferricyanide plotted against square root of scan rate.....	99
Figure 3-16 Linearity of peak oxidation current vs square root of scan rate for various LIG samples in potassium ferricyanide .....	100
Figure 3-17 Peak current of various LIG samples in potassium ferricyanide plotted against scan rate.....	101
Figure 3-18 Linearity of peak oxidation current vs scan rate for various LIG samples in potassium ferricyanide .....	102
Figure 3-19 Comparing LIG CV profiles with EPPG, LSG, BPPG and GCE in 1,1'-ferrocene dimethanol.....	103
Figure 3-20 Comparing LIG CV profiles with EPPG, LSG, BPPG and GCE in potassium ferricyanide .....	105

Figure 3-21 Concentration dependent CV profiles of 30 % LIG in 1,1'-ferrocene dimethanol .....	107
Figure 3-22 Concentration dependent CV profiles of 30 % LIG in potassium ferricyanide .....	107
Figure 3-23 Entrapment of redox species in close proximity to the electrode surface within the pores of LIG shown by CV profiles .....	109
Figure 4-1 Synthesis of dopamine from tyrosine.....	114
Figure 4-2 Electrochemical redox reactions for (A) dopamine, (B) ascorbic acid, (C) uric acid and (D) NADH.....	116
Figure 4-3 X-ray photoelectron spectroscopy of GO and LSG.....	120
Figure 4-4 Cyclic voltammograms of electrodes in electroactive analytes .....	122
Figure 4-5 Differential Pulse Voltammetry profiles of various analytes with EPPG and LSG electrodes.....	123
Figure 4-6 Differential Pulse Voltammograms of solution containing multiple analytesat various electrodes.....	126
Figure 4-7 Dopamine calibration curves with LSG and LIG electrodes.....	128

## Glossary

BPPG	basal-plane pyrolytic graphite
CV	cyclic voltammetry
CVD	Chemical vapour deposition
DOS	density of states
DPV	differential pulse voltammetry
$E_p$	peak potential
$E_{pa}$	peak anodic potential
$E_{pc}$	peak cathodic potential
EPPG	edge-plane pyrolytic graphite
ESEM	environmental scanning electron micrograph
GCE	glassy carbon electrode
GO	Graphene oxide
FD	1,1'-ferrocene dimethanol
$i_p$	peak current
$i_{pa}$	peak anodic current
$i_{pc}$	peak cathodic current
LIG	laser-induced graphene
LSG	laser-scribed graphene
LSG SA	stand alone laser-scribed graphene sensor
PBS	phosphate buffered saline
PET	polyethylene terephthalate
PF	potassium ferricyanide
POC	point of care
rGO	reduced graphite oxide
RSD	relative standard deviation
SEM	scanning electron micrograph
SLG	Single layer graphene produced by chemical vapour deposition
XPS	X-ray photoelectron spectroscopy
$\Delta E_p$	Peak potential separation

## Chapter 1. Introduction

### 1.1 Graphene

Graphene has become an extremely popular material in many research areas since the ground-breaking experiments performed by Novoselov and Geim in 2004 and 2005. In essence they demonstrated single layer graphene to be stable using a simple and economical method for exfoliating few and single layer graphene from graphite, which became known as the Scotch Tape Method (Novoselov *et al.*, 2004) (Novoselov *et al.*, 2005). The use of this simple method and an ability to easily visualise the graphene with optical microscopy when on silicon oxide substrates (Blake *et al.*, 2007) (Figure 1-1) has made it possible for many people to study graphene. Graphene isolated by mechanical exfoliation allowed the initial characterisation of the physical properties of graphene. Due to its 2D atomic structure graphene demonstrated high electrical and thermal conductivity properties, mechanical strength, flexibility, transparency, impermeability to gases (Novoselov *et al.*, 2012) and highest possible surface area, thus has potential in many areas. These properties make graphene a candidate for replacing silicon in computers, for making flexible display screens, as a protective coating material, in energy storage and also for bio-applications including diagnostic biosensors (Novoselov *et al.*, 2012). However the barrier to moving such uses forward is the manufacture of high quality graphene and scaling up the process for mass manufacture. Graphene of varying quality is required dependent upon use as defects, chemical modifications and aggregation can significantly affect the properties of graphene. A simple method of graphene detection which is not dependent upon the support should also be developed in order to aid in moving forward the research and development of graphene (Singh *et al.*, 2011).

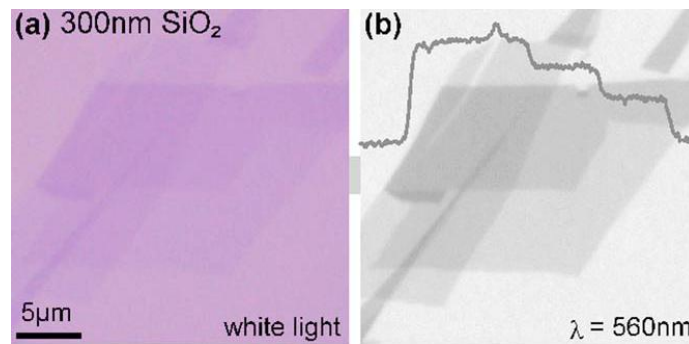


Figure 1-1 Graphene can be visualised optically on silicon dioxide

Adapted from (Blake *et al.*, 2007) (a) Graphene crystallites on 300 nm SiO<sub>2</sub> imaged with white light. Single-layer graphene is clearly visible on the left image (a). The flakes were chosen to contain areas of different thickness so that one can see changes in graphene's visibility with increasing numbers of layers. The trace in (b) shows step-like changes in the contrast for 1, 2, and 3 layers (trace averaged over 10 pixel lines). This proves that the contrast can also be used as a quantitative tool for defining the number of graphene layers on a given substrate.

### 1.1.1 History

Carbon based nanomaterials are nothing new, graphene's predecessor as a wonder material was carbon nanotubes (Thostenson *et al.*, 2001). The explosion of interest in graphene (Figure 1-2) has been spurred by the crucial experiments of Novoselov and Geim isolating graphene and determining the basic electrical properties (Novoselov *et al.*, 2004; Novoselov *et al.*, 2005). However this was not the 'discovery of graphene', which was investigated at least as early as 1962 (Boehm *et al.*, 1962), with attempts back as far as 1859 (Brodie, 1859) and the term graphene was coined in the 1980s (Boehm *et al.*, 1986). Graphene can be produced in several other ways including "by a combination of electrophoretic deposition (EPD) and heat-treatment of diamond nano-particles on a highly oriented pyrolytic graphite (HOPG) substrate" (Affoune *et al.*, 2001) and "grown by thermal decomposition on the surface of 6H-SiC" (Berger *et al.*, 2004). Its manufacture has continued to be optimised to this date with developments in chemical vapour deposition (CVD) graphene (Li *et al.*, 2011b), liquid exfoliation (Green and Hersam, 2009; Lu *et al.*, 2012; Coleman, 2013) and laser scribed graphene (El-Kady *et al.*, 2012).

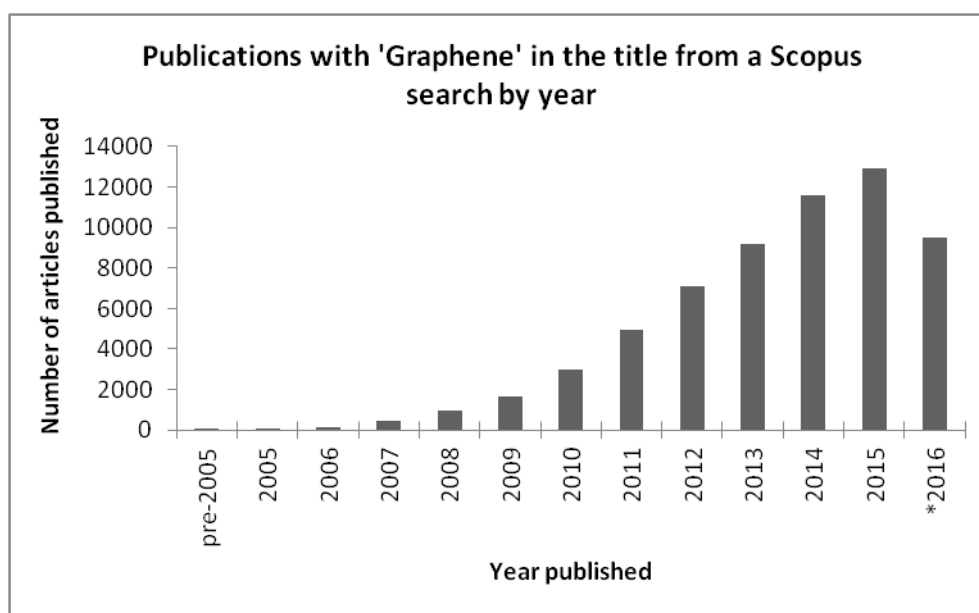


Figure 1-2 Trend in publications in graphene research. Performing a search in Scopus for articles published with “graphene” in the title shows an explosion of research since 2005. Prior to this fewer than 10 articles per year were published containing graphene in the Title. The trend appears to be continuing with almost 10000 published in the first 8 months of 2016. (\*up to 11th September 2016)

### 1.1.2 Properties

Graphene has revealed many unique properties from being the thinnest known material (0.35 nm (Brownson *et al.*, 2012)), having the highest possible surface area to volume ratio at  $2600 \text{ m}^2 \text{ g}^{-1}$ . It is almost transparent (Nair *et al.*, 2008), yet is stronger than steel with a Young's modulus of approx. 1 TPa (Edwards and Coleman, 2013). This amazing material demonstrates impermeability to gases (Bunch *et al.*, 2008) and it has revealed an electron transfer rate of up to  $230\,000 \text{ cm}^2 \text{ V}^{-1} \text{ s}^{-1}$  (Bolotin *et al.*, 2008), therefore having good conductivity and thermal stability and room temperature. The quantum hall effect has also been observed with graphene (Geim and Novoselov, 2007; Novoselov *et al.*, 2007; Barlas *et al.*, 2012). These properties deduced from fundamental studies have generally been elicited from the use of high quality graphene, most often very small mechanically exfoliated flakes. However, in order to exploit these properties and translate into useful electronics, sensors or energy storage devices, larger scale manufacture of graphene of various qualities is required.

The properties of graphene can be altered by p or n-type doping (Giovannetti *et al.*, 2008; Zhou *et al.*, 2008) and also vary dependent upon the number of layers of graphene (Hibino *et al.*, 2009). These changes need to be considered when bonding to and immobilising onto graphene, whether intentionally or as a by-product of the processing methods. There is much debate over what should be called graphene and what should be more correctly termed as graphene-like materials due to variation from the true 2D lattice structure of

pure graphene with the introduction of defects, increased oxygen content and multiple layers.

### **1.1.3 Manufacture**

There are now many different methods available for the manufacture of graphene. These methods produce graphene of varying quality, cost and size, which in turn make them suitable for different applications (Novoselov *et al.*, 2012).

#### **1.1.3.1 Exfoliation**

Mechanical exfoliation (Novoselov *et al.*, 2004; Novoselov *et al.*, 2005) produces excellent graphene samples, suitable for determination of its physical properties. However it is time consuming and results in relatively small graphene flakes, thus being unsuitable for scale up of manufacture. It is also possible to perform chemical exfoliation, many different methods are available in the literature (Lotya *et al.*, 2009; Lu *et al.*, 2012; Nuvoli *et al.*, 2012; Coleman, 2013; Yang *et al.*, 2013) these offer a more scalable method but often introduce problems of their own, as many of the solvents used can be hazardous and difficult to remove.

#### **1.1.3.2 Chemical Vapour Deposition**

Electrochemical deposition of graphene onto transition metal substrates such as copper or nickel can be performed producing large sheets via simple thermal decomposition of hydrocarbons on the surface (Mattevi *et al.*, 2011). The graphene must be transferred to substrates such as SiO<sub>2</sub> or SiC for use in electronic or sensing applications or flexible substrates for use in display screens. This transfer can be done by wet etching of the metal, for example copper with ferric chloride once the graphene has been attached to a polymer such as PMMA which can then be removed in acetone (Tao *et al.*, 2012). PDMS and thermal release tape (Bae *et al.*, 2010) have been used in place of PMMA. Recent improvements to this method produce graphene with excellent electronic properties (Mattevi *et al.*, 2011) where previously there were problems with grain boundaries and wrinkles in the graphene sheet. Yet the multi-stage process still offers opportunities for damage to the delicate graphene sheets with introduction of tears and impurities.

#### **1.1.3.3 Thermal Decomposition**

Graphene can be epitaxially grown on SiC and this could provide opportunities for large scale manufacture. This method requires heating of SiC to temperatures in excess of 1000°C to allow sublimation of silicon, this leaves behind carbon atoms at the surface which re-arrange to form graphene (Shivaraman *et al.*, 2009). The properties of such graphene may vary from freestanding graphene due to its interactions with its substrate

(Bolotin *et al.*, 2008). However it is possible to etch the SiC substrate using a photoelectrochemical etch (Kato *et al.*, 2003) with aqueous potassium hydroxide (1%) as the electrolyte, using a 100 W mercury arc lamp as the source of UV light in order to study freestanding graphene. Again where the graphene is to be removed from the substrate the process can lead to surface impurities and defects altering the properties of the material.

#### **1.1.3.4 Reduction of Graphene Oxide**

A popular method of producing graphene like material utilises graphite oxide, this can be exfoliated to give graphene oxide and reduced to form reduced graphene oxide.

Traditionally oxidising agents and strong acids have been used, the modified Hummers method is particularly common, in which graphite is treated with sulphuric acid and potassium permanganate to create graphite oxide. Sonication then separates layers to produce single layer graphene oxide which can then be reduced thermally, chemically or electrochemically to graphene (Brownson *et al.*, 2012).

A reduction and patterning method using laser scribe technology has demonstrated that electrochemical based devices can be produced in a simple and inexpensive way from reduced graphene oxide. "A simple low-energy, inexpensive infrared laser is used as a powerful tool for the effective reduction and subsequent expansion and exfoliation and fine patterning of graphite oxide" (Strong *et al.*, 2012). This highly reduced graphene has potential in sensors, energy storage and electrochemical growth of nanoparticles. This work was rapidly followed by the use of higher powered lasers to convert non graphite materials such as Kapton<sup>®</sup> into a graphene-like material with the excellent electrical properties suited to electrochemical energy storage and sensing applications (Lin *et al.*, 2014; Nayak *et al.*, 2016; Tehrani and Bavarian, 2016).

#### **1.1.3.5 Summary of Production Methods**

The above sections give only a brief insight into the methods used in the manufacture of graphene. There are constantly new and reviewed methods reported and reviewed in the literature (Johnson *et al.*, 2015; Huang *et al.*, 2016; Khan *et al.*, 2016; König *et al.*, 2016; Li *et al.*, 2016; Ma *et al.*, 2016; Zhang *et al.*, 2016) from using new novel carbon sources (Qu *et al.*, 2013) to use of different reduction and exfoliation methods (Lu *et al.*, 2012). Each method has its own advantages and limitations which vary, dependent upon its intended use.

#### **1.1.4 Characterisation**

The methods used in characterisation of pure graphene of most importance are Light microscopy and Raman spectroscopy. When on silicon oxide substrate, the graphene can be visualised despite its almost transparent properties and varying contrasts on the substrate can aid in identifying single and few layer graphene (Blake *et al.*, 2007). Without this realisation early on in the study of graphene it would have been impossible to make the progress that has been made to date, but these simple methods to exfoliate (Novoselov *et al.*, 2004; Novoselov *et al.*, 2005), isolate and visualise (Blake *et al.*, 2007) graphene flakes opened up the opportunity for research teams to study graphene, even on limited budgets.

Raman spectroscopy can be used to further confirm the presence of graphene, and variation in peak intensities, ratios, location and shape can identify between single, few and multilayer graphene as shown in Figure 1-3 and Figure 1-4 (Blake *et al.*, 2007). Although it should be noted that the graphene support can also affect the graphene bonds and thus the spectra (Wang *et al.*, 2008). Several excellent reviews have been written on the subject describing in far more detail than discussed within the scope of this study (Malard *et al.*, 2009; Ferrari and Basko, 2013; Ryan *et al.*, 2015). The case for using Raman spectroscopy in the analysis of the reduced graphene oxide materials used in these studies is discussed in more detail alongside the results in Chapter 2 and Chapter 3.

X-ray photoelectron spectroscopy (XPS) is a quantitative technique that can be used to confirm the presence of graphene as it gives information about the elements present at the surface, their percentage and their chemical states. This can be useful in characterising graphene devices to confirm successful deposition, etching or immobilisation. In the studies utilising reduced graphene oxide materials it has been useful in quantifying the oxygen content following processing from graphite to graphene oxide and of the residual oxygen content following laser reduction. It is useful in supporting evidence gathered from methods such as Raman spectroscopy.

Other methods typically used to characterise graphene include atomic force microscopy (Schniepp *et al.*, 2006; Lee *et al.*, 2008) or scanning tunnelling microscopy (Biedermann *et al.*, 2009) to visualise surfaces at the atomic level, these can give information on height changes. From an electrochemical perspective cyclic voltammetry can be used to assess its suitability as an electrode material (Alwarappan *et al.*, 2009; Strong *et al.*, 2012).

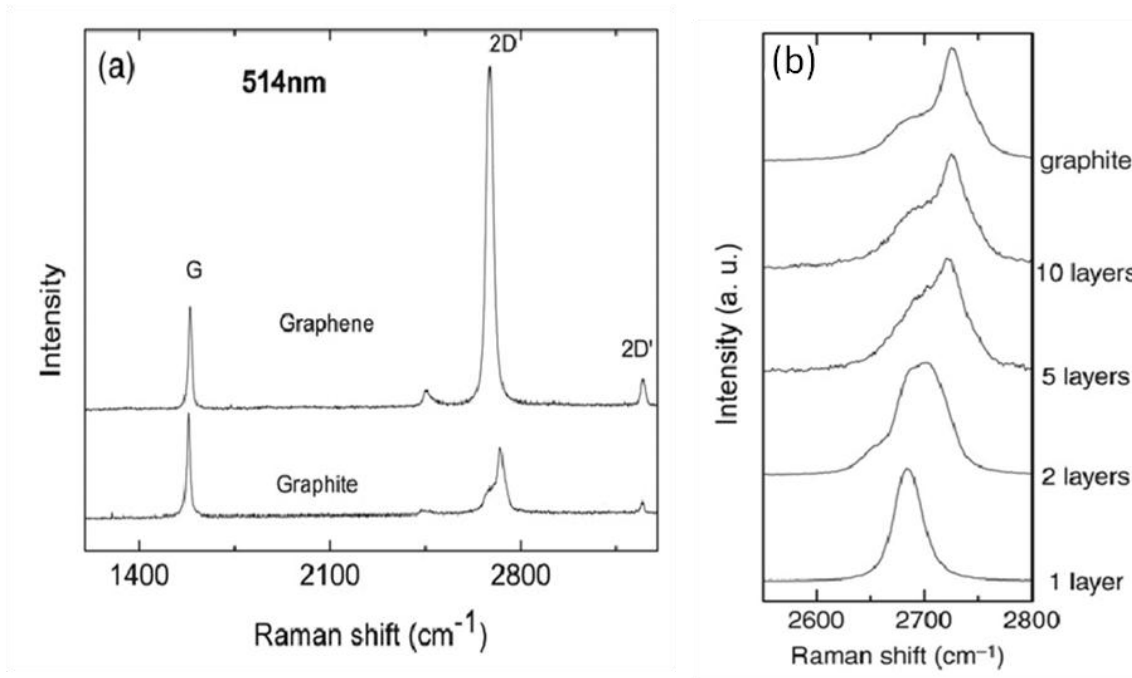


*Figure 1-3 Comparison of the Raman spectra of graphene and graphite*

*The spectra in (a) measured at 514 nm highlights the important peaks used in the distinction of graphene from graphite, where an increased intensity of the 2D and 2D' peak as well as a more symmetrical 2D peak is indicative of graphene material. The spectra in (b) shows the evolution of the 2D peak as number of layers of graphene decrease from multilayered graphite to single layered graphene with a sharper, larger peak and reduced Raman shift. Adapted from (Ferrari, 2007).*

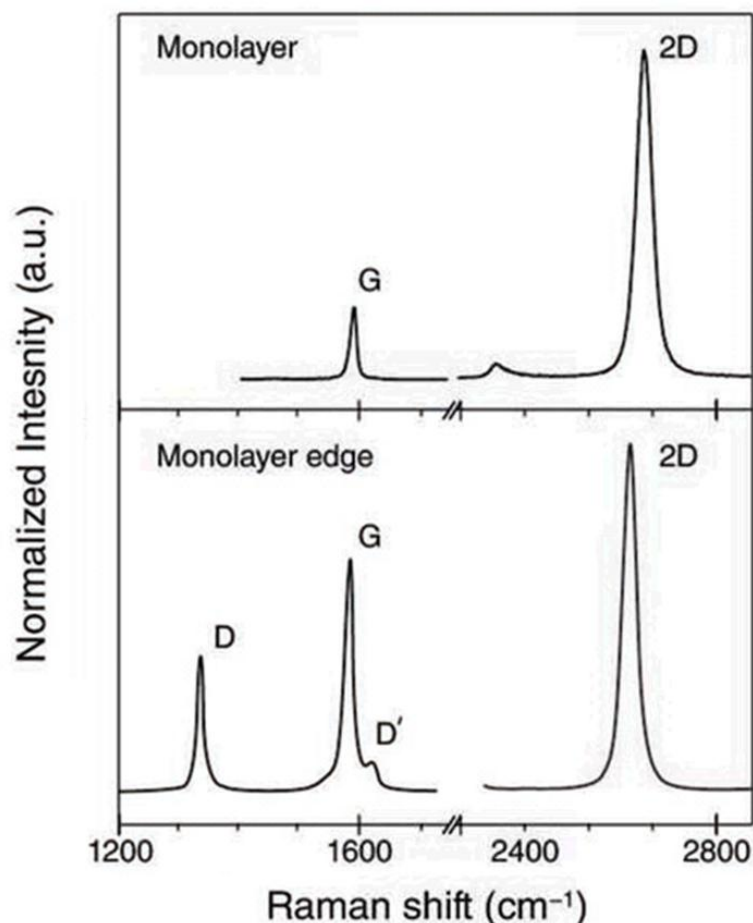


Figure 1-4 Raman spectroscopy of pristine (upper) and an edge (lower) of a monolayer graphene. Showing D, G, D' and 2D (G') peak height. Thus the D and D' peak signify the presence of defects in the graphene structure and would be expected in multilayered graphene materials and can be useful in the case of electrochemistry where edge defects and oxygen functionalities can aid in the transfer of electrons from solution to electrodes. Adapted from (Weiss *et al.*, 2012).

## 1.2 Graphene's Potential in Sensing Applications

Many examples of graphene sensors have been published. These vary from the use of graphene in the improvement of existing SPR sensors (Wu *et al.*, 2010) and use of composites on glassy carbon electrodes (Zhang *et al.*, 2012) through to the use of graphene in microfabricated sensors (Huang *et al.*, 2015).

A simple graphene chemiresistor pH sensor has been described (Lei *et al.*, 2011), using graphene membranes suspended over trenches in a silicon oxide substrate. This allowed the measurement of changes of pH as a function of change in resistance. Graphene chemical sensors have been developed that rely upon the doping effect on graphene when chemicals bind to the surface. Chemical targets have included NO<sub>2</sub> and NH<sub>3</sub> (Fowler *et al.*, 2009; Yavari *et al.*, 2011), detection of NO<sub>2</sub> to 20 ppm and reversibility of the binding and thus re-usability of a graphene foam chemical sensor was demonstrated. However this offers no specificity, only binding of the molecule in question in the absence of any interfering substances.

Graphene resonators have been demonstrated, these began as exfoliated graphene sheets suspended across trenches in silicon oxide (Bunch *et al.*, 2007) and moved on to arrays of Chemical Vapour Deposition grown graphene resonators (Zande *et al.*, 2010) where it was shown that clamping of all sides of the membrane improved both the performance and reproducibility of the resonators. Barton went on to illustrate the use of graphene in circular mechanical resonators and that their increased size improved the quality factor (Barton *et al.*, 2011). There is potential for further research in this area with the use of graphene grown on silicon carbide via thermal decomposition and investigation of immobilising a biological recognition layer and specific detection.

In regards to biosensors, Mohanty and Berry reported to have detected both a single bacterium and ssDNA binding to a reduced graphene oxide (Mohanty and Berry, 2008). Functionalisation of epitaxial graphene with antibodies via nitrobenzene has also been demonstrated (Guy *et al.*, 2010). More recently a very simple graphene biosensor has been demonstrated by Labroo for detection of 5-aminosalicylic acid using an enzyme based sensing technique (Labroo and Cui, 2013a) and a flexible graphene biosensor for lactate (Labroo and Cui, 2013b) capable of rapid and sensitive detection. Although these do not confirm that common sample interferences such as paracetamol and ascorbic acid are not also oxidised at the high potentials used.

### **1.2.1 What Does the Future Hold for Graphene?**

The future holds endless opportunities for graphene. New methods and results are reported weekly about its properties, manufacturing techniques and uses and many large companies are investing in this 'wonder' material such as IBM and Samsung. Also, recently the European Commission has announced funding of €1 billion towards graphene research. So will graphene deliver on its expectations? There is clearly huge potential for graphene in electronics, sensors, energy storage and many other areas. However there is also contradicting research and drawbacks in manufacturing methods. These are sure to be overcome with the current level of interest in this material, and the real developments may still be to come with novel uses rather than use in replacing existing materials such as silicon.

Over the coming years it is likely to be flexible screens, and simpler electronic uses that could emerge onto the market initially. Development of biosensors and uses in medicine are expected to take much longer and not become widely available for more than 15-20 years.

As for graphene biosensors moving forward on previous work done using laser scribed graphene (El-Kady *et al.*, 2012; Strong *et al.*, 2012) will be important, determining its usefulness as an electrode material and comparing to conventional materials such as gold and carbon. It may then be possible to introduce a biorecognition element such as glucose oxidase often used with carbon paste electrodes (Gorton, 1995) and pyrolytic graphite electrodes (Salimi *et al.*, 2004). The laser scribed graphene has potential to be used in amperometric, chemiresistor and impedance sensors due to its simple and low cost manufacturing method.

Other avenues being investigated include the use of graphene grown on silicon carbide as a chemiresistor and resonator. Graphene resonators can be difficult to make due to its 2D structure making freestanding graphene difficult to work with. However with use of high quality graphene and optimisation of resonator geometry (Khaled *et al.*, 2012) it should be possible to visually and mechanically characterise novel graphene resonators capable of single molecule measurements.

### **1.3 Graphene in Electrochemical Sensing**

Graphene is studied extensively in electrochemical sensing and covered by many review articles (Bollella *et al.*; Shao *et al.*, 2010; Wu *et al.*, 2013; Ambrosi *et al.*, 2014; Pandikumar *et al.*, 2014). As an excellent conductor of electricity with a large surface area graphene may appear an obvious choice as an electrode, but does true monolayer graphene offer the most suitable characteristics for electrochemistry? The basic requirement of an electrochemical sensing system is that a reduction or oxidation reaction can occur at an electrode surface, this transfer of electrons from or to the working electrode can then be measured as a change in current, voltage or impedance. Often to aid this exchange at the surface, functional groups are required, which are not present in pristine graphene sheets. Thus a more suitable material for electrodes is likely to have the highly conductive characteristics of graphene but with many edge or defect sites to allow the surface exchange, opening the door for the use of various graphene and graphene like materials in the area of electrochemical sensing. Pumera provides an excellent summary of electrochemistry with some of these graphene materials in his mini review (Pumera, 2013) as a starting point but there are several very extensive reviews covering the area of graphene use in electrochemistry available from the leading electrochemistry and graphene groups (Pumera *et al.*, 2010; Brownson *et al.*, 2012; Ambrosi *et al.*, 2014; Ambrosi *et al.*, 2016).

### 1.3.1 Basic graphene electrochemistry

Before delving specifically into the electrochemistry of graphene it is useful to consider the basics of electrochemistry and the commonly used carbon based electrodes that have been used widely for many years in industrial and academic settings and reported throughout the literature. These include highly ordered pyrolytic graphite (Patel *et al.*, 2012; Zhang *et al.*, 2015), carbon paste electrodes (Shigemitsu *et al.*, 1979) and screen printed electrodes made from various components and with countless treatments (Wang *et al.*, 2009; Randviir *et al.*, 2014). This will provide a good starting point for comparison with the graphene materials.

Electrochemistry is the study of charge separation and transfer between an electrode and solution, where the reduction and oxidation of redox species (Figure 1-5) can be performed and monitored. The potential is controlled externally and most often a three electrode system is employed, with a working, reference and counter electrode. The technique is useful in the study of and detection of redox reactions of substances such as biomolecules, drugs, toxins and metabolites (Fernandez-Sanchez *et al.*, 2004; Batra and Pundir, 2013; Diaz Toro *et al.*, 2015; Feng *et al.*, 2015).

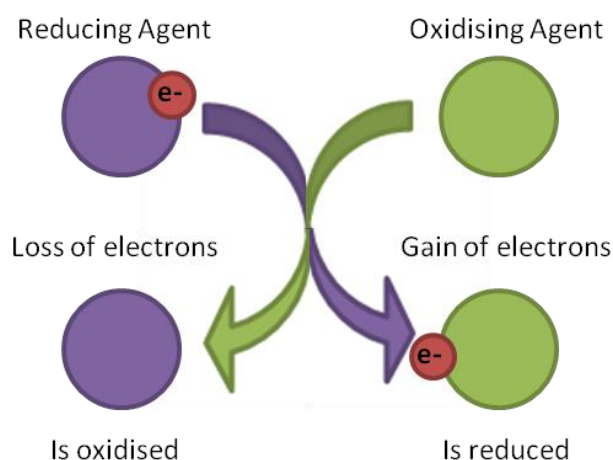


Figure 1-5 Redox reactions

The working electrodes at which these redox reactions occur can be made of numerous different electrically conductive materials. Metals such as gold and platinum have proven to be excellent but whilst these are useful for research purposes they are not suitable to mass production of electrochemical sensors for diagnostic purposes due to the expense of such materials. Carbon electrodes can offer a more affordable alternative, they have lower conductivity than metal electrodes and performance is widely variable dependent upon the

carbon composition used. Carbon based electrodes that have been used widely in electrochemical sensors and are supported with a wealth of studies include edge plane pyrolytic graphite (EPPG) (Banks and Compton, 2005), basal plane pyrolytic graphite (BPPG) (Moore *et al.*, 2004) (Figure 1-6), glassy carbon electrodes (Diaz Toro *et al.*, 2015) and screen printed carbon electrodes (Karuwan *et al.*, 2013). Although all are carbon structures the electrochemical performance is vastly different, this can be attributed to both the functional groups at the electrode surface and the overall conductivity of the material. In the case of EPPG and BPPG, both electrodes are created from the same highly conductive material highly ordered pyrolytic graphite, however their electrochemical performance can be vastly different. The way in which the electrode surface is presented as shown in Figure 1-6 results in a very different surface behaviour despite the underlying material being the same. EPPG could be termed the 'Gold standard' of carbon electrodes as it behaves well with both inner- and outer- sphere redox couples, yet a true pristine graphene layer would be more akin to BPPG. Many reported results suggest otherwise, that is they claim that graphene has behaviour more similar to or surpassing EPPG (Li *et al.*, 2011a). Yet in fact this is more likely due to graphitic islands or defects in the graphene layer introducing functional groups than to true 'catalytic' effects of pristine graphene and use of graphene flakes may in fact even inhibit transfer of electrons to underlying electrodes dependent upon the layering and orientation at the electrode surface (Brownson and Banks, 2011; Brownson *et al.*, 2011a; Brownson *et al.*, 2011b) and these arguments are acknowledged further in Chapter 2.

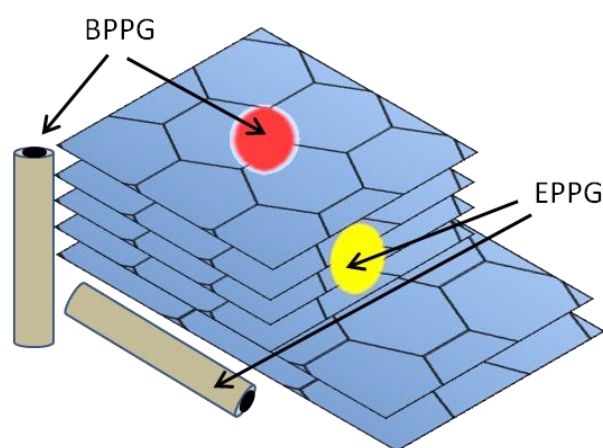


Figure 1-6 Achieving edge- and basal-plane electrodes from highly ordered pyrolytic graphite

Of the electrochemical sensors to be commercialised, the most successful and most well-known is the glucose biosensor. These utilise screen printed carbon electrodes which offer

a balance between cost and performance for mass manufacture of disposable planar electrodes. However these sensors do not compare favourably with gold or EPPG electrodes and so for increased sensitivity of commercialised electrochemical sensors, the future graphene like materials may hold the answer. As described above, graphene with a pristine structure as described by the IUPAC definition is not only troublesome to produce, but also unlikely to be the most promising of electrode materials, however graphene like materials such as reduced graphene oxide may be the future of electrochemical sensing. Graphene itself is said to have a wide stable electrochemical window, with increasing oxygen content this decreases and in the case of graphite oxide, by -700 mV unwanted electrochemical responses occur interfering in specific measurements thus limiting its use (Pumera, 2013). However this is dependent upon the use in question, as for any biological electrochemical sensors, the intention would be to keep any measurement potentials below this level in order to reduce interferences from biological samples. The high oxygen content of graphite oxide also results in a relatively slow electron transfer rate, however as the oxygen content is reduced the heterogeneous electron transfer rate increases. A further consideration in the use of these 'graphene like' materials is that many examples require multi-step processing and each level of processing has the potential to introduce contaminants at a significant level on a structure consisting of only a single atomic layer. Reduced graphene oxides can be produced with thermal, chemical or electrochemical reduction. Thermal reduction in an inert atmosphere should produce the reduced graphene oxide of highest purity. Teamed with the use of a laser it is possible to not only reduce the graphene oxide but to cause a rapid expansion ensuring that graphene layers remain separated maintaining high surface area, graphene like properties yet with low levels of functional groups remaining for efficient electrochemical transfer as described in the work produced by the Kaner group on laser scribed graphene supercapacitors (El-Kady *et al.*, 2012; Strong *et al.*, 2012). This laser scribed graphene must be produced from graphite oxide which by its nature will contain impurities, particularly metals which can alter the electrochemical properties of the resultant electrodes, however a modified Hummers method of producing the graphite oxide which includes multiple wash steps, results in a high purity starting material (Tung *et al.*, 2009; El-Kady *et al.*, 2012; Strong *et al.*, 2012; El-Kady and Kaner, 2013; Griffiths *et al.*, 2014). Of course this material still requires multiple processing steps and in that effect was improved upon by the work that came out of Tours group at Rice university at the end of 2014. This work was quite revolutionary in producing a graphene like expanded structure from a polyimide film (Kapton<sup>®</sup>) with the use of a CO<sub>2</sub> laser (Lin *et al.*, 2014). This material and the resultant experiments performed on its use in

electrochemistry are discussed in detail in Chapters 3 and 4, but essentially a planar electrode with graphene like properties could be printed in a one step process using low cost equipment available in many university departments. This method forms a graphene like material from sublimation of the polyimide containing carbon ring structures which turns the highly insulating and smooth Kapton<sup>®</sup> film into a highly conductive expanded porous structure with a large surface area highly suited to use as an electrochemical sensor (Lin *et al.*, 2014).

Many other variations of graphene materials have been studied as electrochemical sensors. From various forms of reduction, sheets or flakes, as standalone electrodes or as an additive to underlying electrodes, doped material or using biological recognition molecules. These have been reported and reviewed extensively (Pumera *et al.*, 2010; Brownson and Banks, 2011; Brownson *et al.*, 2011a; Brownson *et al.*, 2011b; Brownson *et al.*, 2012; Pumera, 2013; Ambrosi *et al.*, 2014) and even updated to cover the most recent advances as there is such an expanse of research in this field (Ambrosi *et al.*, 2016). Despite this plethora of graphene electrochemical sensor research reported, the most promising for scaleable, reproducible and cost effective manufacture of high performance disposable planar electrodes is the use of laser induced graphene. This will be reported across the following chapters.

### **1.3.2 Voltammetry and Amperometry**

The electrochemical sensing with graphene that has been focused on in the studies reported here was based on voltammetric and amperometric methods. Amperometric techniques are used widely as a means to understanding a materials electrochemical behaviour. Simple techniques such as cyclic voltammetry where the potential is ramped whilst measuring the current allows the study of both analyte and electrode material. This technique has been used extensively to characterise the laser fabricated graphene electrodes herein coupled with the use of defined inner- and outer- sphere redox couples potassium ferricyanide and 1,1'-ferrocene dimethanol allowing the determination of the heterogeneous electron transfer rate of the LSG and probing of the electrode porosity of the LIG. However when moving from electrode material characterisation to use of the electrode for sensing of electrochemically active molecules more sensitive techniques such as differential pulse voltammetry (DPV) and chronoamperometry become more important. DPV is particularly useful when working with graphene based electrodes with an enhanced surface area as a roughened electrode surface can introduce an increased charging current and the use of DPV enhances detection of the faradaic response. Once

moving beyond this onto the use of biological recognition elements such as redox enzymes chronoamperometric methods can be useful in monitoring real time changes in analyte concentrations.

#### **1.4 Biosensors**

The broader aim of development of simple to manufacture electrodes with enhanced electrochemical performance is for the use in biosensing and diagnostics. The term biosensor relates to a device which combines a biological detection system with a transducer and a signal output system. IUPAC have defined a biosensor as “A device that uses specific biochemical reactions mediated by isolated enzymes, immunosystems, tissues, organelles or whole cells to detect chemical compounds usually by electrical, thermal or optical signals” (McNaught *et al.*, 2006), see Figure 1-7. Biosensors lend themselves for many uses including medical diagnostics, food safety, drug discovery, environmental monitoring and biological/chemical defence.

Biosensors came about in the 1960s, when Clark and Lyons described a method for testing glucose levels in blood (Clark, 1962), this became known as the “enzyme electrode”. The initial glucose sensors were amperometric, and the enzyme glucose oxidase (GOx) was captured next to the electrodes using dialysis membrane. It allowed the measurement of oxygen consumption which was proportional to the concentration of glucose present in the sample (Morrison *et al.*, 2007). First generation biosensors were commercialised in the 1970s by the Yellow Springs Instrument company (Song *et al.*, 2006), the concept was further developed and in 1977 the use of whole cells as biorecognition systems was described (Rechnitz *et al.*, 1977). Rechnitz *et al.* used an ammonium gas sensing electrode with *Streptococcus faecium*, a bacterium which could metabolise L-arginine into ammonia to detect the amino acid arginine.

Research and development of biosensors has continued, particularly over the past 10 years. Major advancements have occurred with the use of nanomaterials such as carbon nanotubes (CNT) (Jacobs *et al.*, 2010), nanoparticles (Ali *et al.*, 2013; Kaur *et al.*, 2013; Wang *et al.*, 2013) and nanowires (Kumar and Jung, 2011; Ma *et al.*, 2016) and fashionable materials such as graphene could open up new avenues. Despite the huge potential of biosensors commercialisation is slow and glucose tests still account for 85% of the world market of biosensors (Morrison *et al.*, 2007; Zhu *et al.*, 2012) which is estimated to reach \$20.7 billion by 2020 (Grand view research 2015). The reasons behind the slow movement from research to commercial products can be largely attributed to cost implications, biosensors must lend themselves useful for multiple target analytes and/or be

sold in vast quantities in order to make the cost of transition through development, optimisation, manufacturing and validation commercially viable.

The greatest impact of biosensors is likely to be in the field of point of care (POC) diagnostics (D'Orazio, 2011). Commercial Biosensors do not need to be cheaper per test than existing technology, if overall cost benefit can be argued. "POC tests can indirectly, sometimes drastically, lower medical costs: sample mislabelling and mishandling, along with misdirection of results, are less likely. Results are provided more quickly, enabling more effective treatment of rapidly progressing afflictions, even making a life-or-death difference with some infections" (Gubala *et al.*, 2012). Consideration should be given to sample handling and pre-treatment. Dependent on the required use of the biosensor these should be minimised and simplified in order to produce an easy to use product. A quick and effective POC biosensor should use the least invasive sample with minimum process steps and ideally, sample separation or pre-treatment should be incorporated into the device along with data analysis and presentation of results (Luong *et al.*, 2008).

Once some of these limitations are overcome, biosensors have the potential to revolutionise clinical diagnostics and offer both, disposable, single use options or continuous real time monitoring solutions.

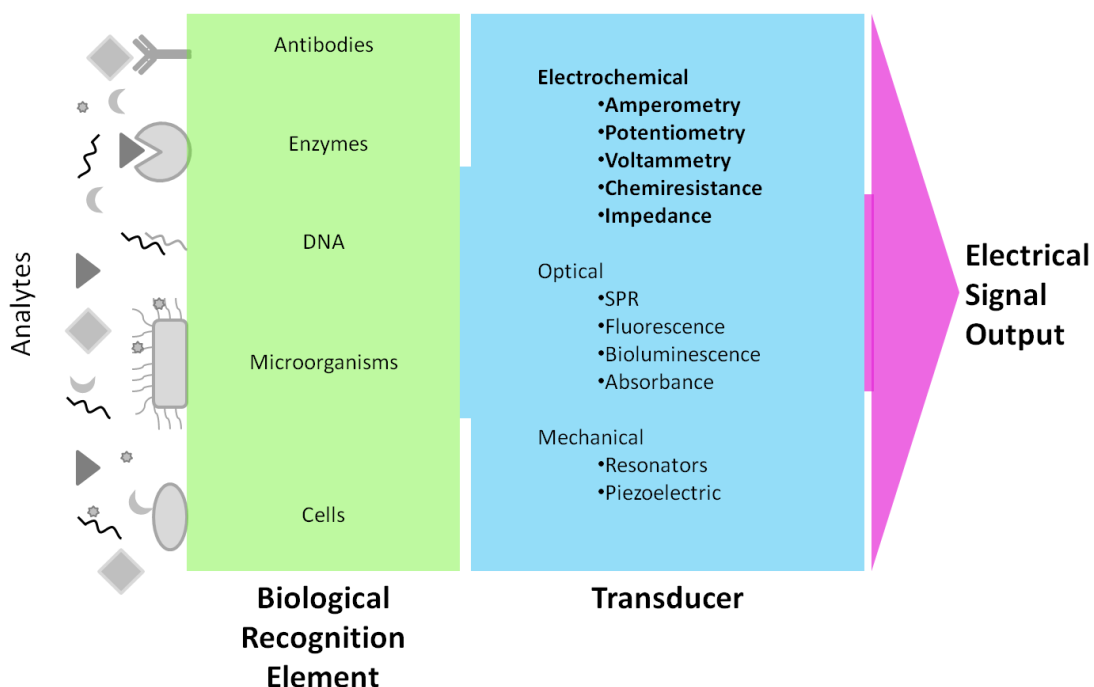


Figure 1-7 Basic structure of a biosensor

The specificity of biosensors is conferred by the biological recognition molecule. Biosensors have shown extremely good sensitivity, for example, Mohanty *et al.* demonstrated detection of a single bacterium using a chemically modified graphene biosensor (Mohanty and Berry, 2008). Sensitivity is determined by the underlying transducer and/or the strength and specificity of interaction between the biological recognition molecule and the target. It can also be affected by non specific binding, however this can often easily be addressed. Sensitivity is defined as the slope of the calibration curve (Currie, 1999). It should also be considered during development how the biosensor will perform in various matrices (Luong *et al.*, 2008), with sample matrix effects, and when performed under various conditions.

As well as medical diagnostics biosensors have uses in food analysis (McGrath *et al.*, 2012; Eissa *et al.*, 2013), whether this be food safety, quality control, or, monitoring for genetically modified organisms in agricultural settings. This could include quantitative detection of bacteria, microbial toxins, or pesticides that could be found in food. In these circumstances the rapid results and real time monitoring available with biosensors would be a clear advantage over typical ELISA, chromatography, spectroscopy or cell culture techniques that have been more commonly utilised.

Drug discovery can be aided with the use of biosensors, as they often allow the use of nanolitre (nl) volumes of valuable samples, leading to significant cost savings when screening potential drug candidates. Biosensors can also be used for target identification, validation, assay development (Jain, 2009) and monitoring during clinical trials.

In environmental monitoring the portability and rapid analysis of biosensors offers benefits above many traditional techniques. Biosensors can allow for testing in 'the field' for a variety of tests from assessing environmental damage to modelling climate change (Frense *et al.*, 1998; Marrazza *et al.*, 1999; Culkova *et al.*, 2013).

In Biological and Chemical defence detection of chemical agents, microbiological agents and toxins could be performed with the use of many different forms of biosensor. Chemical agents of interest may include nerve agents such as Sarin, blood agents such as Hydrogen cyanide or blister agents such as sulphur mustard (Paddle, 1996).

Microbiological agents that may be key targets for biosensors in the field of defence include viruses such as Variola, Ebola or Haemorrhagic fever, bacteria such as *Bacillus anthracis*, *Rickettsia rickettsi* and fungi such as *Coccidioides immitis* and *Nocardia asteroid* (Paddle, 1996). There are also many natural toxins that are classified as potential

chemical or biological weapons. Within this classification are Aflatoxins and Botulinum. Examples of biosensors to detect such weapons have been reported in the literature and include potentiometric (Mulchandani *et al.*, 1999), amperometric (Lei *et al.*, 2005) and acoustic/mechanical resonator based transducers (Pohanka and Skládal, 2005; Carter *et al.*, 1995) which will be described in more detail later.

Most often, biosensors are designed for use in the life sciences, for use in medical diagnostics. In this area there is a much greater potential for commercialisation of biosensor technology. If the technology is not competitive on cost, provided it can offer advantages in terms of sensitivity, rapid results or real time monitoring, it could open new areas of testing and treatment opportunities. The biosensor for detection of glucose in blood, remains the market leading biosensor, most probably due to the vast number of patients with diabetes along with their need for regular monitoring of blood glucose levels.

The large interest in biosensors in both academia and industry stems from the need for assays that are suitable for use at the point of need and for use by non-skilled personnel. Commercialisation of effective biosensors for infectious disease such as HIV, Chlamydia, Flu and malaria could have massive impacts on reducing transmission, increasing treatment rates and overall reducing the worldwide costs of managing such diseases. Taking HIV as an example, in 2011 UNAIDS (UNAIDS, 2012) reported that 34.2 million people were living with HIV and that global investments into the fight against HIV totalled \$16.8 billion. Despite this investment many people living with HIV are unaware of their status and are not receiving anti-retroviral therapy. If a successful biosensor was developed for the detection of HIV, transmission and cases could be significantly reduced as those receiving anti-retroviral treatment have a 96% reduced rate of transmission to sexual partners.

In the case of breast, colon, lung and ovarian cancer  $\geq 60\%$  of patients already have metastases at the stage when they are first diagnosed (Morrison *et al.*, 2007). More sensitive and cost effective biosensor tests could allow for wider screening/testing policies and earlier detection in order to improve cancer patient outcomes.

In 2004 the world health organisation released a report in which it claimed that of the 57,029,000 annual worldwide deaths, 26% of these were due to infectious disease (WHO, 2004). This area could be vastly improved with the potential offered by biosensors. The key offering of rapid results at location could offer a significant reduction in these figures,

not only due to diagnosing infections in individuals but also in environmental monitoring of drinking water in the developing world.

Research and development of biosensors is a rapidly growing field, with great potential. Availability of mass produced biosensors that are small, portable, simple to use and give rapid, sensitive and accurate results could lend benefits to so many areas. Many of the current methods used have limitations that could be improved with biosensor technology, however biosensors are not always the most suitable option and research should focus on those areas to which a real benefit could be gained and commercialisation could become reality.

Although the commercialisation process has been slow, R&D continues at an exponential rate which can be seen in the number of annual publications and company start ups related to biosensors. Biofire Diagnostics Inc. have released Filmarray, a miniaturised diagnostic PCR system with a respiratory virus in vitro diagnostic panel and research use only panels for Blood culture (Pathogens and antibiotic resistance) and Gastro intestinal infections. Their Respiratory panel screens for 20 pathogens in 65 minutes, from a single sample. The 3M integrated cycler with Simplexa real-time PCR assays is a similar benchtop biosensor available for detection of a variety of bacterial and viral targets including CMV, EBV and *C. difficile*. The systems are not yet point of care (POC), but have reduced testing time and complexity and as competing technology are demonstrating a clear need for rapid, miniaturised on the market. Many other companies are investing their time and money in Biosensors suited to POC, such as OJ-Bio, a company working towards manufacture of a surface acoustic wave based biosensor for the detection of respiratory viral infections, enzymes and sexually transmitted infections. It can be imagined that POC testing may become commonplace in over the counter testing where consumers can purchase tests to be performed at home for example a test to detect Streptococcal infection may help someone in deciding whether to self-medicate for a sore throat or to seek guidance from a GP. Biosensors offering the ability to integrate with consumer electronics may have the potential for huge markets.

Since the enzyme electrode, the concept has expanded significantly and the term now encompasses many different biological recognition elements, transducer designs and materials. The enzyme electrodes themselves were further developed with the immobilisation of enzymes onto electrodes rather than the enzyme being confined within a permeable membrane (Wang, 2008). There has been a move towards micro- and nano-

technologies as the ability to manufacture smaller designs has become available and new materials such as carbon nanotubes and graphene have been isolated and characterised. Microbeads have also been used in signal visualisation, signal amplification and in capturing and concentrating the sample (Murphy, 2006). Nanoparticles are also used on the surface of biosensor devices to increase the surface area and therefore increase sensitivity, performance and stability (Justino *et al.*, 2010). Improvements in the performance of immunosensors have also been reported but it is claimed that this is largely due to improvements in antibodies rather than in the underlying sensor mechanisms (Justino *et al.*, 2010). Nanowires (NW) have been used as field effect transistor (FET) devices with silicon nanowire devices reported to have achieved 10 fM sensitivity and device reproducibility for deoxyribonucleic acid (DNA) detection using a peptide nucleic acid receptor (Patolsky *et al.*, 2006). However the paper does state that blood samples require pre-treatment before use as the high ionic strength of blood will interfere with the sensor performance.

Recently a 3D graphene 'foam' sensor has been described that has the potential to be developed into a biosensor. This sensor used a polymerised polydopamine linker to attach thionine to the 3D graphene structure, it was then used to detect hydrogen peroxide down to 80 nM (Xi *et al.*, 2013). They claim to have good stability, recovery and low interference when the sensor is used with 1:5 Bovine serum. This has great potential but remains at very early developmental stages. Cantilevers have shown high sensitivities but are limited in that they cannot be functionalised reproducibly to an acceptable level (Boisen and Thundat, 2009). Quantum dots have also shown potential but, with heavy metal as the core material these are toxic to cells (Morrison *et al.*, 2007). Even 50 years after the first biosensor, much improvement and further research is still required, before biosensors can fully achieve their potential/fulfil their promise.

Biosensors are the future in point of need clinical analysis. Commercial products continue to see sales growth and there is continually increasing interest from both academia and industry. However the slow transfer from research to commercialisation should be thoroughly understood by all those starting out on research in this area. New materials and techniques continue to open new avenues of research but all scientists should be aware of the limitations of their devices. Working well as part of multi-disciplinary teams is essential in this field. A concerted effort across conventional discipline boundaries, such as MEMS, nanotechnology, microfluidics and materials science and clinical diagnostics could provide the missing link to improved biosensor outputs.

### 1.4.1 Classes of Biosensor

Biosensors can be broken down into several classes in terms of the transduction mechanism or the biological recognition element.

Transducer can be broken down into three key groups, electrochemical, optical and piezoelectric (Justino *et al.*, 2010). Examples are shown in Table 1-1. This study focuses solely on graphene electrochemical sensors.

Transducing Element	Biorecognition Element	Analyte	Performance	Reference
<b>Electrochemical (amperometric)</b>	Enzyme-Glucose oxidase	Glutamate	LD: 1.6 $\mu$ M	(Batra and Pundir, 2013)
<b>Electrochemical (amperometric)</b>	Genetically modified <i>E.coli</i> displaying Glucose dehydrogenase	d-glucose	LD: 4 $\mu$ M	(Liang <i>et al.</i> , 2013)
<b>Electrochemical (potentiometric)</b>	Enzyme- Urease	<i>Urea</i>	0.1-80 mM	(Ali <i>et al.</i> , 2013)
<b>Electrochemical (Differential pulse voltammetry)</b>	Antibody	B-lactoglobulin	LD: 0.85 pg ml <sup>-1</sup>	(Eissa <i>et al.</i> , 2012)
<b>Electrochemical (chronopotentiometry)</b>	ssDNA	Target DNA (20 bases)	LD: 2.13 $\times 10^{-13}$ mol L <sup>-1</sup>	(Du <i>et al.</i> , 2010)
<b>Optic (SPR)</b>	Antibody	<i>L. pneumophila</i>	10 <sup>3</sup> CFU ml <sup>-1</sup>	(Enrico <i>et al.</i> , 2013)
<b>Optic (fluorescence)</b>	Enzyme- Acetylcholinesterase and choline oxidase	H <sub>2</sub> O <sub>2</sub> from metabolism of dichlorovos a pesticide	4.49 – 6780 nM	(Meng <i>et al.</i> , 2013)
<b>Optic (bioluminescence)</b>	Genetically engineered bioluminescent bacteria	l-arabinose monosaccharides	LD: 0.009 g L <sup>-1</sup>	(Łukasiak <i>et al.</i> , 2013)
<b>Optic (fibre optic)</b>	Antigen (Transglutaminase)	Antibody against transglutaminase	30-3000 nM	(Cennamo <i>et al.</i> , 2013)
<b>Resonator (Piezoelectric)</b>	Antibody	Prostate Specific Antigen	0.25 ng ml <sup>-1</sup>	(Su <i>et al.</i> , 2013)

Table 1-1 Examples of biosensors with various transduction elements.

#### 1.4.1.1 Electrochemical

Electrochemical sensors rely on the use of electrodes or FETs to measure changes in electrical outputs due to chemical changes such as oxidation or reduction of molecules at the electrode surface. This can include amperometric, potentiometric, voltammetric, conductimetric and impedance measurement (Justino *et al.*, 2010). Electrochemical biosensors are probably the most common, with blood glucose monitors being an example of amperometry. Examples of potentiometric microbial biosensors have been described that detect organophosphate nerve agents with the use of immobilised recombinant *E.coli* on the electrodes (Mulchandani *et al.*, 1998). Impedance sensors offer real potential for

the future of biosensors as very low voltages can be used which leaves the biorecognition layer intact compared to other electrochemical sensors where this can become damaged. Recently a simple graphene impedance biosensor has been described, utilising ssDNA immobilised onto electrochemically reduced graphene oxide (Loo *et al.*, 2013).

#### 1.4.1.2 Optical

Optical transducers used in biosensors can include the use of fluorescence, reflectance, absorbance, chemiluminescence, scattering or refractive index (Morrison *et al.*, 2007) (Luong *et al.*, 2008). The surface plasmon resonance (SPR) instrument is an optical biosensor, such as the Biacore instruments (GE Healthcare). Digital lateral flow tests also fall into this category relying on optical detection of coloured nanoparticles (See Figure 1-8).

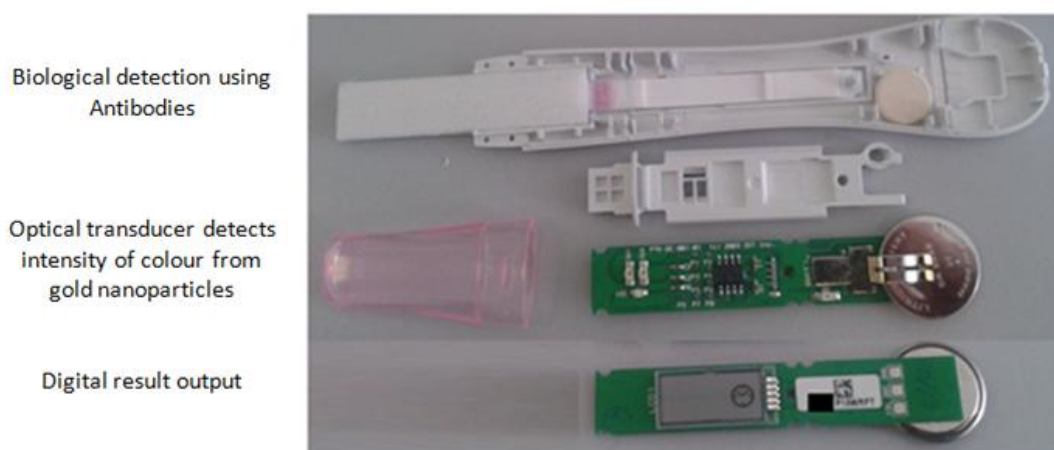


Figure 1-8 Human Chorionic Gonadotropin digital lateral flow test

This photograph shows the internal components of a commercial biosensor. Sample is wicked through an immunostrip. If antigen is present this binds to the antibody labelled gold nanoparticles (Pink band on strip) as the mixture of sample and labelled antibodies move along the strip antigen is captured on a test line. This results in a red line appearing which varies in intensity with antigen concentration. In these digital versions the coloured band is analysed optically to give a digital readout of positive or negative result.

#### 1.4.1.3 Resonators

Materials that resonate under the application of an external alternating electrical field, such as quartz crystals (Justino *et al.*, 2010) fall into the category of resonators. Binding of molecules results in a change of mass at the surface of the device which in turn causes a change in frequency of the resonance. Examples include Shear horizontal-surface acoustic wave, Bulk acoustic wave and quartz crystal microbalance (QCM) devices. These devices have proven successful in detection of viruses, bacteria and various analytes with sensitivity comparable to standard ELISA. The SAW biosensor described by Onen detected urinary Bcl-2 at  $500 \text{ pg ml}^{-1}$  (Onen *et al.*, 2012) similar to commercial assays such as the Bcl-2 ELISA from Millipore QIA23 with sensitivity reported as  $<1 \text{ ng ml}^{-1}$  and

with assay times of 10 min (SAW), 3.5 hours (ELISA). They may rely on the piezoelectric effect for actuation or detection.

This category also includes cantilevers, clamped resonators and circular diaphragm resonators. Ndeiyira has demonstrated the use of cantilevers for “the label-free detection of vancomycin binding to bacterial cell wall precursor analogues (mucopeptides) on cantilever arrays, with 10 nM sensitivity” (Ndeiyira *et al.*, 2008). Circular diaphragm resonators have been demonstrated as biosensors, to detect S100 $\beta$  protein to levels as low as 9 pg added mass (Ismail *et al.*, 2008). Resonators have been investigated as biosensors and characterised. For example poly silicon germanium micro-electro mechanical double clamped beam resonators were assessed for effect of resonator length and dampening with each immobilisation step (Khaled *et al.*, 2012). This group found that longer resonator beams failed more frequently and were more vulnerable to stop functioning with fewer immobilisation layers than shorter beams.

## **1.4.2 Biological Detection**

### **1.4.2.1 Antibodies**

The use of antibodies at biosensor surfaces for specific detection of required antigens is a logical step from the many immunoassay techniques used in wet laboratory conditions (Figure 1-9). They have been successfully used in a wide variety of assays from ELISA, western blots, Immunohistochemistry, agglutination assays and lateral flow. The techniques all take advantage of the positive attributes of antibodies, such as, high affinities and high selectivity toward their specific antigen (Albrecht *et al.*, 2010). In addition, they can be developed to the analyte of interest, are widely available commercially, can be raised in different hosts to give more flexibility and many immobilisation methods are well understood. A good antibody can confer improved sensitivity of orders of magnitude to a system compared to a poor antibody. Since the advent of monoclonal antibodies, they can be manufactured reproducibly and in large volumes, which makes them a good option for diagnostics. Antibodies may be monoclonal or polyclonal. A polyclonal antibody preparation often contains antibodies raised against the same antigen but able to bind various epitopes and is taken from the sera of an immunised host. These antibodies can show greater sensitivity than monoclonals but can also result in greater non-specific binding resulting in lowered selectivity. Monoclonal antibodies can show lower binding levels as they are specific to one epitope, effectively clones of one another, but in general show lower cross-reactivity, and therefore improved selectivity in samples.

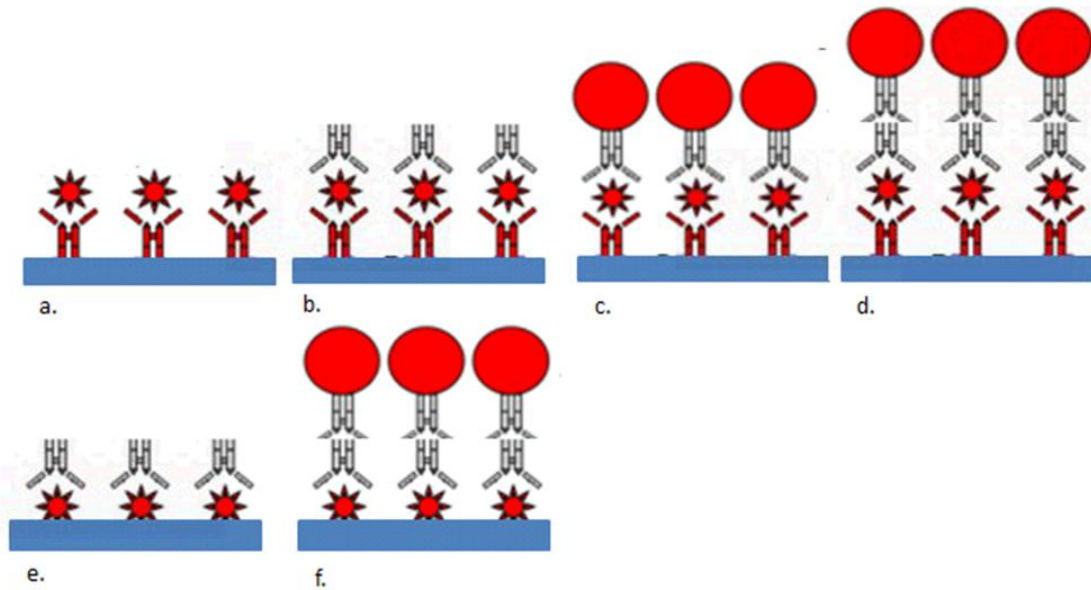


Figure 1-9 Typical immunoassay methods.

a. direct detection of antigen using antibody capture surface. b. sandwich assay. c. use of labelled detection antibody. d. addition of labelled secondary antibody for further signal enhancement. e. detection of antibodies to immobilised antigen. f. detection of antibodies with signal enhancement.

Secondary antibodies can also be used for signal visualisation or enhancement. These are often anti species antibodies raised against the primary antibody species and can be used alone or with a tag dependent upon their purpose in the system. The tag can be a fluorescent molecule, an enzyme, a particle or many other alternatives.

### 1.4.2.2 Enzymes

Enzymes are another good option for specific biological detection due to their binding and catalytic properties. Being proteins, they are also easily immobilised onto various surfaces using the same techniques as used for antibodies. The method of detection with enzymes can vary, the signal is generated by the catalysis of the reaction by the enzyme. This reaction leads to a change such as light emission, reflectance, absorption, production of heat, release of gas or change in ion concentration that can be detected by the transducer. The transducer then converts these changes into a measurable signal output. Enzymes can also be used in signal enhancement to increase sensitivity (Luong *et al.*, 2008).

### 1.4.2.3 Nucleic Acid

Biosensors can be developed using the binding affinities of the DNA bases to bind complimentary strands. Such detection typically require pre-treatment of sample to lyse cells releasing the genetic material and to perform the polymerase chain reaction, the DNA strands also need to be 'unzipped' to be detected. Nucleic acids can be immobilised

covalently, or, non-covalently onto surfaces, although specific covalent binding should increase the specificity of the recognition (Loo *et al.*, 2013). Oligodeoxynucleotides can be attached to the surfaces of sensors such as gold using a thiol group, and these can form self-assembled monolayers (SAM) with the ability to bind and therefore detect nucleic acid sequences of choice (Palek and Fojta, 2001). Avidin-biotin systems have also been demonstrated for immobilisation of DNA biosensors, for example a QCM biosensor for detection of  $\beta$ -thalassaemia (Zhou *et al.*, 2001).

## 1.5 Conclusions

Graphene offers a real opportunity to re-invigorating the field of electrochemical sensors which has not progressed commercially beyond the glucose biosensor used by millions in the monitoring of diabetes. Graphene's high conductivity, strength, large surface area all make it amenable to electrochemical sensing, if a suitable production method can be identified to produce large volumes of reproducible, cost effective sensors. This is more likely to be fulfilled with the use of 'graphene like' materials as opposed to pristine graphene as described by IUPAC. Their availability of low levels of oxygen defects can aid the electrochemical transfer. A balance in defects, dopants or oxygen is imperative to achieve this improved transfer state whilst maintaining the excellent conductivities is required. From the abundance of examples in the literature, some of those offering the greatest opportunity are the laser fabricated graphene like materials which require limited processing, can be used as standalone electrodes and have potential for printing of planar electrode structures (El-Kady *et al.* 2012; Strong *et al.* 2012; Lin *et al.* 2014). These carbon based materials should also offer favourable characteristics for combining with biological recognition elements with well understood immobilisation chemistries being available to attach covalently to carbon oxygen groups such as carboxylic acid and hydroxyl groups.

## 1.6 References

- Affoune, A.M., Prasad, B.L.V., Sato, H., Enoki, T., Kaburagi, Y. and Hishiyama, Y. (2001) 'Experimental evidence of a single nano-graphene', *Chemical Physics Letters*, 348, pp. 17-20.
- Albrecht, C., Fechner, P., Honcharenko, D., Baltzer, L. and Gauglitz, G. (2010) 'A new assay design for clinical diagnostics based on alternative recognition elements', *Biosensors and Bioelectronics*, 25(10), pp. 2302-2308.
- Ali, A., Alsalhi, M.S., Atif, M., Ansari, A.A., Israr, M.Q., Sadaf, J.R., Ahmed, E., Nur, O. and Willander, M. (2013) 'Potentiometric urea biosensor utilizing nanobiocomposite of chitosan-iron oxide magnetic nanoparticles', *Journal of Physics: Conference Series*, 414(1).
- Alwarappan, S., Erdem, A., Liu, C. and Li, C.-Z. (2009) 'Probing the Electrochemical Properties of Graphene Nanosheets for Biosensing Applications', *The Journal of Physical Chemistry C*, 113(20), pp. 8853-8857.
- Ambrosi, A., Chua, C.K., Bonanni, A. and Pumera, M. (2014) 'Electrochemistry of Graphene and Related Materials', *Chemical Reviews*, 114(14), pp. 7150-7188.
- Ambrosi, A., Chua, C.K., Latiff, N.M., Loo, A.H., Wong, C.H.A., Eng, A.Y.S., Bonanni, A. and Pumera, M. (2016) 'Graphene and its electrochemistry - an update', *Chemical Society Reviews*, 45(9), pp. 2458-2493.
- Bae, S., Kim, H., Lee, Y., Xu, X., Park, J.-S., Zheng, Y., Balakrishnan, J., Lei, T., Ri Kim, H., Song, Y.I., Kim, Y.-J., Kim, K.S., Ozyilmaz, B., Ahn, J.-H., Hong, B.H. and Iijima, S. (2010) 'Roll-to-roll production of 30-inch graphene films for transparent electrodes', *Nature Nanotechnology*, 5(8), pp. 574-578.
- Banks, C. E. and R. G. Compton (2005) 'Edge Plane Pyrolytic Graphite Electrodes in Electroanalysis: An Overview.' *Analytical Sciences* 21(11): 1263-1268.
- Barlas, Y., Yang, K. and Macdonald, A.H. (2012) 'Quantum Hall effects in graphene-based two-dimensional electron systems', *Nanotechnology*, 23(5).
- Barton, R.A., Ilic, B., van der Zande, A.M., Whitney, W.S., McEuen, P.L., Parpia, J.M. and Craighead, H.G. (2011) 'High, Size-Dependent Quality Factor in an Array of Graphene Mechanical Resonators', *Nano Letters*, 11(3), pp. 1232-1236.
- Batra, B. and Pundir, C.S. (2013) 'An amperometric glutamate biosensor based on immobilization of glutamate oxidase onto carboxylated multiwalled carbon nanotubes/gold nanoparticles/chitosan composite film modified Au electrode', *Biosensors and Bioelectronics*, 47, pp. 496-501.
- Berger, C., Song, Z., Li, T., Li, X., Ogbazghi, A.Y., Feng, R., Dai, Z., Marchenkov, A.N., Conrad, E.H., First, P.N. and de Heer, W.A. (2004) 'Ultrathin Epitaxial Graphite: 2D Electron Gas Properties and a Route toward Graphene-based Nanoelectronics', *The Journal of Physical Chemistry B*, 108(52), pp. 19912-19916.
- Biedermann, L.B., Bolen, M.L., Capano, M.A., Zemlyanov, D. and Reifengerger, R.G. (2009) 'Insights into few-layer epitaxial graphene growth on 4H-SiC(0001[over  $\bar{1}$ ]) substrates from STM studies', *Physical Review B*, 79(12), p. 125411.
- Blake, P., Hill, E.W., Castro Neto, A.H., Novoselov, K.S., Jiang, D., Yang, R., Booth, T.J. and Geim, A.K. (2007) 'Making graphene visible', *Applied Physics Letters*, 91(6).
- Boehm, H.P., Clauss, A., Fischer, G.O. and Hofmann, U. (1962) 'Das Adsorptionsverhalten sehr dünner Kohlenstoff-Folien', *Zeitschrift für anorganische und allgemeine Chemie*, 316(3-4), pp. 119-127.
- Boehm, H.P., Setton, R. and Stumpp, E. (1986) 'Nomenclature and terminology of graphite intercalation compounds', *Carbon*, 24(2), pp. 241-245.

- Boisen, A. and Thundat, T. (2009) 'Design & fabrication of cantilever array biosensors', *Materials Today*, 12(9), pp. 32-38.
- Bollella, P., Fusco, G., Tortolini, C., Sanzò, G., Favero, G., Gorton, L. and Antiochia, R. 'Beyond graphene: Electrochemical sensors and biosensors for biomarkers detection', *Biosensors and Bioelectronics*, 89(1), pp. 152-166.
- Bolotin, K.I., Sikes, K.J., Jiang, Z., Klima, M., Fudenberg, G., Hone, J., Kim, P. and Stormer, H.L. (2008) 'Ultrahigh electron mobility in suspended graphene', *Solid State Communications*, 146(9–10), pp. 351-355.
- Brodie, B.C. (1859) 'On the Atomic Weight of Graphite', *Philosophical Transactions of the Royal Society of London*, 149, pp. 249-259.
- Brownson, D.A.C. and Banks, C.E. (2011) 'Graphene electrochemistry: Fabricating amperometric biosensors', *Analyst*, 136(10), pp. 2084-2089.
- Brownson, D.A.C., Gomez-Mingot, M. and Banks, C.E. (2011a) 'CVD graphene electrochemistry: biologically relevant molecules', *Physical Chemistry Chemical Physics*, 13(45), pp. 20284-20288.
- Brownson, D.A.C., Kampouris, D.K. and Banks, C.E. (2012) 'Graphene electrochemistry: fundamental concepts through to prominent applications', *Chemical Society Reviews*, 41(21), pp. 6944-6976.
- Brownson, D.A.C., Munro, L.J., Kampouris, D.K. and Banks, C.E. (2011b) 'Electrochemistry of graphene: not such a beneficial electrode material?', *RSC Advances*, 1(6), pp. 978-988.
- Bunch, J.S., van der Zande, A.M., Verbridge, S.S., Frank, I.W., Tanenbaum, D.M., Parpia, J.M., Craighead, H.G. and McEuen, P.L. (2007) 'Electromechanical Resonators from Graphene Sheets', *Science*, 315(5811), pp. 490-493.
- Bunch, J.S., Verbridge, S.S., Alden, J.S., Van Der Zande, A.M., Parpia, J.M., Craighead, H.G. and McEuen, P.L. (2008) 'Impermeable atomic membranes from graphene sheets', *Nano letters*, 8(8), pp. 2458-2462.
- Carter, R.M., Jacobs, M.B., Lubrano, G.J. and Guilbault, G.G. (1995) 'Piezoelectric Detection of Ricin and Affinity-Purified Goat Anti-ricin Antibody', *Analytical Letters*, 28(8), pp. 1379-1386.
- Cennamo, N., Varriale, A., Pennacchio, A., Staiano, M., Massarotti, D., Zeni, L. and D'Auria, S. (2013) 'An innovative plastic optical fiber-based biosensor for new bio/applications. The case of celiac disease', *Sensors and Actuators B: Chemical*, 176(0), pp. 1008-1014.
- Clarke, L.C. (1962) *Annals of the New York Academy of Sciences*, 102, pp. 29-45.
- Coleman, J.N. (2013) 'Liquid Exfoliation of Defect-Free Graphene', *Accounts of Chemical Research*, 46(1), pp. 14-22.
- Culková, E., Švorc, L., Tomčík, P., Durdiak, J., Rievaj, M., Bustin, D., Brescher, R. and Lokaj, J. (2013) 'Boron-doped diamond electrode as sensitive and selective green electroanalytical tool for heavy metals environmental monitoring: Zinc detection in rubber industry waste.' *Polish Journal of Environmental Studies* 22(5): 1317-1323.
- Currie, L.A. (1999) 'Nomenclature in evaluation of analytical methods including detection and quantification capabilities: (IUPAC Recommendations 1995)', *Analytica Chimica Acta*, 391(2), pp. 105-126.
- Díaz Toro, P. C., F. J. Arévalo, M. A. Zon and H. Fernández (2015) 'Studies of the electrochemical behavior of moniliformin mycotoxin and its sensitive determination at pretreated glassy carbon electrodes in a non-aqueous medium.' *Journal of Electroanalytical Chemistry* 738: 40-46.

- D'Orazio, P. (2011) 'Biosensors in clinical chemistry - 2011 update', *Clinica Chimica Acta*, 412(19-20), pp. 1749-1761.
- Du, M., Yang, T. and Jiao, K. (2010) 'Rapid DNA electrochemical biosensing platform for label-free potentiometric detection of DNA hybridization', *Talanta*, 81(3), pp. 1022-1027.
- Edwards, R.S. and Coleman, K.S. (2013) 'Graphene synthesis: relationship to applications', *Nanoscale*, 5(1), pp. 38-51.
- Eissa, S., Tlili, C., L'Hocine, L. and Zourob, M. (2012) 'Electrochemical immunosensor for the milk allergen  $\beta$ -lactoglobulin based on electrografting of organic film on graphene modified screen-printed carbon electrodes', *Biosensors and Bioelectronics*, 38(1), pp. 308-313.
- Eissa, S., L'Hocine, M. Sij and M. Zourob (2013) 'A graphene-based label-free voltammetric immunosensor for sensitive detection of the egg allergen ovalbumin.' *Analyst* 138(15): 4378-4384.
- El-Kady, M.F. and Kaner, R.B. (2013) 'Scalable fabrication of high-power graphene micro-supercapacitors for flexible and on-chip energy storage', *Nature Communications*, 4, p. 1475.
- El-Kady, M.F., Strong, V., Dubin, S. and Kaner, R.B. (2012) 'Laser Scribing of High-Performance and Flexible Graphene-Based Electrochemical Capacitors', *Science*, 335(6074), pp. 1326-1330.
- Enrico, D.L., Manera, M.G., Montagna, G., Cimaglia, F., Chiesa, M., Poltronieri, P., Santino, A. and Rella, R. (2013) 'SPR based immunosensor for detection of Legionella pneumophila in water samples', *Optics Communications*, 294, pp. 420-426.
- Feng, X., Y. Zhang, J. Zhou, Y. Li, S. Chen, L. Zhang, Y. Ma, L. Wang and X. Yan (2015) 'Three-dimensional nitrogen-doped graphene as an ultrasensitive electrochemical sensor for the detection of dopamine.' *Nanoscale* 7(6): 2427-2432.
- Fernández-Sánchez, C., C. J. McNeil, K. Rawson and O. Nilsson (2004) 'Disposable Noncompetitive Immunosensor for Free and Total Prostate-Specific Antigen Based on Capacitance Measurement.' *Analytical Chemistry* 76(19): 5649-5656.
- Ferrari, A.C. (2007) 'Raman spectroscopy of graphene and graphite: Disorder, electron-phonon coupling, doping and nonadiabatic effects', *Solid State Communications*, 143(1-2), pp. 47-57.
- Ferrari, A.C. and Basko, D.M. (2013) 'Raman spectroscopy as a versatile tool for studying the properties of graphene', *Nature Nanotechnology*, 8(4), pp. 235-246.
- Fowler, J.D., Allen, M.J., Tung, V.C., Yang, Y., Kaner, R.B. and Weiller, B.H. (2009) 'Practical Chemical Sensors from Chemically Derived Graphene', *American Chemical Society Nano*, 3(2), pp. 301-306.
- Frense, D., A. Müller and D. Beckmann (1998) 'Detection of environmental pollutants using optical biosensor with immobilized algae cells.' *Sensors and Actuators B: Chemical* 51(1-3): 256-260.
- Geim, A.K. and Novoselov, K.S. (2007) 'The rise of graphene', *Nature Materials*, 6(3), pp. 183-191.
- Giovannetti, G., Khomyakov, P.A., Brocks, G., Karpan, V.M., van den Brink, J. and Kelly, P.J. (2008) 'Doping Graphene with Metal Contacts', *Physical Review Letters*, 101(2), p. 026803.
- Gorton, L. (1995) 'Carbon paste electrodes modified with enzymes, tissues, and cells', *Electroanalysis*, 7(1), pp. 23-45.

- Green, A.A. and Hersam, M.C. (2009) 'Solution Phase Production of Graphene with Controlled Thickness via Density Differentiation', *Nano Letters*, 9(12), pp. 4031-4036.
- Griffiths, K., Dale, C., Hedley, J., Kowal, M.D., Kaner, R.B. and Keegan, N. (2014) 'Laser-scribed graphene presents an opportunity to print a new generation of disposable electrochemical sensors', *Nanoscale*, 6(22), pp. 13613-13622.
- Gubala, V., Harris, L.F., Ricco, A.J., Tan, M.X. and Williams, D.E. (2012) 'Point of Care Diagnostics: Status and Future', *Analytical Chemistry*, 84(2), pp. 487-515.
- Guy, O.J., Castaing, A., Tehrani, Z. and Doak, S.H. (2010) *Proceedings of IEEE Sensors*.
- Hibino, H., Kageshima, H., Kotsugi, M., Maeda, F., Guo, F.Z. and Watanabe, Y. (2009) 'Dependence of electronic properties of epitaxial few-layer graphene on the number of layers investigated by photoelectron emission microscopy', *Physical Review B*, 79(12), p. 125437.
- Huang, L., Zhang, Z., Li, Z., Chen, B., Ma, X., Dong, L. and Peng, L.-M. (2015) 'Multifunctional Graphene Sensors for Magnetic and Hydrogen Detection', *ACS Applied Materials & Interfaces*, 7(18), pp. 9581-9588.
- Huang, S.Y., Ji, Y., Wen, H., Zhang, K., Yuen, M.M.F., Fu, X.Z., Sun, R. and Wong, C.P. (2016) *China Semiconductor Technology International Conference 2016, CSTIC 2016*. Available at: <https://www.scopus.com/inward/record.uri?eid=2-s2.0-84974623060&partnerID=40&md5=6488c93f1ab5383014ee15c34c3825eb>.
- Ismail, A.K., Burdess, J.S., Harris, A.J., Suarez, G., Keegan, N., Spoor, J.A., Chang, S.C., McNeil, C.J. and Hedley, J. (2008) 'The fabrication, characterization and testing of a MEMS circular diaphragm mass sensor', *Journal of Micromechanics and Microengineering*, 18.
- Jacobs, C. B., M. J. Peairs and B. J. Venton (2010). 'Review: Carbon nanotube based electrochemical sensors for biomolecules.' *Analytica Chimica Acta* 662(2): 105-127.
- Jain, K.K. 655 (2009) 'The role of nanobiotechnology in drug discovery' *Advances in Experimental Medicine and Biology*. pp. 37-43. Available at: <http://www.scopus.com/inward/record.url?eid=2-s2.0-77955486440&partnerID=40&md5=7fe619dab10372b0992bb9b60b583771>.
- Johnson, D.W., Dobson, B.P. and Coleman, K.S. (2015) 'A manufacturing perspective on graphene dispersions', *Current Opinion in Colloid and Interface Science*, 20(5-6), pp. 367-382.
- Justino, C.I.L., Rocha-Santos, T.A. and Duarte, A.C. (2010) 'Review of analytical figures of merit of sensors and biosensors in clinical applications', *Trends in Analytical Chemistry*, 29(10), pp. 1172-1183.
- Karuwan, C., A. Wisitsoraat, D. Phokharatkul, C. Sriprachuabwong, T. Lomas, D. Nacapricha and A. Tuantranont (2013). "A disposable screen printed graphene-carbon paste electrode and its application in electrochemical sensing." *Royal Society of Chemistry Advances* 3(48): 25792-25799.
- Kato, M., Ichimura, M., Arai, E. and Ramasamy, P. (2003) 'Electrochemical Etching of 6H-SiC Using Aqueous KOH Solutions with Low Surface Roughness', *Japanese Journal of Applied Physics*, 42(Part 1, No. 7A), pp. 4233-4236.
- Kaur, B., T. Pandiyan, B. Satpati and R. Srivastava (2013) 'Simultaneous and sensitive determination of ascorbic acid, dopamine, uric acid, and tryptophan with silver nanoparticles-decorated reduced graphene oxide modified electrode.' *Colloids and Surfaces B: Biointerfaces* 111(0): 97-106.

- Khaled, A., Raoof, M., Cherman, V., Jans, K., Abbas, M., Ebrahim, S., Bryce, G., Verheyen, P., Witvrouw, A. and De Wolf, I. (2012) 'Effect of the functionalization process on the performance of SiGe MEM resonators used for bio-molecular sensing', *Microelectronics Reliability*, 52, pp. 2272-2277.
- Khan, Z.U., Kausar, A., Ullah, H., Badshah, A. and Khan, W.U. (2016) 'A review of graphene oxide, graphene buckypaper, and polymer/graphene composites: Properties and fabrication techniques', *Journal of Plastic Film and Sheeting*, 32(4), pp. 336-379.
- König, M., Ruhl, G., Batke, J.M. and Lemme, M.C. (2016) 'Self-organized growth of graphene nanomesh with increased gas sensitivity', *Nanoscale*, 8(34), pp. 15490-15496.
- Kumar, A. and S. Jung (2011) 'Protein biosensors based on polymer nanowires, carbon nanotubes and zinc oxide nanorods.' *Sensors* 11(5): 5087-5111.
- Labroo, P. and Cui, Y. (2013a) 'Electrical, enzymatic graphene biosensing of 5-aminosalicylic acid', *Analyst*, 138(5), pp. 1325-1328.
- Labroo, P. and Cui, Y. (2013b) 'Flexible graphene bio-nanosensor for lactate', *Biosensors and Bioelectronics*, 41(0), pp. 852-856.
- Lee, C., Wei, X., Kysar, J.W. and Hone, J. (2008) 'Measurement of the Elastic Properties and Intrinsic Strength of Monolayer Graphene', *Science*, 321(5887), pp. 385-388.
- Lei, N., Li, P., Xue, W. and Xu, J. (2011) 'Simple graphene chemiresistors as pH sensors: Fabrication and characterization', *Measurement Science and Technology*, 22(10).
- Lei, Y., Mulchandani, P., Wang, J., Chen, W. and Mulchandani, A. (2005) 'Highly Sensitive and Selective Amperometric Microbial Biosensor for Direct Determination of p-Nitrophenyl-Substituted Organophosphate Nerve Agents', *Environmental Science & Technology*, 39(22), pp. 8853-8857.
- Li, J., Zhang, G., Sun, R. and Wong, C.P. (2016) *China Semiconductor Technology International Conference 2016, CSTIC 2016*. Available at: <https://www.scopus.com/inward/record.uri?eid=2-s2.0-84974577686&partnerID=40&md5=52da02be60e1fe3c051b71f1957e9730>.
- Li, W., Tan, C., Lowe, M.A., Abruña, H.D. and Ralph, D.C. (2011a) 'Electrochemistry of Individual Monolayer Graphene Sheets', *American Chemical Society Nano*, 5(3), pp. 2264-2270.
- Li, X., Magnuson, C.W., Venugopal, A., Tromp, R.M., Hannon, J.B., Vogel, E.M., Colombo, L. and Ruoff, R.S. (2011b) 'Large-area graphene single crystals grown by low-pressure chemical vapor deposition of methane on copper', *Journal of the American Chemical Society*, 133(9), pp. 2816-9.
- Liang, B., Li, L., Tang, X., Lang, Q., Wang, H., Li, F., Shi, J., Shen, W., Palchetti, I., Mascini, M. and Liu, A. (2013) 'Microbial surface display of glucose dehydrogenase for amperometric glucose biosensor', *Biosensors and Bioelectronics*, 45(1), pp. 19-24.
- Lin, J., Peng, Z., Liu, Y., Ruiz-Zepeda, F., Ye, R., Samuel, E.L.G., Yacaman, M.J., Yakobson, B.I. and Tour, J.M. (2014) 'Laser-induced porous graphene films from commercial polymers', *Nature Communications*, 5.
- Loo, A.H., Bonanni, A. and Pumera, M. (2013) 'Soldering DNA to graphene via 0, 1 and 2-point contacts: Electrochemical impedance spectroscopic investigation', *Electrochemistry Communications*, 28, pp. 83-86.
- Lotya, M., Hernandez, Y., King, P.J., Smith, R.J., Nicolosi, V., Karlsson, L.S., Blighe, F.M., De, S., Wang, Z., McGovern, I.T., Duesberg, G.S. and Coleman, J.N. (2009) 'Liquid Phase Production of Graphene by Exfoliation of Graphite in Surfactant/Water Solutions', *Journal of the American Chemical Society*, 131(10), pp. 3611-3620.

- Lu, W., Liu, S., Qin, X., Wang, L., Tian, J., Luo, Y., Asiri, A.M., Al-Youbi, A.O. and Sun, X. (2012) 'High-yield, large-scale production of few-layer graphene flakes within seconds: using chlorosulfonic acid and H<sub>2</sub>O<sub>2</sub> as exfoliating agents', *Journal of Materials Chemistry*, 22(18), pp. 8775-8777.
- Łukasiak, J., Olsen, K., Georgiou, C.A. and Georgakopoulos, D.G. (2013) 'Bioluminescence and ice-nucleation microbial biosensors for l-arabinose content analysis in arabinoxylans', *European Food Research and Technology*, pp. 1-8.
- Luong, J.H.T., Male, K.B. and Glennon, J.D. (2008) 'Biosensor technology: Technology push versus market pull', *Biotechnology Advances*, 26(5), pp. 492-500.
- Ma, H., Zeng, J., Song, J., Chen, X. and Ma, Y. (2016) *China Semiconductor Technology International Conference 2016, CSTIC 2016*. Available at: <https://www.scopus.com/inward/record.uri?eid=2-s2.0-84974528520&partnerID=40&md5=8c2a0b24d30e04b27f5d4dda2e9dd919>.
- Malard, L.M., Pimenta, M.A., Dresselhaus, G. and Dresselhaus, M.S. (2009) 'Raman spectroscopy in graphene', *Physics Reports*, 473(5–6), pp. 51-87.
- Marrazza, G., I. Chianella and M. Mascini (1999) 'Disposable DNA electrochemical biosensors for environmental monitoring.' *Analytica Chimica Acta* 387(3): 297-307.
- Mattevi, C., Kim, H. and Chhowalla, M. (2011) 'A review of chemical vapour deposition of graphene on copper', *Journal of Materials Chemistry*, 21(10), pp. 3324-3334.
- McGrath, T. F., C. T. Elliott and T. L. Fodey (2012) 'Biosensors for the analysis of microbiological and chemical contaminants in food.' *Analytical and Bioanalytical Chemistry* 403(1): 75-92.
- McNaught, A., D., Wilkinson, A. and IUPAC (2006-) *Compendium of Chemical Terminology, 2nd ed (the "Gold Book")*. update 2012-08-19, version 2.3.2 edn. Oxford: Blackwell Scientific Publications.
- Meng, X., Wei, J., Ren, X., Ren, J. and Tang, F. (2013) 'A simple and sensitive fluorescence biosensor for detection of organophosphorus pesticides using H<sub>2</sub>O<sub>2</sub>-sensitive quantum dots/bi-enzyme', *Biosensors and Bioelectronics*, 47, pp. 402-407.
- Mohanty, N. and Berry, V. (2008) 'Graphene-based single-bacterium resolution biodevice and DNA transistor: Interfacing graphene derivatives with nanoscale and microscale biocomponents', *Nano Letters*, 8(12), pp. 4469-4476.
- Moore, R. R., C. E. Banks and R. G. Compton (2004). "Basal Plane Pyrolytic Graphite Modified Electrodes: Comparison of Carbon Nanotubes and Graphite Powder as Electrocatalysts." *Analytical Chemistry* 76(10): 2677-2682.
- Morrison, D.W.G., Dokmeci, M.R., Demirci, U. and Khademhosseini, A. (2007) 'Clinical Applications of Micro- and Nanoscale Biosensors', *Biomedical Nanostructures*. John Wiley & Sons, Inc., pp. 439-460.
- Mulchandani, A., Mulchandani, P., Chauhan, S., Kaneva, I. and Chen, W. (1998) 'A Potentiometric Microbial Biosensor for Direct Determination of Organophosphate Nerve Agents', *Electroanalysis*, 10(11), pp. 733-737.
- Mulchandani, P., Mulchandani, A., Kaneva, I. and Chen, W. (1999) 'Biosensor for direct determination of organophosphate nerve agents. 1. Potentiometric enzyme electrode', *Biosensors and Bioelectronics*, 14(1), pp. 77-85.
- Murphy, L. (2006) 'Biosensors and bioelectrochemistry', *Current Opinion in Chemical Biology*, 10(2), pp. 177-184.

- Nair, R.R., Blake, P., Grigorenko, A.N., Novoselov, K.S., Booth, T.J., Stauber, T., Peres, N.M.R. and Geim, A.K. (2008) 'Fine structure constant defines visual transparency of graphene', *Science*, 320(5881), p. 1308.
- Nayak, P., Kurra, N., Xia, C. and Alshareef, H.N. (2016) 'Highly Efficient Laser Scribed Graphene Electrodes for On-Chip Electrochemical Sensing Applications', *Advanced Electronic Materials*.
- Ndieyira, J.W., Watari, M., Barrera, A.D., Zhou, D., Vogtli, M., Batchelor, M., Cooper, M.A., Strunz, T., Horton, M.A., Abell, C., Rayment, T., Aeppli, G. and McKendry, R.A. (2008) 'Nanomechanical detection of antibiotic-mucopeptide binding in a model for superbug drug resistance', *Nature Nanotechnology*, 3(11), pp. 691-6.
- Novoselov, K.S., Falko, V.I., Colombo, L., Gellert, P.R., Schwab, M.G. and Kim, K. (2012) 'A roadmap for graphene', *Nature*, 490(7419), pp. 192-200.
- Novoselov, K.S., Geim, A.K., Morozov, S.V., Jiang, D., Zhang, Y., Dubonos, S.V., Grigorieva, I.V. and Firsov, A.A. (2004) 'Electric Field Effect in Atomically Thin Carbon Films', *Science*, 306(5696), pp. 666-669.
- Novoselov, K.S., Jiang, D., Schedin, F., Booth, T.J., Khotkevich, V.V., Morozov, S.V. and Geim, A.K. (2005) 'Two-dimensional atomic crystals', *Proceedings of the National Academy of Sciences of the United States of America*, 102(30), pp. 10451-10453.
- Novoselov, K.S., Jiang, Z., Zhang, Y., Morozov, S.V., Stormer, H.L., Zeitler, U., Maan, J.C., Boebinger, G.S., Kim, P. and Geim, A.K. (2007) 'Room-Temperature Quantum Hall Effect in Graphene', *Science*, 315(5817), p. 1379.
- Nuvoli, D., Alzari, V., Sanna, R., Scognamillo, S., Piccinini, M., Peponi, L., Kenny, J.M. and Mariani, A. (2012) 'The production of concentrated dispersions of few-layer graphene by the direct exfoliation of graphite in organosilanes', *Nanoscale Research Letters*, 7, pp. 1-7.
- Onen, O., Sisman, A., Gallant, N.D., Kruk, P. and Guldiken, R. (2012) 'A urinary Bcl-2 surface acoustic wave biosensor for early ovarian cancer detection', *Sensors (Basel, Switzerland)*, 12(6), pp. 7423-7437.
- Paddle, B.M. (1996) 'Biosensors for chemical and biological agents of defence interest', *Biosensors and Bioelectronics*, 11(11), pp. 1079-1113.
- Palek, E. and Fojta, M. (2001) 'Detecting DNA Hybridization and Damage', *Analytical Chemistry*, 73(3), pp. 74 A-83 A.
- Pandikumar, A., Soon How, G.T., See, T.P., Omar, F.S., Jayabal, S., Kamali, K.Z., Yusoff, N., Jamil, A., Ramaraj, R., John, S.A., Lim, H.N. and Huang, N.M. (2014) 'Graphene and its nanocomposite material based electrochemical sensor platform for dopamine', *Royal Society of Chemistry Advances*, 4(108), pp. 63296-63323.
- Patel, A. N., M. G. Collignon, M. A. O'Connell, W. O. Y. Hung, K. McKelvey, J. V. Macpherson and P. R. Unwin (2012) 'A New View of Electrochemistry at Highly Oriented Pyrolytic Graphite.' *Journal of the American Chemical Society* 134(49): 20117-20130.
- Patolsky, F., Zheng, G. and Lieber, C.M. (2006) 'Nanowire-based biosensors', *Analytical Chemistry*, 78(13), pp. 4260-4269.
- Pohanka, M. and Skládal, P. (2005) 'Piezoelectric Immunosensor for Francisella tularensis Detection Using Immunoglobulin M in a Limiting Dilution', *Analytical Letters*, 38(3), pp. 411-422.
- Pumera, M. (2013) 'Electrochemistry of graphene, graphene oxide and other graphenoids: Review', *Electrochemistry Communications*, 36, pp. 14-18.

- Pumera, M., Ambrosi, A., Bonanni, A., Chng, E.L.K. and Poh, H.L. (2010) 'Graphene for electrochemical sensing and biosensing', *Trends in Analytical Chemistry*, 29(9), pp. 954-965.
- Qu, J., Luo, C.Q., Zhang, Q., Cong, Q. and Yuan, X. (2013) 'Easy synthesis of graphene sheets from alfalfa plants by treatment of nitric acid', *Materials Science and Engineering B-Advanced Functional Solid-State Materials*, 178(6), pp. 380-382.
- Randviir, E. P., D. A. C. Brownson, J. P. Metters, R. O. Kadara and C. E. Banks (2014) 'The fabrication, characterisation and electrochemical investigation of screen-printed graphene electrodes.' *Physical Chemistry Chemical Physics* 16(10): 4598-4611.
- Rechnitz, G.A., Kobos, R.K., Riechel, S.J. and Gebauer, C.R. (1977) 'A bio-selective membrane electrode prepared with living bacterial cells', *Analytica Chimica Acta*, 94, pp. 357-365.
- Ryan, B., Luiz Gustavo, C. and Lukas, N. (2015) 'Raman characterization of defects and dopants in graphene', *Journal of Physics: Condensed Matter*, 27(8), p. 083002.
- Salimi, A., Compton, R.G. and Hallaj, R. (2004) 'Glucose biosensor prepared by glucose oxidase encapsulated sol-gel and carbon-nanotube-modified basal plane pyrolytic graphite electrode', *Analytical Biochemistry*, 333(1), pp. 49-56.
- Schniepp, H.C., Li, J.-L., McAllister, M.J., Sai, H., Herrera-Alonso, M., Adamson, D.H., Prud'homme, R.K., Car, R., Saville, D.A. and Aksay, I.A. (2006) 'Functionalized Single Graphene Sheets Derived from Splitting Graphite Oxide', *The Journal of Physical Chemistry B*, 110(17), pp. 8535-8539.
- Shao, Y., Wang, J., Wu, H., Liu, J., Aksay, I.A. and Lin, Y. (2010) 'Graphene Based Electrochemical Sensors and Biosensors: A Review', *Electroanalysis*, 22(10), pp. 1027-1036.
- Shigemitsu, T., G. Matsumoto and S. Tsukahara (1979) 'Electrical properties of glassy-carbon electrodes.' *Medical and Biological Engineering and Computing* 17(4): 465-470.
- Shivaraman, S., Barton, R.A., Yu, X., Alden, J., Herman, L., Chandrashekar, M.S.V., Park, J., McEuen, P.L., Parpia, J.M., Craighead, H.G. and Spencer, M.G. (2009) 'Free-standing epitaxial graphene', *Nano Letters*, 9(9), pp. 3100-3105.
- Singh, V., Joung, D., Zhai, L., Das, S., Khondaker, S.I. and Seal, S. (2011) 'Graphene based materials: Past, present and future', *Progress in Materials Science*, 56(8), pp. 1178-1271.
- Song, S., Xu, H. and Fan, C. (2006) 'Potential diagnostic applications of biosensors: current and future directions', *International Journal of Nanomedicine*, 1(4), pp. 433-440.
- Strong, V., Dubin, S., El-Kady, M.F., Lech, A., Wang, Y., Weiller, B.H. and Kaner, R.B. (2012) 'Patterning and Electronic Tuning of Laser Scribed Graphene for Flexible All-Carbon Devices', *American Chemical Society Nano*, 6(2), pp. 1395-1403.
- Su, L., Zou, L., Fong, C.C., Wong, W.L., Wei, F., Wong, K.Y., Wu, R.S.S. and Yang, M. (2013) 'Detection of cancer biomarkers by piezoelectric biosensor using PZT ceramic resonator as the transducer', *Biosensors and Bioelectronics*, 46, pp. 155-161.
- Tao, L., Lee, J., Holt, M., Chou, H., McDonnell, S.J., Ferrer, D.A., Babenco, M.G., Wallace, R.M., Banerjee, S.K., Ruoff, R.S. and Akinwande, D. (2012) 'Uniform Wafer-Scale Chemical Vapor Deposition of Graphene on Evaporated Cu (111) Film with Quality Comparable to Exfoliated Monolayer', *Journal of Physical Chemistry C*, 116(45), pp. 24068-24074.

Tehrani, F. and Bavarian, B. (2016) 'Facile and scalable disposable sensor based on laser engraved graphene for electrochemical detection of glucose', *Scientific Reports*, 6, p. 27975.

Thostenson, E.T., Ren, Z. and Chou, T.-W. (2001) 'Advances in the science and technology of carbon nanotubes and their composites: a review', *Composites Science and Technology*, 61(13), pp. 1899-1912.

Tung, V.C., Allen, M.J., Yang, Y. and Kaner, R.B. (2009) 'High-throughput solution processing of large-scale graphene', *Nature Nanotechnology*, 4(1), pp. 25-29.

UNAIDS (2012) *Together we will end AIDS* (UNAIDS / JC2296E). UNAIDS. [Online]. Available at: <http://www.unaids.org/en/resources/publications/2012/> (Accessed: 20121113).

Wang, J. (2008) 'Electrochemical glucose biosensors', *Chemical Reviews*, 108(2), pp. 814-825.

Wang, Y.y., Ni, Z.h., Yu, T., Shen, Z.X., Wang, H.m., Wu, Y.h., Chen, W. and Shen Wee, A.T. (2008) 'Raman Studies of Monolayer Graphene: The Substrate Effect', *The Journal of Physical Chemistry C*, 112(29), pp. 10637-10640.

Wang, S. C., K. S. Chang and C. J. Yuan (2009) 'Enhancement of electrochemical properties of screen-printed carbon electrodes by oxygen plasma treatment.' *Electrochimica Acta* 54(21): 4937-4943.

Wang, L., D. Lu, S. Yu, X. Shi, C. Wang and Y. Zhang (2013) 'Voltammetric determination of alkannin using an Au nanoparticles–poly(diallyldimethylammonium chloride)-functionalized graphene nanocomposite film.' *Journal of Applied Electrochemistry* 43(8): 855-863.

Weiss, N.O., Zhou, H., Liao, L., Liu, Y., Jiang, S., Huang, Y. and Duan, X. (2012) 'Graphene: An emerging electronic material', *Advanced Materials*, 24(43), pp. 5782-5825.

WHO. (2004) *The Annual World Health Statistics Report 2004(Annexes)*. [http://www.who.int/gho/publications/world\\_health\\_statistics/en/index.html](http://www.who.int/gho/publications/world_health_statistics/en/index.html): World Health Organisation. [Online]. Available at: [http://www.who.int/gho/publications/world\\_health\\_statistics/en/index.html](http://www.who.int/gho/publications/world_health_statistics/en/index.html) (Accessed: 15th November 2012).

Wu, L., Chu, H.S., Koh, W.S. and Li, E.P. (2010) 'Highly sensitive graphene biosensors based on surface plasmon resonance', *Opt. Express*, 18(14), pp. 14395-14400.

Wu, S., He, Q., Tan, C., Wang, Y. and Zhang, H. (2013) 'Graphene-Based Electrochemical Sensors', *Small*, 9(8), pp. 1160-1172.

Xi, F., Zhao, D., Wang, X. and Chen, P. (2013) 'Non-enzymatic detection of hydrogen peroxide using a functionalized three-dimensional graphene electrode', *Electrochemistry Communications*, 26, pp. 81-84.

Yang, H., Hernandez, Y., Schlierf, A., Felten, A., Eckmann, A., Johal, S., Louette, P., Pireaux, J.J., Feng, X., Mullen, K., Palermo, V. and Casiraghi, C. (2013) 'A simple method for graphene production based on exfoliation of graphite in water using 1-pyrenesulfonic acid sodium salt', *Carbon*, 53(0), pp. 357-365.

Yavari, F., Chen, Z., Thomas, A.V., Ren, W., Cheng, H.M. and Koratkar, N. (2011) 'High sensitivity gas detection using a macroscopic three-dimensional graphene foam network', *Scientific reports*, 1, p. 166.

Zande, A.M.v.d., Barton, R.A., Alden, J.S., Ruiz-Vargas, C.S., Whitney, W.S., Pham, P.H.Q., Park, J., Parpia, J.M., Craighead, H.G. and McEuen, P.L. (2010) 'Large-Scale Arrays of Single-Layer Graphene Resonators', *Nano Letters*, 10(12), pp. 4869-4873.

Zhang, D.D., Fu, L., Liao, L., Liu, N., Dai, B.Y. and Zhang, C.X. (2012) 'Preparation, characterization, and application of electrochemically functional graphene nanocomposites by one-step liquid-phase exfoliation of natural flake graphite with methylene blue', *Nano Research*, 5(12), pp. 875-887.

Zhang, G., A. S. Cuharuc, A. G. Guell and P. R. Unwin (2015) 'Electrochemistry at highly oriented pyrolytic graphite (HOPG): lower limit for the kinetics of outer-sphere redox processes and general implications for electron transfer models.' *Physical Chemistry Chemical Physics* 17(17): 11827-11838.

Zhang, Y.F., Han, D., Fang, H. and Bai, S.L. (2016) *China Semiconductor Technology International Conference 2016, CSTIC 2016*. Available at: <https://www.scopus.com/inward/record.uri?eid=2-s2.0-84974589118&partnerID=40&md5=c21f03c71be1ed2a28e329a251375191>.

Zhou, S.Y., Siegel, D.A., Fedorov, A.V. and Lanzara, A. (2008) 'Metal to Insulator Transition in Epitaxial Graphene Induced by Molecular Doping', *Physical Review Letters*, 101(8).

Zhou, X.C., Huang, L.Q. and Li, S.F.Y. (2001) 'Microgravimetric DNA sensor based on quartz crystal microbalance: comparison of oligonucleotide immobilization methods and the application in genetic diagnosis', *Biosensors and Bioelectronics*, 16(1-2), pp. 85-95.

Zhu, Z., Garcia-Gancedo, L., Flewitt, A.J., Xie, H., Moussy, F. and Milne, W.I. (2012) 'A critical review of Glucose biosensors based on Carbon nanomaterials: Carbon nanotubes and graphene', *Sensors (Switzerland)*, 12(5), pp. 5996-6022.

## Chapter 2. Laser-scribed Graphene Presents an Opportunity to Print a New Generation of Disposable Electrochemical Sensors

This chapter has been published as a research paper in *Nanoscale* (Griffiths *et al.*, 2014).

### 2.1 Introduction

A diverse range of chemical and biochemical analytes have been detected using carbon materials as electrodes, or components of electrodes, in electrochemical assays. The composition of carbon electrodes used in electrochemistry are highly heterogeneous in nature with examples including glassy carbon (O'Neill *et al.*, 2004), carbon paste (Kulys, 1999), screen printed carbon (Albareda-Sirvent *et al.*, 2000), edge-plane pyrolytic graphite (EPPG)/basal-plane pyrolytic graphite (BPPG) (Banks and Compton, 2005; Banks and Compton, 2006), carbon nanotubes (Musameh *et al.*, 2002) and graphene (Pumera *et al.*, 2010). Interestingly, the electron transfer rate and analytical performance of these electrodes are dramatically influenced by the structural nature of the carbon material itself, which is largely due to differences in the density of electronic states and edge-plane sites available on the carbon electrode surface (McCreery and McDermott, 2012). This is well demonstrated by the now common method of modifying underlying carbon electrodes with carbon nanotubes, engendering enhanced electrochemical performance. The original demonstration was performed by Wang's group who discovered the addition of carbon nanotubes allowed a large reduction in the overpotential for NADH detection compared with unmodified glassy carbon electrodes (Musameh *et al.*, 2002). In further work, Wang's group used multi-walled carbon nanotubes as the underlying electrode by screen printing them as an ink, which gave increased current densities and reduced overpotentials for numerous electro-active species compared with a commercial carbon ink (Wang and Musameh, 2004). However, a fundamental observation by Compton's group is worth bearing in mind. The electro-catalytic performance reported for carbon nanotubes should be substantiated using the relevant controls when modifying a pre-existing electrode, for example, substituting carbon nanotubes for graphite powder (Moore *et al.*, 2004). In fact, the same group wrote two illuminating and extensive reviews advocating that EPPG electrodes were often advantageous over carbon nanotubes and other carbon based electrodes in electrochemical sensing, due to the increased edge plane/defect sites they possess (Banks and Compton, 2005; Banks and Compton, 2006). It appears likely that EPPG has been sidelined to academic endeavours due to the manufacturing route and operation. It is cut from highly ordered pyrolytic graphite and housed in an external casing

before operation using macroscale external reference and counter electrodes, making commercial exploitation problematic due to difficulties in mass production and miniaturisation. In contrast, screen printed carbon electrodes heralded a turning point in mass production of whole systems for numerous electrochemical sensing applications, utilising in-built reference and counter electrodes on a planar substrate, ultimately producing a notable commercial success, namely the multi-billion dollar glucose sensor (Albareda-Sirvent *et al.*, 2000). Any material that can be very simply printed with properties akin to or even better than EPPG should be very appealing.

Considering the rich history of carbon based materials in electrochemical sensing it is hardly surprising that graphene has become a focal point of electrochemical research over recent years. Graphene in its truest form represents a single, or few layers of carbon in an atomic scale honeycomb lattice (an unrolled carbon nanotube), as per the 2004 seminal experiments performed by Geim and Novoselov (Novoselov *et al.*, 2004). Even within the landscape of ongoing materials optimisation using numerous alternative processing routes (Berger *et al.*, 2004; Novoselov *et al.*, 2004; Li *et al.*, 2009; Peltekis *et al.*, 2012), the scientific community has revealed many advantageous properties for the emergent material, such as high thermal conductivity, mechanical strength and unique electronic properties (Novoselov, 2007). In contrast, the fundamental electrochemical properties of graphene are not deciphered to the same degree as its electronic properties. This is hardly surprising as the plethora of scientific literature on graphene electrochemistry actually revolves around solution miscible graphene derivatives that are easier to produce, such as graphene oxide (GO) (Dreyer *et al.*, 2010), which can be chemically (Alwarappan *et al.*, 2010; Zhou *et al.*, 2010), thermally (Kang *et al.*, 2009), or electrochemically (Wang *et al.*, 2009) reduced to generate structure and properties similar to pristine graphene. The reduced GO will inevitably still contain numerous defect sites, but in electrochemistry this can be very advantageous regarding heterogeneous electron transfer, which will mainly occur at edge-plane defect sites (Ratinac *et al.*, 2011). The solution miscible graphene derivatives are predominantly drop-cast onto underlying electrodes – in essence the graphene derivatives are acting in concert with the underlying electrode – producing summative electrochemical effects (Kang *et al.*, 2009; Wang *et al.*, 2009; Zhou *et al.*, 2010; Ratinac *et al.*, 2011).

Papers that use graphene as the standalone electrode have been published, but such studies are sparsely represented. One example showed that an epitaxial graphene electrode required significant anodisation to improve on poor initial electrochemical

behaviour towards the inner sphere redox couple potassium ferricyanide (Lim *et al.*, 2010). However, the redox electrochemistry of monolayer CVD graphene towards the outer sphere redox couple ferrocenemethanol was demonstrated to be ten-fold faster than basal plane pyrolytic graphite (Li *et al.*, 2011). A subsequent paper using monolayer CVD graphene as the electrode concluded that CVD graphene was akin to EPPG with regard to simple biological redox couples, while biological analytes that require surface oxygen species to act as adsorption mediators show poor electrochemistry compared to EPPG. The authors concluded that a pristine graphene electrode should be akin to BPPG electrodes, which lacks edge sites for superior electrochemistry and that graphitic islands within their layers may be responsible for the results (Brownson *et al.*, 2011a). In fact, the same group was even more conservative in a paper directed at a fundamental examination of graphene as an electrochemical sensing material. Here they concluded that flakes of pristine graphene monolayers deposited on an EPPG electrode block electron transfer from solution to the electrode and increase the peak to peak separation ( $\Delta E_p$ ) of the underlying EPPG electrode. In short, the conclusion was that the edge- to basal-plane ratio is critical, so a true monolayer of pristine graphene would possess a low concentration of edge-plane sites, exhibiting poor electrochemical behaviour in response to many analytes of interest (Brownson *et al.*, 2011b). The theoretical and experimental conjectures surrounding pristine graphene in a continuous layer seem reasonable and follow the accepted view that carbon materials with a basal-plane structure will have a low density of states and scarcity of surface adsorption sites for electron transfer from the solution phase, but the empirical results have been slightly better than one would expect, which could be due to the overall quality of the starting material.

Interestingly, the fabrication of laser irradiated reduced graphite oxide films as standalone electrodes were demonstrated as a route to fabrication of super-capacitors in 2011 (Gao *et al.*, 2011). This was followed by simplification of the laser source and generation of laser-scribed graphene (LSG) as a new member of the graphene family, which is produced by thermally reducing a film of graphite oxide at predefined positions using a LightScribe DVD burner (El-Kady *et al.*, 2012; Strong *et al.*, 2012). The laser-irradiated graphite oxide areas were very effectively reduced demonstrating a rapid expansion and exfoliation of the layers, producing a film with excellent conductivity, high porosity and providing a surface area of  $1520 \text{ m}^2 \text{ g}^{-1}$  (El-Kady *et al.*, 2012; Strong *et al.*, 2012). The rapid exfoliation and increase in surface area is indicative of the graphene layers existing as individual monolayers with limited restacking into graphitic sheets (Strong *et al.*, 2012). The

reduction process also drastically altered the films C/O ratio finishing with a carbon content of 96.5% and residual oxygen content of 3.5% (Gao *et al.*, 2011). Laser-scribed graphene has already demonstrated promise in super-capacitors (El-Kady *et al.*, 2012), gas sensors (Strong *et al.*, 2012) and more recently strain sensors (Tian *et al.*, 2014). The LSG gas sensor work also discusses the possibility that the LSG material should have a high degree of edge plane content, which would open up many avenues of research regarding electrochemical biosensors (Strong *et al.*, 2012).

The current work validates previous physiochemical characterisation of laser-scribed graphene and performs an in-depth study of the utility of laser-scribed graphene as an electrochemical transducer. The LSG fabrication method allows the facile production of scalable and flexible electrochemical sensors whose electrodes are made exclusively of graphene with no underlying electrode material and no added composites. The study uses well-characterised inner- sphere and outer-sphere redox couples to probe the properties of LSG and benchmarks performance against various all-carbon electrodes, including EPPG, BPPG and monolayer CVD graphene (SLG). In the initial experiments 3 mm diameter LSG working electrodes were used in conjunction with macroscale external reference and counter electrodes. However, in the final experiments the LSG fabrication process was used to produce a planar three electrode system consisting of an all-graphene working electrode, counter electrode and a graphene base for the simple Ag/AgCl pseudo-reference electrode. The whole process was accomplished without the requirement of lithographic masks or photoresist.

## **2.2 Experimental**

### **2.2.1 Materials**

Chemicals were purchased from Sigma-Aldrich and were analytical grade unless otherwise stated. Potassium ferricyanide and 1,1'-ferrocene dimethanol were used as inner- and outer-sphere redox probes at 1 mM in 1 M potassium chloride as supporting electrolyte.

Graphene oxide was prepared using a modified Hummers' method (Hummers and Offeman, 1958; Tung *et al.*, 2009) beginning with graphite from Bay Carbon, Inc. Polyethylene terephthalate (PET, Niceday Guilbert) was used as a flexible substrate for GO and was attached to a Lightscribe DVD using SprayMount (RS Components, Northants). The HP lightscribe DVD RW drive was used with Lightscribe software for

designing the laser-scribe patterns of the electrodes. Silver paint, conductive copper tape and Kapton<sup>®</sup> tape were purchased from RS components (Northants). Platinum foil 99.99% trace metals basis (Sigma Aldrich) was purchased for use as a counter electrode. The Ag/AgCl reference electrode was from BASi (Indiana, USA). EPPG and BPPG electrodes (3 mm diameter) from IJ Cambria Scientific Ltd were used for comparison purposes as was CVD 1 cm<sup>2</sup> single layer graphene on 285 nm silicon dioxide/silicon (p-doped) (Graphene Supermarket).

### **2.2.2 Manufacture of Laser-scribed Graphene**

The GO suspension was diluted in deionized water (dH<sub>2</sub>O), 1.5 g of GO suspension was added to 20 ml dH<sub>2</sub>O and sonicated at 55 °C for 90 min. The suspension was then drop-cast onto a PET covered Lightscribe enabled DVD and allowed to dry overnight on a level surface. Once dry, the disc was placed label and GO side down into a Lightscribe enabled disc drive and the GO was laser reduced to the desired pattern. Each laser irradiation cycle takes approximately 20 minutes to complete dependent upon design required. The laser scribing procedure was repeated ten times in order to ensure maximum reduction of the GO, optimal expansion and increased conductivity. It has previously been shown that the level of laser reduction can be tuned for electrical conductivity over five orders of magnitude using one, two, or three reduction steps and the grey scale power settings, eventually saturating the attainable conductivity (Strong *et al.*, 2012). The number of cycles chosen reflects our wish to saturate the reduction process, but it is possible that fine tuning the oxygen content may be appropriate for specific electrochemical analysis. The LSG was then removed from the disc on the flexible substrate and cut into individual electrodes. It is worthy of note that the resolution of the LightScribe 780 nm laser is 20 microns (El-Kady and Kaner, 2013).

### **2.2.3 Laser-scribed Graphene Characterisation**

Environmental scanning electron microscopy was performed to visualise changes from GO to LSG following laser reduction. An FEI-Philips XL30 ESEM was used to image the surface of GO and LSG. The GO and LSG films were carefully separated from the acetate substrate prior to imaging in order to reduce any charging effects.

XPS analysis of the GO and LSG was performed by NEXUS at nanoLAB (Newcastle University). Full spectrum surveys were performed as well as high resolution analysis of the C<sub>1s</sub> and O<sub>1s</sub> peaks at 284 eV and 532 eV, respectively. Measurements were taken at five positions across the surface of the films. Peak fitting was performed using Casa XPS

in order to determine bonding configurations and carbon : oxygen changes due to the reduction by laser irradiation.

The Raman spectra were performed using a Horiba Jobin Yvon HR800 Raman spectrometer with a 532 nm excitation laser.

#### **2.2.4 Laser-scribed Graphene Electrodes**

The LSG standalone electrodes were initially prepared using a disc of GO that had been entirely laser-scribed to form a continuous surface of LSG. This sheet of LSG could then be cut to size and prepared for use as an electrode. Conductive silver paint was used in order to contact the LSG to copper tape. Contact lines of silver paint were drawn around a 1 cm<sup>2</sup> piece of LSG, to one edge a strip of copper foil was attached to allow contact for electrochemical measurement. The electrode was then passivated using Kapton<sup>®</sup> tape, leaving only a 3 mm diameter LSG surface available for electrochemical activity. A similar method was used with the 1 cm<sup>2</sup> single layer graphene (SLG) to create a SLG electrode of 3 mm diameter for comparison.

The disposable three electrode system, including tracking for electrical connections, was produced by specifically patterning LSG on a GO covered disc by laser irradiation. The LSG working electrode was standardised to an area of 7.1 mm<sup>2</sup> for easy comparison to other electrodes unless otherwise stated. Once laser reduced, the three-electrode design was removed from the disc and cut to size. A copper tape contact was made to each electrode and a Ag/AgCl reference electrode was added by hand using silver paint. Chloride ions were available in the 1 M KCl supporting electrolyte. The tracking was passivated with Kapton<sup>®</sup> tape leaving only the silver reference, LSG working and counter electrodes exposed.

#### **2.2.5 Electrochemistry**

A three-electrode system was employed. A platinum counter electrode was created using platinum foil, copper tape and Kapton<sup>®</sup> tape to produce a platinum electrode surface of 2.5 cm<sup>2</sup>, and a standard Ag/AgCl reference electrode was used. Carbon based working electrodes were chosen for comparative work including EPPG, BPPG and SLG.

Measurements were performed with an Autolab electrochemical workstation (Ecochemie) and a general purpose electrochemical system. All electrochemistry was performed in 1 M potassium chloride supporting electrolyte. The cyclic voltammetry (CV) step potential was maintained at 1 mV in all experiments and a scan rate of 10 mV s<sup>-1</sup> was used except when directly investigating the effect of scan rate on LSG electrodes. For each CV

experiment, five CV scans were performed with the first being discarded to allow for equilibration at the electrode surface and therefore the mean of four scans was determined. Background scans in the 1 M KCl supporting electrolyte were also monitored and subtracted.

Experiments comparing the different types of working electrode were performed using 1,1'-ferrocene dimethanol and potassium ferricyanide. When using 1,1'-ferrocene dimethanol, the potential was cycled between 0.6 V and 0.0 V, while, using potassium ferricyanide, the potential was cycled between 0.6 V and -0.15 V. When investigating the effect of scan rate on the peak current and the  $\Delta E_p$ , CVs were performed at 10, 25, 50, 75 and 100 mV s<sup>-1</sup>.

## 2.3 Results and Discussion

### 2.3.1 *Physicochemical Characterisation of Laser-scribed Graphene Electrodes*

The LSG electrodes were fabricated at wafer level using the LightScribe DVD label writing technology and a GO film to produce individual LSG electrode devices. The LightScribe technology allows direct laser writing of DVD labels into user-defined designs utilising the same drive that writes the data. In short, the process is adopted so that the laser thermally reduces an insulating GO film at predefined positions programmed into the software, thus creating bespoke conducting LSG electrodes. A schematic of the process can be seen in Figure 2-1 in which a PET film allows flexible handling of the devices for ease of packaging. This one-step patterning process can be carried out in any lab with basic computer facilities and requires no masks for fabrication, or expensive lithography, which are required for screen-printed and microfabricated electrochemical sensors, respectively.

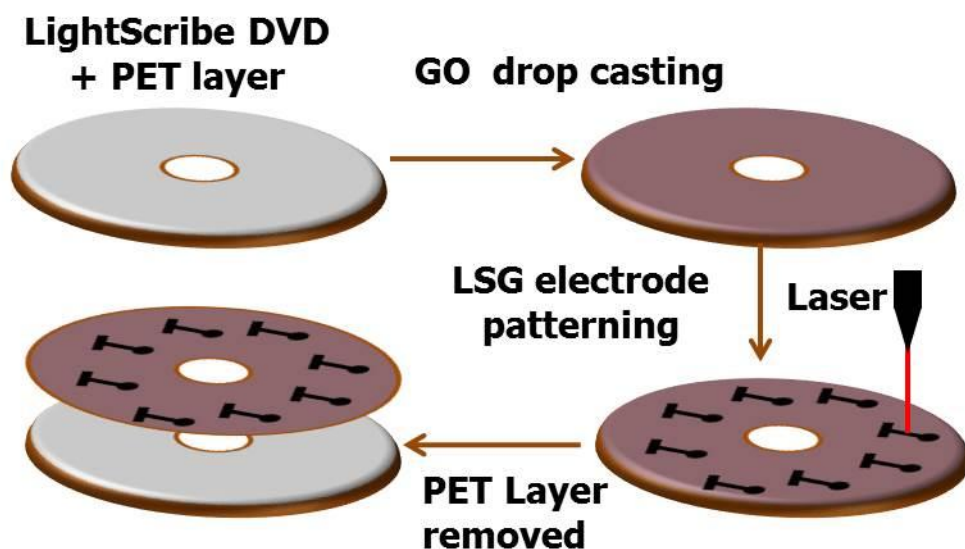


Figure 2-1 The process of patterning LSG electrodes on a flexible PET substrate

Scanning electron microscopy images of the LSG surfaces were in line with previous literature that states the stacked GO sheets undergo rapid thermal shock on laser ablation causing reduction, exfoliation and expansion of the film indicative of graphene sheets, which do not restack (El-Kady *et al.*, 2012; Strong *et al.*, 2012; Tian *et al.*, 2014). Figure 2-2 shows that the thermal reduction induces a large scale expansion on the LSG area as opposed to the original GO film. Across the samples the expanded LSG height was approximately 10  $\mu\text{m}$ , this is qualitative as the SEM images were tilted, but is in fair agreement with the previous literature at 7.6  $\mu\text{m}$  (El-Kady *et al.*, 2012). Cross-sections of the GO film and LSG material are clearly indicative of the chemical change from stacked graphitic sheets in the GO film to an unordered network structure with high edge plane content in the LSG film.

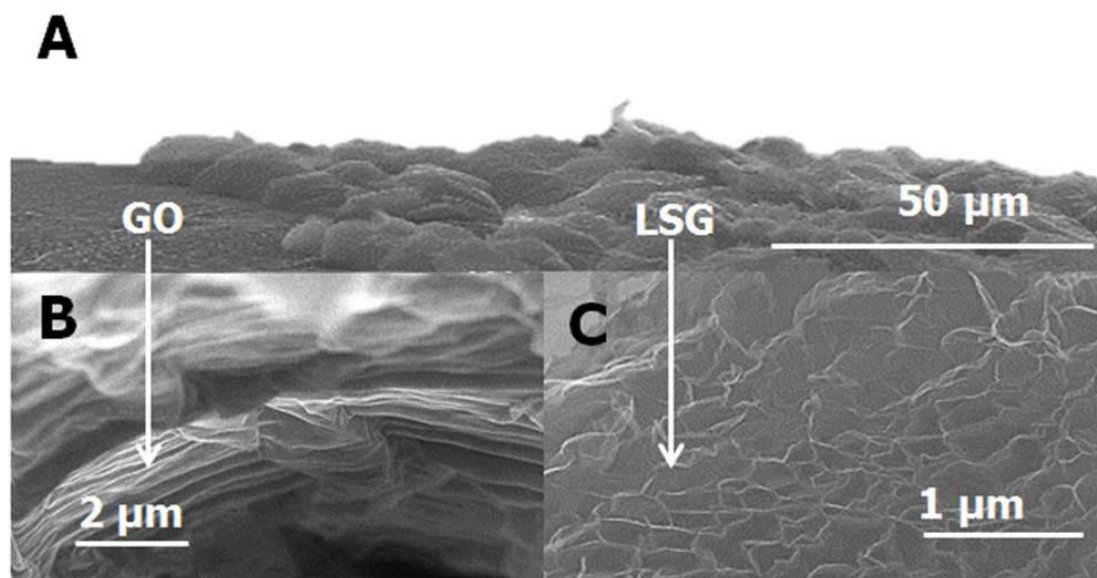


Figure 2-2 SEM images of GO and LSG.

Panel A shows the contrast between the initial GO film and the LSG area, which demonstrates the characteristic exfoliation of layers and increased surface area brought about by the laser-irradiation. Panel B shows a magnified image of the GO cross section clearly visualising stacked layers. Panel C shows a magnified image of a LSG cross section confirming the formation of a porous network structure with high edge plane content.

The sheet resistance of the GO film in this study was essentially insulating at  $13.6 \text{ M}\Omega \text{ sq}^{-1}$  while the laser reduction process produced LSG with a sheet resistance of  $589 \text{ }\Omega \text{ sq}^{-1}$ . This transformation into a conductor is in agreement with the earlier report by Strong *et al* (Strong *et al.*, 2012) which stated a sheet resistance value of  $80 \text{ }\Omega \text{ sq}^{-1}$  for LSG, significantly reduced from that of the GO film at more than  $20 \text{ M}\Omega \text{ sq}^{-1}$ . Raman spectroscopy of the layers in a previous study by the Kaner group detailed the effectiveness of the process in controllably producing few layer laser-scribed graphene with high edge plane content (Strong *et al.*, 2012). In our study, the oxygen/carbon ratio was used as a quality control method to ensure the reduction process was effective and X-ray photoelectron spectroscopy (XPS) analysis was performed to this end. Figure 2-3 shows both a decrease in and shift of the O1s peak when GO is reduced to LSG, signifying a loss of oxygen during the reduction process. The C1s peak also confirms a decrease in oxygen content as shown in image B which demonstrates the change from a double peak at the C1s location for GO to a prominent single peak following reduction to LSG. This variation in peak arrangement supports evidence of an alteration in bond configuration, which can be seen further detailed in image C. In the case of GO the ratio of carbon-oxygen to carbon-carbon bonds is greater than in the case of LSG where the largest peak is clearly  $\text{sp}^2$  bonded carbons, with considerably lowered carbon-oxygen

bonds. In the case of LSG there is also a small peak at 293 eV attributable to the  $sp^2$  bonded carbon ring structure. This XPS data indicates that the oxygen content is reduced from 42.4% in the GO film to 6.5% in the LSG film immediately after the thermal reduction process, thus confirming the effective reduction of oxygen and a return to the  $sp^2$  bonded carbon structure across the basal plane of the individual few layer graphene sheets. This level of oxygen content is known to be advantageous for numerous electrochemical redox reactions that are termed inner sphere, due to their reliance on surface species such as oxygen derived functional groups to aid electron transfer at the electrode surface (McCreery and McDermott, 2012).

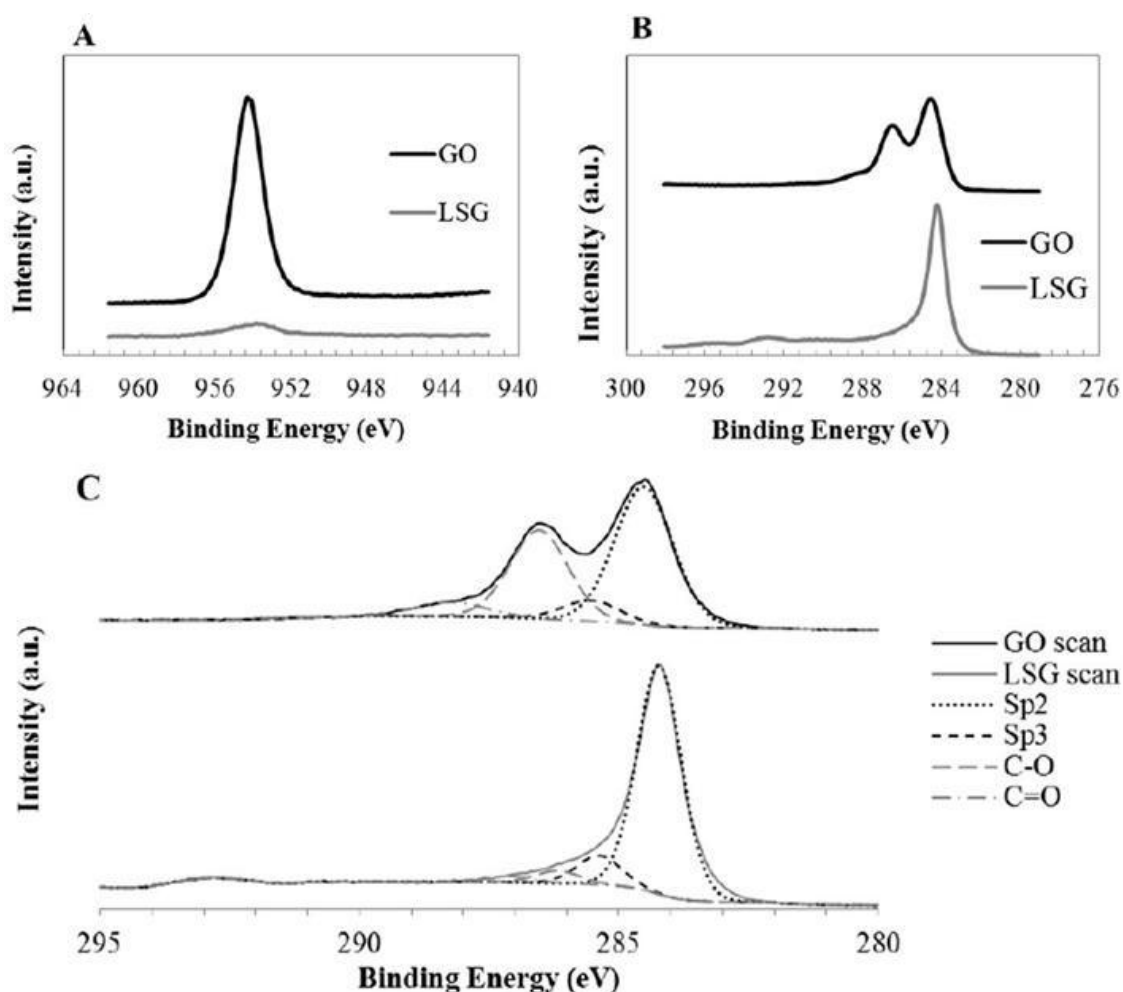


Figure 2-3 X-ray photoelectron spectroscopy data for GO and LSG. Panel A shows the high resolution O1s peak, panel B the C1s peak and panel C the peak fitting to the C1s peak.

Ultimately, the prevalence of edge plane content within LSG electrodes should compare favourably with existing state-of-the-art carbon electrodes whilst offering the advantage of scalable cost effective manufacture. To evaluate this hypothesis, both inner and outer

sphere redox reactions were analysed using single LSG working electrodes in conjunction with external reference and counter electrodes. The electrochemical performance was compared with established carbon electrodes and single layer graphene (SLG).

### 2.3.2 Electrochemical Sensing of Inner- and Outer-sphere Redox Probes Using LSG Electrodes

Cyclic voltammetry was used for electrode characterisation, CV potential forward and reverse scans were performed with respect to a standard Ag/AgCl reference electrode and platinum counter electrode unless otherwise stated. A photograph of the LSG electrode set-up can be seen in Figure 2-4. Image A is a schematic of the LSG working electrode, while B is a photograph of all the electrodes required in the setup. In B, the working LSG electrode is centre, the macroscale platinum counter electrode on the left and the standard Silver/silver chloride reference electrode on the right are easily connected to a standard laboratory potentiostat via crocodile clips and immersed in the solution under test.

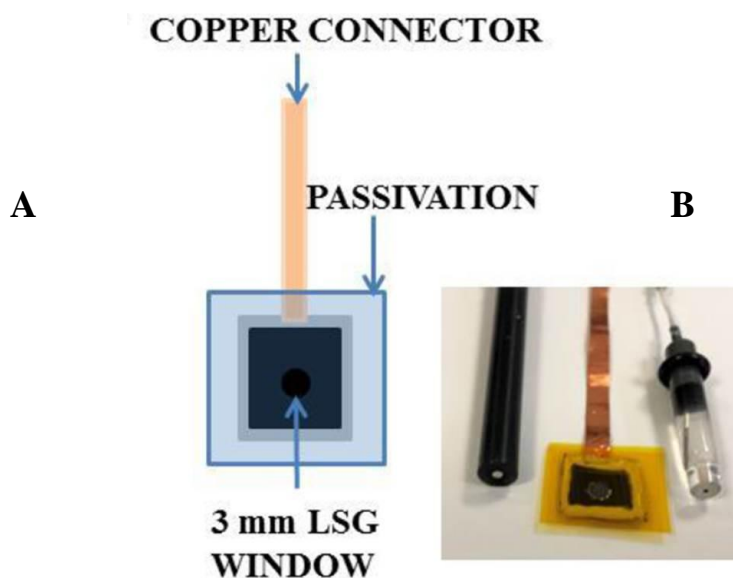


Figure 2-4 Diagram and photograph of an LSG working electrode  
The LSG working electrode requires no underlying electrodes or composites and is connected to a potentiostat via conductive silver paint and copper tape, with Kapton<sup>®</sup> tape passivation to create a 3 mm diameter electrode.

A range of carbon-based electrodes were selected for comparison with LSG electrodes and the diameter of the working electrode standardised at 3 mm. EPPG was chosen as the gold standard comparator, as it has good heterogeneous electron transport rates as a consequence of its high proportion of edge plane sites (Randviir *et al.*, 2012). BPPG was selected as a comparator due to the multitude of examples in the literature that

demonstrate reduced electrode performance due to its lack of oxygen defects and edge plane sites as compared to EPPG (Strong *et al.*, 2012). Finally, SLG electrodes were investigated to assess the benefits of using the network structure of LSG over the pristine single layer graphene structure. First, CVs were performed in 1,1'-ferrocene dimethanol, an outer-sphere redox species, insensitive to surface oxides. The response was thus solely dependent upon density of states (DOS). Second, experiments were conducted in potassium ferricyanide, an inner-sphere redox species that is known to be sensitive to surface oxides (McCreery and McDermott, 2012).

In 1,1'-ferrocene dimethanol, the BPPG electrodes demonstrated the lowest peak potentials and LSG produced the greatest peak currents of all the electrodes tested, as seen in Figure 2-5.

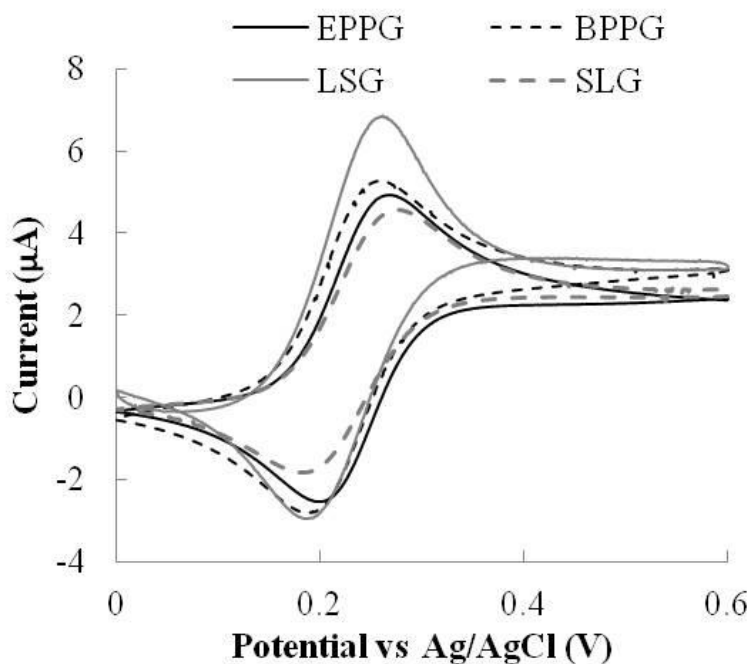


Figure 2-5 Cyclic voltammograms of four carbon electrodes in 1,1'-ferrocene dimethanol Redox mediator in 1 M KCl supporting electrolyte and performed at a scan rate of  $10 \text{ mV s}^{-1}$  with unmodified 3 mm diameter EPPG, BPPG, LSG and SLG electrode surfaces.

Table 2-1 details the comparative electrochemical parameters taken from the scans. The peak separation for the LSG, EPPG and the BPPG remained close to the 59 mV theoretical ideal for a one electron transfer process, with a  $\Delta E_p$  of 54 mV, 58 mV and 59 mV, respectively. The SLG performance was poor in comparison to the pyrolytic graphite and LSG in terms of peak current response. In addition, the  $\Delta E_p$  of SLG was also inferior with a peak separation of 79 mV, which is suggestive of a much slower electron transfer

rate. Interestingly, previous reports have commented on the presence of graphitic islands in commercially available graphene samples providing better than expected SLG electrochemistry (Brownson *et al.*, 2011a), whereas our SLG samples appear to be very high quality, as detailed in Raman spectra found in Figure 2-6. Raman spectroscopy is a commonly employed technique to characterise graphene (Ferrari *et al.*, 2006; Malard *et al.*, 2009; Ferrari and Basko, 2013) as it provides vital information relating to the quality of the material (defects) and the number of layers present. The Raman spectrum in Figure 2-6 is characteristic of single layer CVD graphene situated on a 285 nm SiO<sub>2</sub>/Si (p-doped) substrate. It can be clearly observed that the three main characteristic peaks of graphene are present; the D peak (1350 cm<sup>-1</sup>), the G peak (1580 cm<sup>-1</sup>) and the 2D peak (2680 cm<sup>-1</sup>). The ratio of the 2D peak to the G peak alongside the symmetric nature of the 2D peak confirms that the graphene is single layer. Whereas the small intensity of the D peak in comparison to the G peak indicates the graphene is of high quality containing only a small number of defects. The D peak intensity has been reported to increase with the number of defects within the graphene material (Banhart *et al.*, 2011; Cançado *et al.*, 2011).

Table 2-1  $\Delta E_p$  values for selected electrode materials

Electrode material <sup>a</sup>	$\Delta E_p$ /mV in 1,1'-ferrocene dimethanol	$\Delta E_p$ /mV in potassium ferricyanide
EPPG	58	85
BPPG	59	176
SLG	79	NA <sup>b</sup>
LSG average ( $n = 4$ )	54	59
RSD	5.5%	5.1%

<sup>a</sup> Two redox species were investigated, 1,1'-ferrocene dimethanol and potassium ferricyanide. Results of four LSG electrodes are presented to confirm reproducibility of the  $\Delta E_p$  with this new material. <sup>b</sup> SLG did not demonstrate a reversible redox reaction with potassium ferricyanide and so a  $\Delta E_p$  could not be determined.

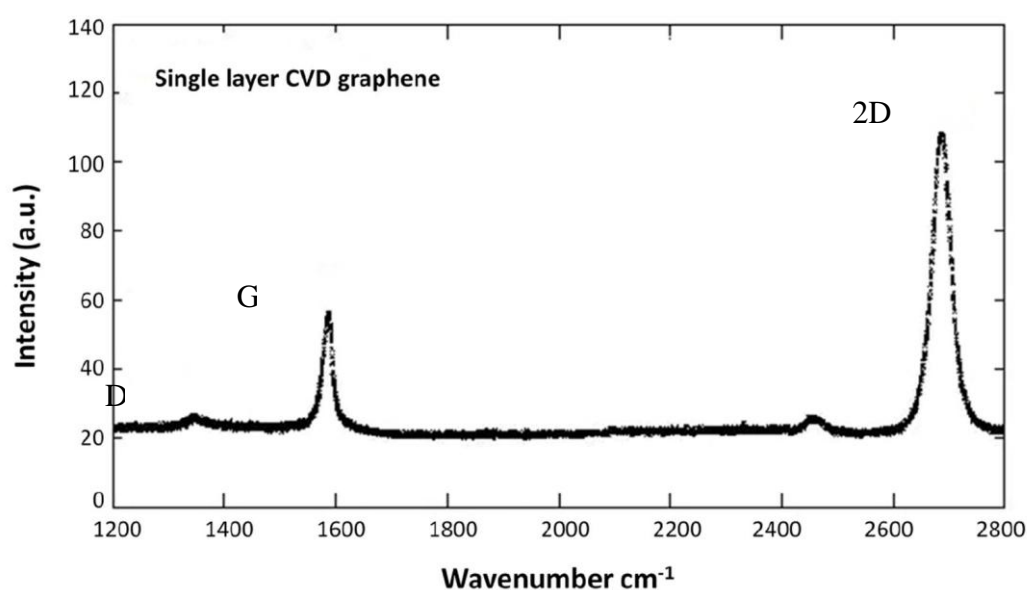


Figure 2-6 Raman spectra of CVD SLG

Figure 2-7 shows the various electrochemical responses for the inner-sphere redox probe potassium ferricyanide. Interestingly, the SLG provides an extremely poor electrochemical response; it presents lower peak currents than LSG, EPPG and BPPG, while the peak separation is essentially irreversible in the window measured, which is indicative of a very slow heterogeneous electron transfer rate. However, this is hardly surprising considering the theoretical structure of pristine graphene with its low edge and oxygen content, which is far from ideal for an inner-sphere redox probe electron transfer rate. Our results are in

line with Brownson *et al.*, who demonstrated that higher quality SLG electrodes have a very poor electrochemical response towards inner-sphere redox probes, with a quoted  $\Delta E_p$  of 1242.7 mV (at 100 mV s<sup>-1</sup>) (Brownson *et al.*, 2014). The clear trend is that SLG performed poorly and is at best analogous to BPPG. In contrast, the LSG electrode demonstrates high current densities, low overpotentials and the smallest peak separation with a  $\Delta E_p$  of only 59 mV compared with the 85 mV of EPPG and 176 mV for BPPG. This clearly demonstrates the superior electrochemical response of LSG even compared with EPPG, the gold standard of carbon electrodes, likely due to an optimal O/C content and accessibility to many edge sites at the electrodes surface. The inner sphere redox probe clearly shows the difference in electrochemical performance of EPPG and BPPG, where the  $\Delta E_p$  of the BPPG (176 mV) is now more than double that of the EPPG (85 mV) with severely decreased peak current responses due to its basal plane configuration.

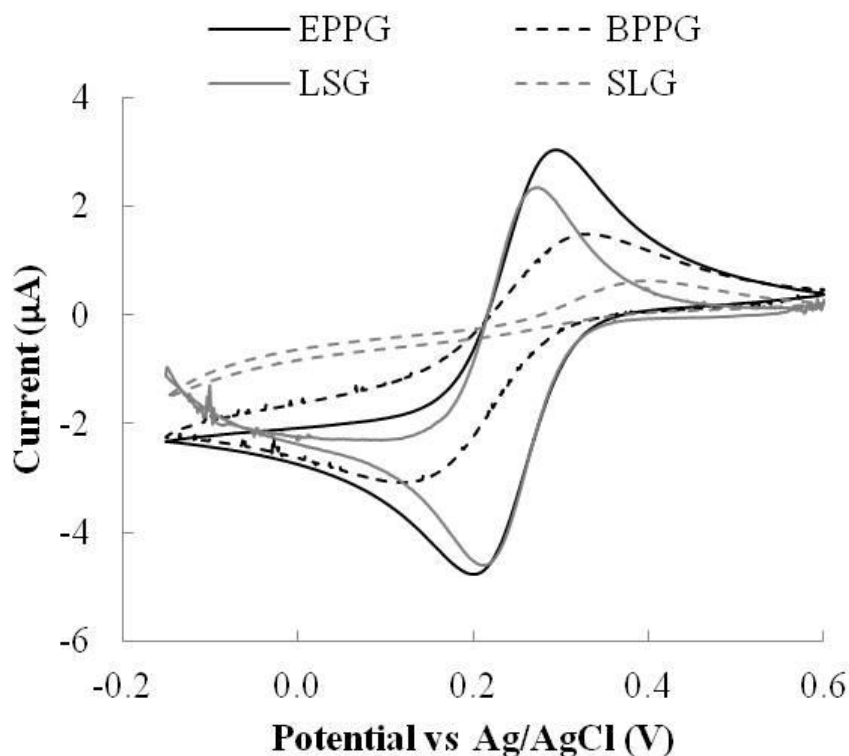


Figure 2-7 Cyclic voltammograms of four carbon based electrodes in potassium ferricyanide. Scans performed in 1 M KCl supporting electrolyte at a scan rate of 10 mV s<sup>-1</sup> at unmodified 3 mm diameter EPPG, BPPG, LSG and SLG electrode surfaces.

These data clearly establish that the LSG electrodes perform better/on par with EPPG for inner-sphere and outer-sphere redox probes. The performance is noteworthy as the LSG electrode is not a composite, unlike the vast proportion of the reduced graphite oxide (rGO) electrodes cited in the literature, which require an underlying electrode, such as

glassy carbon (Eissa *et al.*, 2013; Nguyen *et al.*, 2013; Oprea *et al.*, 2013; Radoi *et al.*, 2013; Song *et al.*, 2013; Wang *et al.*, 2013a; Wang *et al.*, 2013b). The results of the electrochemical studies of LSG along with the XPS analysis (Figure 2-3) suggest that the material offers an optimal balance of oxygenated edge defects. This allows efficient heterogeneous electron transfer, while maintaining a high level of electrical conductivity, resulting in a highly effective electrode.

Inter-reproducibility of the Laser-Scribe method of electrode manufacture was then assessed. Again, using the inner- and outer-sphere redox probes potassium ferricyanide and 1,1'-ferrocene dimethanol, the peak potential ( $E_p$ ) and peak current ( $i_p$ ) were determined for each of four electrodes. The results are presented in

Table 2-2. The relative standard deviation of the anodic and cathodic peak current response were generally good providing an acceptable level of reproducibility. The relative standard deviation of the  $E_p$  was of particular note as all values are well below 2% suggesting that the electrodes have huge potential for specific detection of redox species in voltammetric applications.

Next, the effect of scan rate on the behaviour of LSG electrodes was considered (Figure 2-8). Both the inner- and outer-sphere redox species discussed earlier were used and CVs were performed at scan rates varying from 10 to 100  $\text{mV s}^{-1}$ . The peak current responses were proportional to the square root of the scan rate in both, as shown in Figure 2-8 inset, suggesting a diffusion-controlled voltammetric response.

Table 2-2 Electrochemical parameters of four LSG electrodes

		$E_{pa}$ (V)	$i_{pa}$ ( $\mu$ A)	$E_{pc}$ (V)	$i_{pc}$ ( $\mu$ A)
<b>1,1'-Ferrocene dimethanol</b>	1	0.199	-4.634	0.256	6.523
	2	0.199	-4.576	0.253	5.890
	3	0.204	-5.293	0.254	7.650
	4	0.196	-4.785	0.251	6.223
	Average	0.200	-4.822	0.254	6.572
	RSD	1.7%	6.8%	0.8%	11.6%
<b>Potassium ferricyanide</b>	1	0.212	-4.100	0.274	3.720
	2	0.214	-3.703	0.270	3.959
	3	0.213	-3.602	0.269	3.401
	4	0.211	-3.887	0.271	3.828
	Average	0.213	-3.823	0.271	3.727
	RSD	0.6%	5.7%	0.8%	6.4%

<sup>a</sup> Ferrocene dimethanol and potassium ferricyanide were used as the redox probes. For inter-reproducibility purposes the mean, and percentage relative standard deviation (RSD) are shown for four LSG electrodes with each of the redox probes assessed to confirm reproducibility of electrochemical responses with this new material.

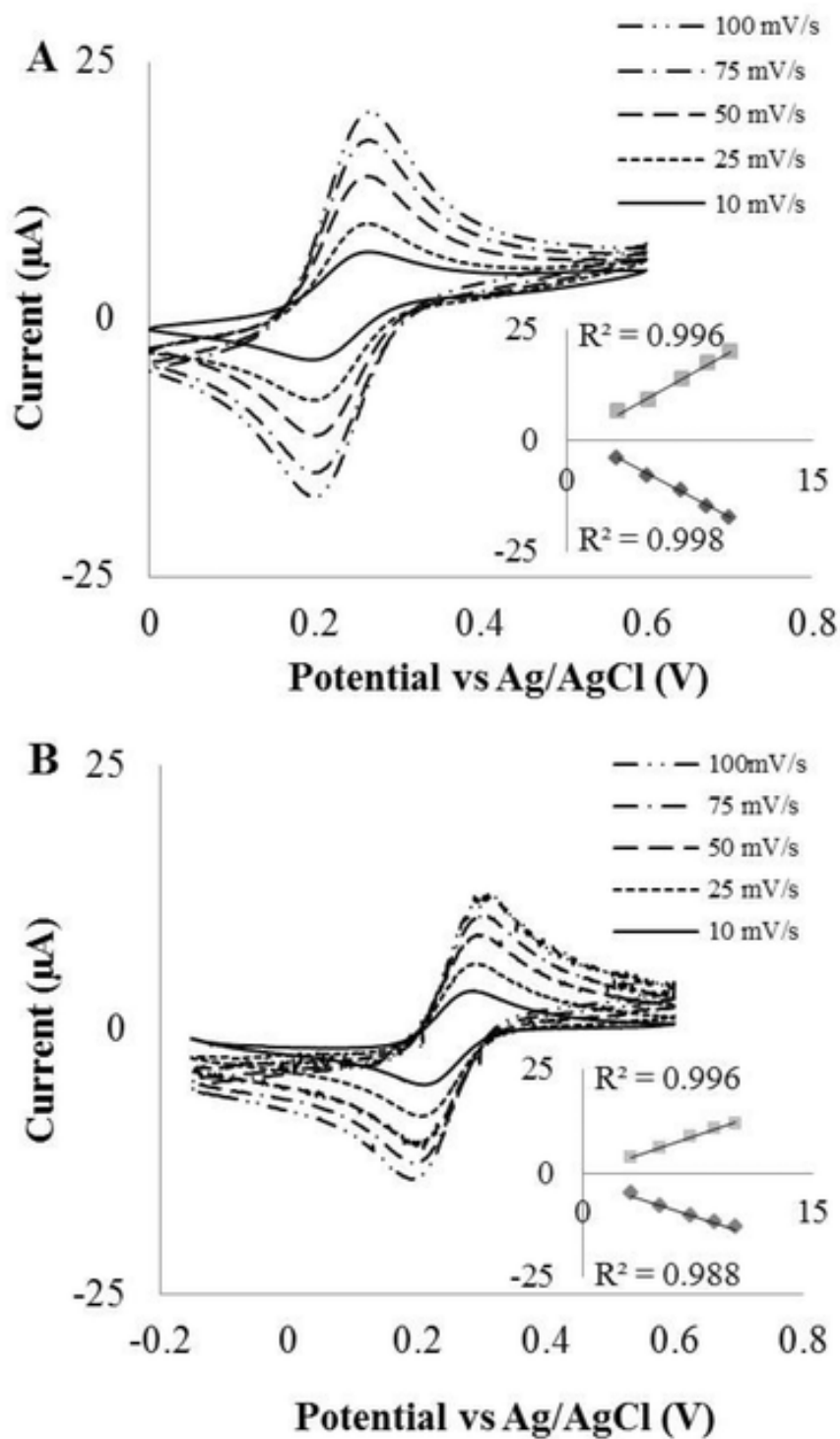


Figure 2-8 Effect of scan rate on peak current and peak potential for LSG electrodes in 1,1'-ferrocene dimethanol (A) and potassium ferricyanide (B). Inset shows that peak current is proportional to square root of scan rate. Scans were performed at 10, 25, 50, 75, 100  $\text{mV s}^{-1}$ .

However, the behaviour of peak separation varied between the two redox species. In 1,1'-ferrocene dimethanol the  $\Delta E_p$  remains close to the theoretical value even with an increased scan rate, but for the potassium ferricyanide the  $\Delta E_p$  widens with increasing

scan rate resulting in quasi-reversible behaviour. The rate constant is lowered due to the equilibrium at the surface being reached more slowly and therefore, an increase in scan rate causes a shift in peak potentials. The scans performed in potassium ferricyanide also demonstrate a quasi-reversible process with EPPG and BPPG (data not shown). Using these data the electrode reaction kinetics can be calculated utilising the Nicholson method (Nicholson, 1965). This allows a direct comparison of LSG with EPPG and BPPG under identical experimental conditions. In order to calculate an estimate of the heterogeneous electrochemical rate constant  $k^0$ , the dimensionless kinetic parameter  $\Psi$  was first determined from Equation 2-1 (Lavagnini *et al.*, 2004).

*Equation 2-1 Determination of  $\Psi$*

$$\Psi = (-0.6288 + 0.0021X)/(1 - 0.017 X)$$

Where  $X$  was equal to the  $\Delta E_p$  of the system multiplied by the number of electrons involved in the electrochemical reaction ( $n$ ), which in the case of the potassium ferricyanide reaction was equal to one. Following the calculation of  $\Psi$  the  $k^0$  could be determined using Equation 2-2 (Nicholson, 1965; Lavagnini *et al.*, 2004).

*Equation 2-2 The Nicholson equation*

$$\Psi = k^0[\pi D n \nu F / (RT)]^{-1/2}$$

Where  $D$  was the diffusion coefficient of the oxidation of the electroactive species,  $\nu$  is the scan rate in  $V s^{-1}$ ,  $F$  is the Faraday constant,  $R$  is the universal gas constant and  $T$  the absolute temperature. The diffusion coefficient was approximated to be  $5.4 \times 10^{-6} \text{ cm}^2 \text{ s}^{-1}$  for potassium ferricyanide, as used by Valota *et al.* in the investigation of electrochemical performance of monolayer and bi-layer graphene (Valota *et al.*, 2011). Thus, in 1 mM potassium ferricyanide the  $k^0$  of LSG was calculated as  $0.02373 \text{ cm s}^{-1}$ , demonstrating a favourable electron transfer rate when compared with EPPG at  $0.002601 \text{ cm s}^{-1}$  and at BPPG  $0.00033 \text{ cm s}^{-1}$ . The order of magnitude difference between the EPPG and BPPG is to be expected due to the availability of defect sites being significantly greater at the edge-plane than at the basal-plane of pyrolytic graphite. What is interesting is that the  $k^0$  of LSG is significantly increased compared with EPPG, further evidencing the practicality of this material for electrochemical biosensors. The results shown here are given further credence and show the same trend as a recent paper investigating Q-graphene and the beneficial effect it had on the electrochemical response of EPPG electrodes (Randviir *et al.*, 2012). The  $k^0$  of potassium ferrocyanide(II) on EPPG was shown to be  $0.00466 \text{ cm s}^{-1}$ , but it underwent a significant increase to  $0.0186 \text{ cm s}^{-1}$  when the

electrode was modified with Q graphene. The LSG is clearly showing strikingly similar advantages to the work carried out by Randviir *et al* (Randviir *et al.*, 2012) but our work is a standalone electrode with no additive effects and is clearly applicable to facile scalable mass production unlike previous work.

### 2.3.3 Electrochemical Evaluation of a Planar Three-electrode LSG System

In the initial characterisation study LSG electrodes were constructed as individual working electrodes, as shown in Figure 2-4, using conventional external reference and counter electrodes. The second aim of our study was to assess the possibility of not only having a stand-alone graphene electrode, but to incorporate that electrode into a fully disposable planar three-electrode system that requires no external reference, or counter electrode, as depicted in the schematic and photograph in Figure 2-9.

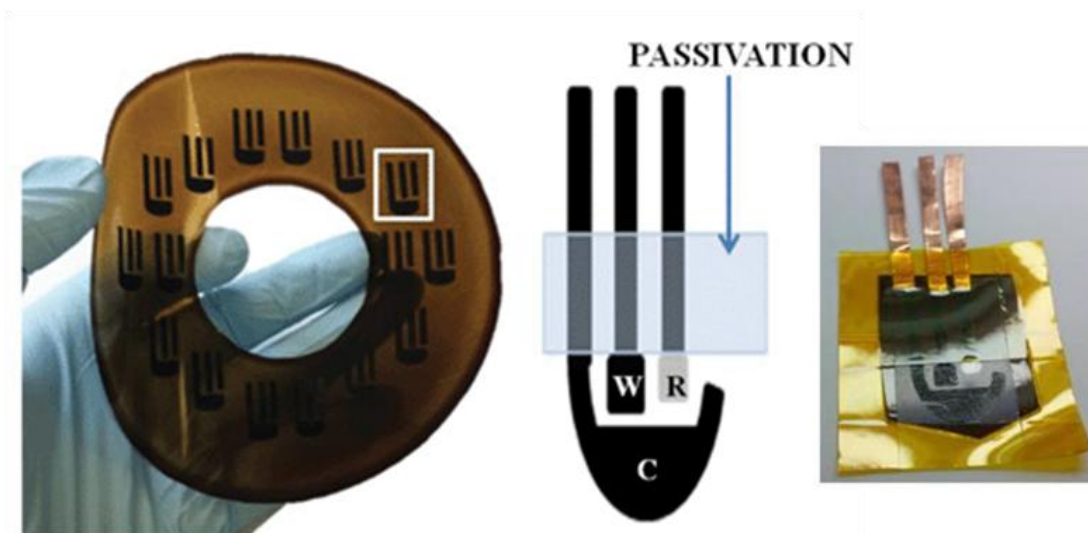


Figure 2-9 Patterned LSG planar three-electrode system

On the left is shown the basis of a planar three-electrode system for electrochemical analysis without the need for an external reference and counter electrode. The schematic to the centre shows the LSG working electrode (W), LSG counter electrode (C) and the reference electrode (R) which is silver adhesive paint manually applied to a LSG base. An example of the prototype device is shown on the right.

Effectively, this is wafer level production of a planar printed three-electrode system, akin to screen printing, or microfabrication of conventional materials such as carbon paste and gold, but updated to utilise mask-free generation of LSG. The GO, which undergoes no thermal patterning and modification, retains its insulating properties, so it can remain *in situ*. Silver was applied to the third electrode which acted as a Ag/AgCl pseudo-reference electrode and the larger LSG electrode was used as a counter electrode. In this work the silver paint was applied by hand and no masking steps were used, although there are many alternative routes, for example electroplating. Pseudo-reference electrodes are

often variable in their performance compared with a standard Ag/AgCl reference electrode, which contains a liquid double junction and inner solution saturated with KCl. However, our pseudo-reference electrode potential only varied from the standard reference electrode potential between 0.99 mV to -1.97 mV in 1,1'-ferrocene dimethanol and 0.60 mV to -4.59 mV in potassium ferricyanide (Data not shown). Hence the voltammetric responses recorded below remain at a similar potential for the pseudo-reference electrode as compared to the standard Ag/AgCl reference electrode and the differences are essentially within the experimental error.

The electrochemical performance of the LSG planar three-electrode system is shown in Figure 2-10 compared with EPPG (the EPPG has macroscale external reference and counter electrodes). It can be seen that when performing CVs in ferrocene dimethanol, the LSG planar three-electrode system performs comparably with the EPPG, the gold standard of carbon electrodes as discussed at length previously in this work. Interestingly, the LSG sensor demonstrates lower peak potentials suggesting that it may be useful in the detection of biological molecules since detection at lower potentials decreases the likelihood of electrochemical interference. Both electrode materials demonstrate a Nernstian response with  $\Delta E_p$  values of 57 mV and 58 mV for LSG and EPPG, respectively. Using the potassium ferricyanide redox probe, the LSG sensor is shown to have a  $\Delta E_p$  of 75 mV, which compares favourably with the 85 mV achieved with the EPPG. The potassium ferricyanide  $\Delta E_p$  value for the planar three electrode system is slightly altered from the external reference electrode system at 59 mV (Table 2-1), a possible explanation for this was investigated using a new batch of graphite oxide and two additional LSG processing runs. Representative potassium ferricyanide CV scans can be seen in Figure 2-11 generating a  $\Delta E_p$  value of 63 mV for the stand-alone LSG electrode and 61 mV for the planar three electrode LSG system, which is in excellent agreement with the original reproducibility data in Table 2-1. It would appear that a subtle change in the electrode processing, most plausibly the surface oxygen content, has marginally altered the electrode performance towards the inner sphere redox probe in Figure 2-10. This highlights the possibility of minor processing differences between batches, however, the effect is minimal, and indeed potassium ferricyanide is well known to be very sensitive to small changes in surface species (McCreery and McDermott, 2012), so the spread of results between batches, as well as within a batch is very small. It is worth noting that the LSG outperformed the EPPG regarding all potassium ferricyanide results.

Representative scans of 1,1'-ferrocene dimethanol can also be found in Figure 2-11 using the two additional processing runs. The  $\Delta E_p$  values of 54 mV and 60 mV were achieved with the stand-alone LSG electrode and the planar three electrode LSG system respectively, which compares well with the results shown in Table 2-1 for 1,1'-ferrocene dimethanol.

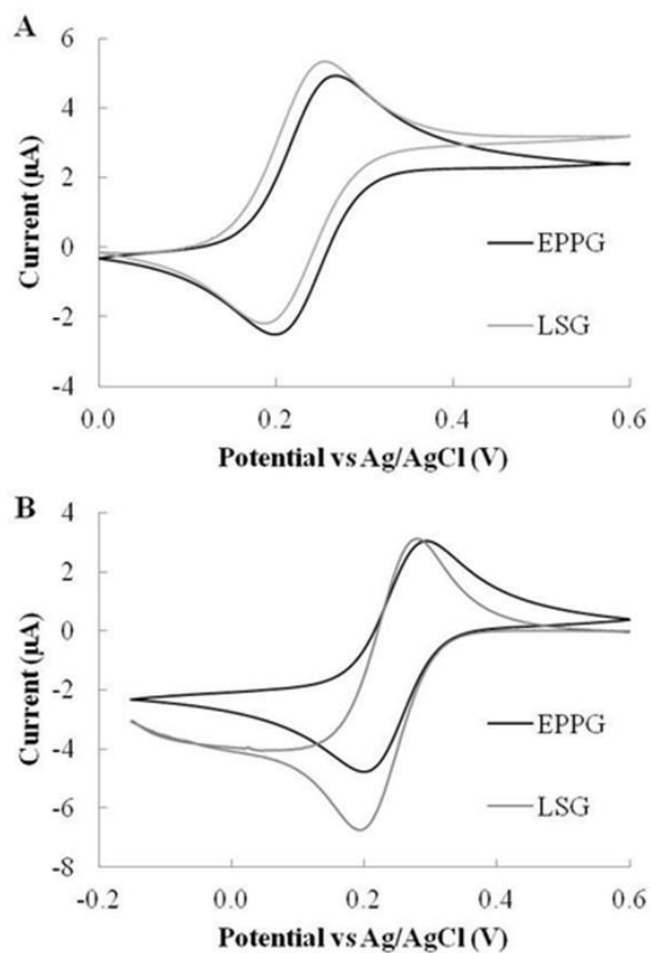


Figure 2-10 Comparing electrochemical performance of the disposable planar three electrode LSG system with EPPPG by CV

Panel A shows cyclic voltammograms of 1,1'-ferrocene dimethanol and panel B potassium ferricyanide at a scan rate of  $10 \text{ mV s}^{-1}$  at EPPG electrode surfaces compared to the disposable planar three electrode LSG system.

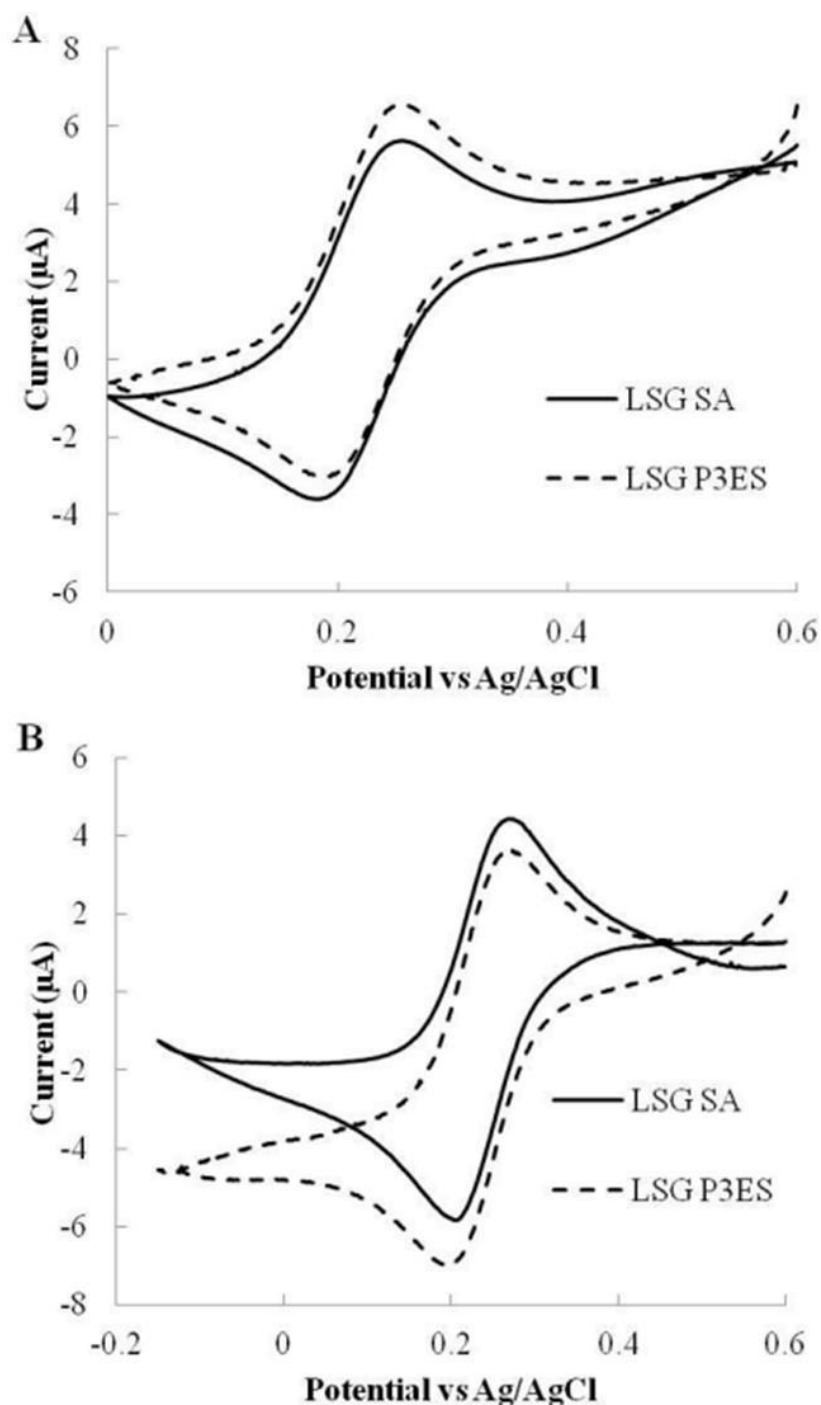


Figure 2-11 Comparing electrochemical performance of the disposable planar three electrode LSG system with the stand alone LSG working electrode by CV  
 Cyclic voltammograms of (A) 1,1'-ferrocene dimethanol and (B) potassium ferricyanide at a scan rate of  $10 \text{ mV s}^{-1}$ . The stand alone LSG electrodes (LSG SA) were made on a new, separate processing run from all other results in this work, using a new batch of GO. In a further additional processing run a new batch of planar three electrode LSG systems (P3ES) were made using the new batch of GO (the area of these electrodes has been normalised from  $4 \text{ mm}^2$  to  $7.1 \text{ mm}^2$  to match the area of stand alone electrodes). This brings the total number of processing runs discussed in this study to four separate wafer depositions and two separate batches of GO.

These data further demonstrate the reproducible nature of the LSG electrodes between processing runs as well as within a processing run (Table 2-1). Ultimately, the LSG three-electrode system is equivalent to, or arguably marginally outperforms, EPPG in terms of peak current response, peak potential and  $\Delta E_p$ . Most importantly, EPPG will always be a macroscale electrode cut from highly ordered pyrolytic graphite and require macroscale external reference and counter electrodes, which are not compatible with mass production. LSG on the other hand is clearly suitable for scalable, inexpensive mass production in a planar three-electrode configuration, which has seen great commercial success in the past using the classical techniques of screen printing and microfabrication. Parallel processing in microfabrication/screen printing would still be superior to a single DVD drive, where the processing, although producing multiple devices, could be thought of as serial in nature. However, due to the attributes of computer technology it is conceivable that a manufacturer could stack hundreds of DVD writers to fabricate LSG devices in a highly parallel manner.

## 2.4 Conclusions

The electrochemical behaviour of LSG has been methodically investigated as a stand-alone electrode by comparing it with highly relevant carbon alternatives, EPPG, BPPG and SLG. Interestingly, SLG performs very poorly with regard to the electrochemical response to both inner- and outer-sphere redox couples, which is in line with an observation made in a 2014 publication (Tian *et al.*, 2014) and also the theory regarding a defect-free basal-plane structure (McCreery and McDermott, 2012). This is important in its own right as graphene used in electrochemical sensing has been widely reported, but in most cases has only been successful as a composite. The graphene flakes seemingly improve the underlying electrodes due to the addition of favourable carbon architectures with a large number of edge plane sites and some degree of surface oxygenation (Randviir *et al.*, 2012). In this study we clearly show that the LSG electrode displays the optimal surface qualities for electrochemistry, in its own right without summative effects, as it compares favourably to the reference carbon electrode, EPPG, in terms of peak current response,  $\Delta E_p$  and heterogeneous electron transfer rates. This dovetails nicely with empirical evidence that the LSG material can be fabricated as a disposable sensor, in a planar three-electrode system, with no loss of performance. The LSG performance, inter-electrode reproducibility and amenability to a disposable format will open up many potential opportunities in the electrochemical bio-sensing arena and the authors are now investigating the material with respect to biological systems.

## 2.5 References

- Albareda-Sirvent, M., Merkoçi, A. and Alegret, S. (2000) 'Configurations used in the design of screen-printed enzymatic biosensors. A review', *Sensors and Actuators B: Chemical*, 69(1–2), pp. 153-163.
- Alwarappan, S., Liu, C., Kumar, A. and Li, C.-Z. (2010) 'Enzyme-Doped Graphene Nanosheets for Enhanced Glucose Biosensing', *The Journal of Physical Chemistry C*, 114(30), pp. 12920-12924.
- Banhart, F., Kotakoski, J. and Krasheninnikov, A.V. (2011) 'Structural Defects in Graphene', *American Chemical Society Nano*, 5(1), pp. 26-41.
- Banks, C.E. and Compton, R.G. (2005) 'Edge Plane Pyrolytic Graphite Electrodes in Electroanalysis: An Overview', *Analytical Sciences*, 21(11), pp. 1263-1268.
- Banks, C.E. and Compton, R.G. (2006) 'New electrodes for old: from carbon nanotubes to edge plane pyrolytic graphite', *Analyst*, 131(1), pp. 15-21.
- Berger, C., Song, Z., Li, T., Li, X., Ogbazghi, A.Y., Feng, R., Dai, Z., Marchenkov, A.N., Conrad, E.H., First, P.N. and de Heer, W.A. (2004) 'Ultrathin Epitaxial Graphite: 2D Electron Gas Properties and a Route toward Graphene-based Nanoelectronics', *The Journal of Physical Chemistry B*, 108(52), pp. 19912-19916.
- Brownson, D.A.C., Gomez-Mingot, M. and Banks, C.E. (2011a) 'CVD graphene electrochemistry: biologically relevant molecules', *Physical Chemistry Chemical Physics*, 13(45), pp. 20284-20288.
- Brownson, D.A.C., Munro, L.J., Kampouris, D.K. and Banks, C.E. (2011b) 'Electrochemistry of graphene: not such a beneficial electrode material?', *Royal Society of Chemistry Advances*, 1(6), pp. 978-988.
- Brownson, D.A.C., Varey, S.A., Hussain, F., Haigh, S.J. and Banks, C.E. (2014) 'Electrochemical properties of CVD grown pristine graphene: monolayer- vs. quasi-graphene', *Nanoscale*, 6(3), pp. 1607-1621.
- Cançado, L.G., Jorio, A., Ferreira, E.H.M., Stavale, F., Achete, C.A., Capaz, R.B., Moutinho, M.V.O., Lombardo, A., Kulmala, T.S. and Ferrari, A.C. (2011) 'Quantifying Defects in Graphene via Raman Spectroscopy at Different Excitation Energies', *Nano Letters*, 11(8), pp. 3190-3196.
- Dreyer, D.R., Park, S., Bielawski, C.W. and Ruoff, R.S. (2010) 'The chemistry of graphene oxide', *Chemical Society Reviews*, 39(1), pp. 228-240.
- Eissa, S., L'Hocine, L., Sijaj, M. and Zourob, M. (2013) 'A graphene-based label-free voltammetric immunosensor for sensitive detection of the egg allergen ovalbumin', *Analyst*, 138(15), pp. 4378-4384.
- El-Kady, M.F. and Kaner, R.B. (2013) 'Scalable fabrication of high-power graphene micro-supercapacitors for flexible and on-chip energy storage', *Nature Communications*, 4, p. 1475.
- El-Kady, M.F., Strong, V., Dubin, S. and Kaner, R.B. (2012) 'Laser Scribing of High-Performance and Flexible Graphene-Based Electrochemical Capacitors', *Science*, 335(6074), pp. 1326-1330.
- Ferrari, A.C. and Basko, D.M. (2013) 'Raman spectroscopy as a versatile tool for studying the properties of graphene', *Nature Nanotechnology*, 8(4), pp. 235-246.
- Ferrari, A.C., Meyer, J.C., Scardaci, V., Casiraghi, C., Lazzeri, M., Mauri, F., Piscanec, S., Jiang, D., Novoselov, K.S., Roth, S. and Geim, A.K. (2006) 'Raman Spectrum of Graphene and Graphene Layers', *Physical Review Letters*, 97(18), p. 187401.
- Gao, W., Singh, N., Song, L., Liu, Z., Reddy, A.L.M., Ci, L., Vajtai, R., Zhang, Q., Wei, B. and Ajayan, P.M. (2011) 'Direct laser writing of micro-supercapacitors on hydrated graphite oxide films', *Nature Nanotechnology*, 6(8), pp. 496-500.

- Griffiths, K., Dale, C., Hedley, J., Kowal, M.D., Kaner, R.B. and Keegan, N. (2014) 'Laser-scribed graphene presents an opportunity to print a new generation of disposable electrochemical sensors', *Nanoscale*, 6(22), pp. 13613-13622.
- Hummers, W.S. and Offeman, R.E. (1958) 'Preparation of Graphitic Oxide', *Journal of the American Chemical Society*, 80(6), pp. 1339-1339.
- Kang, X., Wang, J., Wu, H., Aksay, I.A., Liu, J. and Lin, Y. (2009) 'Glucose Oxidase-graphene-chitosan modified electrode for direct electrochemistry and glucose sensing', *Biosensors and Bioelectronics*, 25(4), pp. 901-905.
- Kulys, J. (1999) 'The carbon paste electrode encrusted with a microreactor as glucose biosensor', *Biosensors and Bioelectronics*, 14(5), pp. 473-479.
- Lavagnini, I., Antiochia, R. and Magno, F. (2004) 'An Extended Method for the Practical Evaluation of the Standard Rate Constant from Cyclic Voltammetric Data', *Electroanalysis*, 16(6), pp. 505-506.
- Li, W., Tan, C., Lowe, M.A., Abruña, H.D. and Ralph, D.C. (2011) 'Electrochemistry of Individual Monolayer Graphene Sheets', *American Chemical Society Nano*, 5(3), pp. 2264-2270.
- Li, X., Zhu, Y., Cai, W., Borysiak, M., Han, B., Chen, D., Piner, R.D., Colombo, L. and Ruoff, R.S. (2009) 'Transfer of Large-Area Graphene Films for High-Performance Transparent Conductive Electrodes', *Nano Letters*, 9(12), pp. 4359-4363.
- Lim, C.X., Hoh, H.Y., Ang, P.K. and Loh, K.P. (2010) 'Direct Voltammetric Detection of DNA and pH Sensing on Epitaxial Graphene: An Insight into the Role of Oxygenated Defects', *Analytical Chemistry*, 82(17), pp. 7387-7393.
- Malard, L.M., Pimenta, M.A., Dresselhaus, G. and Dresselhaus, M.S. (2009) 'Raman spectroscopy in graphene', *Physics Reports*, 473(5-6), pp. 51-87.
- McCreery, R.L. and McDermott, M.T. (2012) 'Comment on Electrochemical Kinetics at Ordered Graphite Electrodes', *Analytical Chemistry*, 84(5), pp. 2602-2605.
- Moore, R.R., Banks, C.E. and Compton, R.G. (2004) 'Basal Plane Pyrolytic Graphite Modified Electrodes: Comparison of Carbon Nanotubes and Graphite Powder as Electrocatalysts', *Analytical Chemistry*, 76(10), pp. 2677-2682.
- Musameh, M., Wang, J., Merkoci, A. and Lin, Y. (2002) 'Low-potential stable NADH detection at carbon-nanotube-modified glassy carbon electrodes', *Electrochemistry Communications*, 4(10), pp. 743-746.
- Nguyen, V., Tang, L. and Shim, J.-J. (2013) 'Electrochemical property of graphene oxide/polyaniline composite prepared by in situ interfacial polymerization', *Colloid and Polymer Science*, 291(9), pp. 2237-2243.
- Nicholson, R.S. (1965) 'Theory and Application of Cyclic Voltammetry for Measurement of Electrode Reaction Kinetics', *Analytical Chemistry*, 37(11), pp. 1351-1355.
- Novoselov, K. (2007) 'Graphene: Mind the gap', *Nature Materials*, 6(10), pp. 720-721.
- Novoselov, K.S., Geim, A.K., Morozov, S.V., Jiang, D., Zhang, Y., Dubonos, S.V., Grigorieva, I.V. and Firsov, A.A. (2004) 'Electric Field Effect in Atomically Thin Carbon Films', *Science*, 306(5696), pp. 666-669.
- O'Neill, R.D., Chang, S.-C., Lowry, J.P. and McNeil, C.J. (2004) 'Comparisons of platinum, gold, palladium and glassy carbon as electrode materials in the design of biosensors for glutamate', *Biosensors and Bioelectronics*, 19(11), pp. 1521-1528.

- Oprea, R., Peteu, S.F., Subramanian, P., Qi, W., Pichonat, E., Happy, H., Bayachou, M., Boukherroub, R. and Szunerits, S. (2013) 'Peroxynitrite activity of hemin-functionalized reduced graphene oxide', *Analyst*, 138(15), pp. 4345-4352.
- Peltekis, N., Kumar, S., McEvoy, N., Lee, K., Weidlich, A. and Duesberg, G.S. (2012) 'The effect of downstream plasma treatments on graphene surfaces', *Carbon*, 50(2), pp. 395-403.
- Pumera, M., Ambrosi, A., Bonanni, A., Chng, E.L.K. and Poh, H.L. (2010) 'Graphene for electrochemical sensing and biosensing', *Trends in Analytical Chemistry*, 29(9), pp. 954-965.
- Radoi, A., Obreja, A., Eremia, S.V., Bragaru, A., Dinescu, A. and Radu, G.-L. (2013) 'l-Lactic acid biosensor based on multi-layered graphene', *Journal of Applied Electrochemistry*, 43(10), pp. 985-994.
- Randviir, E.P., Brownson, D.A.C., Gomez-Mingot, M., Kampouris, D.K., Iniesta, J. and Banks, C.E. (2012) 'Electrochemistry of Q-Graphene', *Nanoscale*, 4(20), pp. 6470-6480.
- Ratinac, K.R., Yang, W., Gooding, J.J., Thordarson, P. and Braet, F. (2011) 'Graphene and Related Materials in Electrochemical Sensing', *Electroanalysis*, 23(4), pp. 803-826.
- Song, H., Ni, Y. and Kokot, S. (2013) 'A novel electrochemical biosensor based on the hemin-graphene nano-sheets and gold nano-particles hybrid film for the analysis of hydrogen peroxide', *Analytica Chimica Acta*, 788(0), pp. 24-31.
- Strong, V., Dubin, S., El-Kady, M.F., Lech, A., Wang, Y., Weiller, B.H. and Kaner, R.B. (2012) 'Patterning and Electronic Tuning of Laser Scribed Graphene for Flexible All-Carbon Devices', *American Chemical Society Nano*, 6(2), pp. 1395-1403.
- Tian, H., Shu, Y., Cui, Y.-L., Mi, W.-T., Yang, Y., Xie, D. and Ren, T.-L. (2014) 'Scalable fabrication of high-performance and flexible graphene strain sensors', *Nanoscale*, 6(2), pp. 699-705.
- Tung, V.C., Allen, M.J., Yang, Y. and Kaner, R.B. (2009) 'High-throughput solution processing of large-scale graphene', *Nature Nanotechnology*, 4(1), pp. 25-29.
- Valota, A.T., Kinloch, I.A., Novoselov, K.S., Casiraghi, C., Eckmann, A., Hill, E.W. and Dryfe, R.A.W. (2011) 'Electrochemical behavior of monolayer and bilayer graphene', *American Chemical Society Nano*, 5(11), pp. 8809-8815.
- Wang, H., Zhang, Y., Li, H., Du, B., Ma, H., Wu, D. and Wei, Q. (2013a) 'A silver-palladium alloy nanoparticle-based electrochemical biosensor for simultaneous detection of ractopamine, clenbuterol and salbutamol', *Biosensors and Bioelectronics*, 49(0), pp. 14-19.
- Wang, J. and Musameh, M. (2004) 'Carbon nanotube screen-printed electrochemical sensors', *Analyst*, 129(1), pp. 1-2.
- Wang, L., Lu, D., Yu, S., Shi, X., Wang, C. and Zhang, Y. (2013b) 'Voltammetric determination of alkannin using an Au nanoparticles-poly(diallyldimethylammonium chloride)-functionalized graphene nanocomposite film', *Journal of Applied Electrochemistry*, 43(8), pp. 855-863.
- Wang, Z., Zhou, X., Zhang, J., Boey, F. and Zhang, H. (2009) 'Direct Electrochemical Reduction of Single-Layer Graphene Oxide and Subsequent Functionalization with Glucose Oxidase', *The Journal of Physical Chemistry C*, 113(32), pp. 14071-14075.
- Zhou, K., Zhu, Y., Yang, X. and Li, C. (2010) 'Electrocatalytic Oxidation of Glucose by the Glucose Oxidase Immobilized in Graphene-Au-Nafion Biocomposite', *Electroanalysis*, 22(3), pp. 259-264.

## Chapter 3. Laser-induced Graphene as an Electrochemical Sensor

### 3.1 Introduction

Carbon materials have been used in electrochemical sensors for many years, they can provide a cost effective alternative to the likes of gold and platinum electrodes. They have been shown to confer advantages such as a wider electrochemical window and adsorption of molecules from solution onto the carbon electrode permitting electrocatalytic reactions that are weaker or absent on metal electrodes and biocompatibility, required for the move towards continuous monitoring and implantable sensors. There is a plethora of carbon materials described in the literature for electrochemical detection including pyrolytic graphite (Banks and Compton, 2005; Banks and Compton, 2006), boron doped diamond (Culková *et al.*, 2013), screen printed carbon electrodes (Chang *et al.*, 2002) and glassy carbon electrodes (GCE) (Díaz Toro *et al.*, 2015). Despite the overabundance of publications describing carbon materials as effective electrochemical sensors for clinical uses, it remains that few have been successfully commercialised due to lack of amenability to mass manufacture and miniaturisation. More recent advances in the field of nanomaterials including carbon nanotubes, graphene and reduced graphene oxide, have shown interesting improvements to electrochemical responses, in most cases these materials require an underlying electrode such as GCE (Keeley and Lyons, 2009; Salinas-Torres *et al.*, 2011; Kutluay and Aslanoglu, 2013; Lim *et al.*, 2014; Wang *et al.*, 2014), pyrolytic graphite (Randviir *et al.*, 2012) or are incorporated into screen printing ink/paste (Ping *et al.*, 2012; Gutierrez *et al.*, 2014). Recently it has also become increasingly acknowledged that many cases in which electrocatalytic behaviour has been attributed to electrode materials, can in fact be traced to changes in the electrode morphology (Punckt *et al.*, 2013; Barnes *et al.*, 2014). Barnes and Compton published a theoretical study on the voltammetric behaviour of porous electrodes in which simulated cyclic voltammograms showed that in an ideal porous electrode with low scan rates or small interconnected pores behaviour will become ultimately 'thin layer' with peak potential separation of 0 mV. In the case of fast scan rates or large pores the response becomes increasingly 'diffusional' (Barnes *et al.*, 2014). This behaviour can lead to more sensitive responses at reduced over-potentials and may even help in the case of simultaneous detection of analytes in a solution if their behaviour within the electrode pores and at the surface varies from one analyte to another. Aksay's group have also published a number of papers experimentally investigating the effect of porosity on graphene electrode performance. They have shown

that a combination of high C/O ratio and porosity have a real effect in decreasing the overpotential for the electrochemical oxidation of NADH, with electrode porosity having an 'amplifying' effect on the apparent electrocatalytic behaviour of porous graphene electrodes (Punckt *et al.*, 2010; Punckt *et al.*, 2013; Punckt *et al.*, 2014). One such paper looks at the common method of applying graphene particles onto a glassy carbon electrode. In similar experiments the graphene has often been attributed with amazing electrocatalytic properties and electrode porosity is neither controlled, nor considered, yet Aksay demonstrates that in the case of both reversible and quasi-reversible systems, diffusion from the bulk electrolyte into the porous electrode can be negligible whilst the 'thin-film' diffusion element becomes dominant. What may be even more interesting is that for irreversible redox reactions such as is the case for NADH, the peak potential can be significantly reduced when using porous electrodes (Punckt *et al.*, 2013). In a more recent paper, the group have demonstrated an ability to tune an electrode material via its pore size and volume, for the separation of redox peaks from interfering species (Punckt *et al.*, 2014).

Real progress in the field of electrochemical sensors requires the development of standalone electrodes that have the benefits offered by carbon nanomaterials and the morphological changes that come with them, but that can also be manufactured on a large scale. Such sensors also need to be suited to miniaturisation into a planar electrode configurations suitable for disposable point of care use. LSG has been shown to possess this capability in Chapter 2 (Griffiths *et al.*, 2014), here a second material with such potential has been identified. Laser-induced graphene (LIG) has recently been reported as a new material with excellent behaviour as a micro-supercapacitor by the Tour group at Rice University (Lin *et al.*, 2014). Sheets of insulating polyimide (Kapton<sup>®</sup>, Figure 3-1) were taken and following CO<sub>2</sub> laser irradiation were shown to have excellent electrical properties with a sheet resistance reduced from >90 M Ω sq<sup>-1</sup> for Kapton<sup>®</sup> to as low as 15 Ω sq<sup>-1</sup> for LIG (Lin *et al.*, 2014).

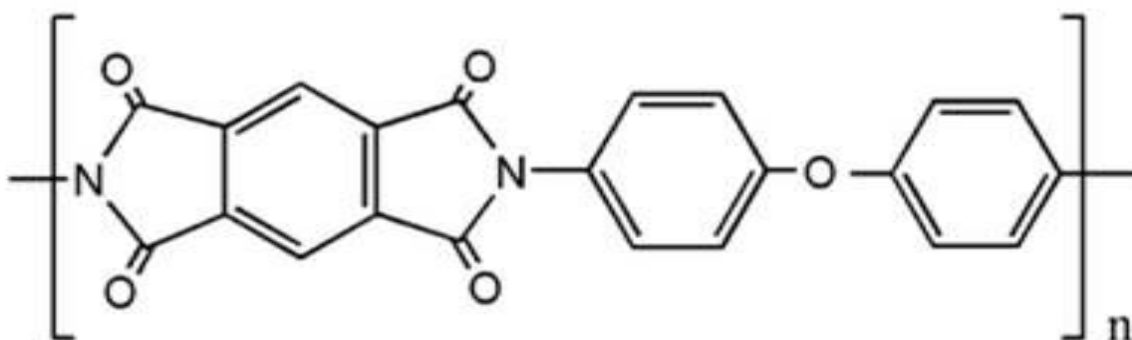


Figure 3-1 Structure of polyimide (Kapton®)

Further characterisation with Raman spectroscopy, X-ray diffraction, X-ray photoelectron spectroscopy, Fourier-transform infrared spectroscopy and scanning electron microscopy have confirmed this to be a graphene material with an expanded porous structure (Lin *et al.*, 2014). These features should confer excellent electrochemical activity due to an enhanced surface area available for electron transfer and a high edge/defect content to allow efficient electron shuttling of surface sensitive inner-sphere redox species. Previous studies have demonstrated the use of lasers to produce electrode materials from polymer films. Studies on polyimide began in the mid-1980s with the use of ultraviolet lasers for the etching of polyimide (Koren and Yeh, 1984; Brannon *et al.*, 1985; Dyer and Sidhu, 1985; Gorodetsky *et al.*, 1985; Srinivasan, 1986), by the early 1990s it was being reported that the use of ultraviolet lasers on polyimide could be used to create electrically conducting features (Srinivasan *et al.*, 1993) leading to further investigation as an electrode for sensing. In 1997 work was published on the use of ultraviolet lasers to induce carbonisation of polyimide films and their use as electrochemical devices, this material was compared with platinum and GCE for electrochemical response with potassium ferro/ferricyanide and shown to have slower electron transfer rates (Wynn and Fountain, 1997). By 2003 a laser carbonised polyimide humidity sensor was reported by the same group. Using an argon ion laser beam they had produced electrically conductive carbonised polyimide filaments (Ingram *et al.*, 2003) but use in electrochemical sensing appears to have been sidelined. The poor electrochemical performance of these carbonised polyimide materials produced via ultraviolet laser irradiation is a probable result of the material being more similar to glassy carbon or amorphous carbon as the UV laser power was insufficient to transform the polymer into a graphene like material consisting of increased  $sp^2$  carbon content. In the case of LIG, produced via  $CO_2$  laser ablation the material has been shown to have graphene like qualities as evidenced by Tours group (Lin

*et al.*, 2014). The more recent developments in the field of creating graphene like materials with lasers for use in supercapacitors (El-Kady *et al.*, 2012; Strong *et al.*, 2012; Lin *et al.*, 2014) has led several groups down the same route in the electrochemical characterisation of such materials and assessment of their use in disposable sensors. Following on from the publication of laser-scribed graphene as a printable disposable electrochemical sensor (Griffiths *et al.*, 2014), Tehrani has published evidence of the use of a 500 mW violet laser engraving machine (400-450 nm wavelength) to fabricate direct laser engraved graphene from Kapton<sup>®</sup> (Tehrani and Bavarian, 2016). Their material was shown to be both sensitive and selective for electrochemical detection of glucose when decorated with electrochemically deposited copper nanocubes. Another group, even more recently, have taken the same route as is described in this chapter, where they have built upon Tour's work of producing LIG from Kapton<sup>®</sup> (Lin *et al.*, 2014) and have electrochemically characterised the material (Nayak *et al.*, 2016). However, they report heterogeneous electron transfer rates in both inner- and outer-sphere redox mediators higher than the standard carbon based electrodes such as EPPG and BPPG and attribute this to the "binder free 3D porous network of LIG and enriched edge plane sites" (Nayak *et al.*, 2016). They fail to identify the full extent of the contribution of the porous 3D structure to the improved peak currents and reduced  $\Delta E_p$  observed in their CV analysis of the LIG which can be seen more clearly from the work described later in this chapter.

Thus the electrochemical characterisation performed in this study is truly novel and has produced some interesting findings. The reported porous graphene nature of LIG has been verified and the material further probed as an electrode for sensing purposes utilising the well characterised inner- and outer-sphere redox probes potassium ferricyanide and 1,1'-ferrocene dimethanol. The electrochemical performance of LIG was compared with EPPG, BPPG, GCE and LSG, adding to the earlier study which demonstrated LSG to be superior in electrochemical performance to pyrolytic graphite and monolayer graphene (Griffiths *et al.*, 2014) (Chapter 2).

## 3.2 Experimental

### 3.2.1 Materials

Unless otherwise stated all chemicals were of analytical grade and purchased from Sigma-Aldrich (Dorset). The polyimide (Kapton<sup>®</sup>) tape was sourced from RS components (Northants). Polyethylene terephthalate (PET, Niceday Guilbert) was used as a flexible support for Kapton<sup>®</sup> and attached to a glass microscope slide (Appleton Woods, Birmingham). Spraymount, conductive copper tape and adhesive silver paint used in creating laser-induced graphene (LIG) electrodes were sourced from RS components (Northants). A standard 1 M potassium chloride solution was used as supporting electrolyte unless otherwise stated and inner- and outer-sphere redox probes potassium ferricyanide and 1,1'-ferrocene dimethanol were prepared at a working concentration of 1 mM. The 40 W CO<sub>2</sub> laser instrument utilised was model LS6040PRO (HPC Laser LTD, West Yorkshire).

Electrochemical measurements were performed as described in Chapter 2 using an Autolab electrochemical workstation (Ecochemie) and general purpose electrochemical system software. Experiments were performed with a standard three electrode configuration with a Ag/AgCl reference electrode (BASi, Indiana, USA) and a platinum counter electrode (BASi, Indiana, USA), using a 3 mm diameter working electrode as specified.

For comparison purposes the LIG working electrodes were compared with carbon electrodes including EPPG, BPPG and GCE electrodes (3 mm diameter) from IJ Cambria Scientific Ltd and LSG electrodes prepared as described in Chapter 2 (Griffiths *et al.*, 2014) also of 3 mm diameter.

### 3.2.2 Manufacture of Laser-induced Graphene

Laser-induced graphene was prepared from Kapton<sup>®</sup>. First a layer of PET was attached to a glass microscope slide using spraymount followed by application of a layer of adhesive Kapton<sup>®</sup> tape. Electrode geometries were then scribed onto the Kapton<sup>®</sup> film utilising a CO<sub>2</sub> laser engraver at various power intensities from 12 W to 17 W were used to create samples of LIG from Kapton<sup>®</sup> by means of altering the 40 W power of the CO<sub>2</sub> laser from 30 % to 42.5 %.

### 3.2.3 Calculation of Sheet Resistance

This electrical transformation was measured as a change in sheet resistance using a four probe method which consisted of passing a current across a strip of material and

measuring the potential between two central points. The four probes were equidistant, with a film thickness less than 40 % of the spacing distance and the edges of the film equated to more than four times the spacing distance of the probes. This allowed the calculation of the sheet resistance in  $\Omega \text{ sq}^{-1}$  following Equation 3-1 developed by Smits (Smits, 1958).

*Equation 3-1 Sheet resistance calculation*

$$R_s = \frac{\pi}{(\log(n)^2)} \times \frac{V}{I} = 4.5324 \times \frac{V}{I}$$

### **3.2.4 Physicochemical Characterisation of Laser-induced Graphene**

The LIG was characterised with the use of SEM, XPS and Raman spectroscopy. Scanning electron microscopy was performed on a benchtop TM3030 (Hitachi High Technologies America, Inc). Elemental composition and bond configurations of Kapton<sup>®</sup> and LIG were compared with the use of XPS. Full survey scans and high resolution scans of C<sub>1s</sub> and O<sub>1s</sub> peaks at 284 eV and 532 eV were performed by NEXUS at NanoLab (Newcastle University) at three points across the material surface. Analysis of the XPS data was performed in CasaXPS software. Raman spectroscopy was performed with a Horiba Jobin Yvon HR800 at 532 nm excitation to analyse the resulting LIG material and to confirm its transition to a graphene like structure.

### **3.2.5 Electrochemical Characterisation**

Electrodes were prepared from LIG where 1 cm<sup>2</sup> LIG were first created with the use of a CO<sub>2</sub> laser on the Kapton<sup>®</sup> surface. The LIG was removed from the glass microscope slides along with the underlying PET layer. These squares were then manufactured into a useable electrode with the use of conductive silver paint, a copper tape connection and Kapton<sup>®</sup> tape as a passivation layer blocking all but a 3 mm diameter circular working area. This electrode design is similar to that for the LSG electrodes in Chapter 2 with the replacement of LSG with LIG. The LIG material was characterised electrochemically by CV with a standard three electrode electrochemical cell utilising a Ag/AgCl reference electrode and 3 mm diameter platinum counter electrode, the working electrode was varied to allow comparison of LIG with LSG, EPPG, BPPG and GCE as required, all of which had a 3 mm diameter. Scan rates were investigated between 10 and 200 mV s<sup>-1</sup> with a step potential of 1 mV, scan windows were dependent upon the redox species used, for potassium ferricyanide 0.6 V to -0.15 V and for 1,1'-ferrocene dimethanol 0.6 V to 0.0 V. In all cases the CV results shown are the average of three scans unless otherwise stated.

### 3.3 Results and Discussion

#### 3.3.1 Characterisation of Laser-induced Graphene

Laser induced graphene was prepared using a CO<sub>2</sub> laser to induce change in the Kapton<sup>®</sup>, forming an expanded porous graphene-like material (LIG). Such a method allowed the preparation of multiple electrodes on a flexible PET substrate held in place on a glass slide (Figure 3-2). The LIG and PET was then removed from the glass slide and cut into individual samples of 1 cm x 1 cm LIG and electrodes created with the use of silver paint to contact with copper tape connections. Kapton<sup>®</sup> tape was used to passivate all but the required 3 mm diameter LIG electrode area. The change in structure from Kapton<sup>®</sup> to LIG could be observed by eye, therefore structural changes were investigated in detail with the use of SEM (Figure 3-3). As found with LSG (Figure 2-2) the material undergoes a rapid expansion following laser irradiation more than doubling in height, resulting in an expanded porous structure, which has significant potential for electrochemistry due to the large surface area and high edge plane content of this material reported as LIG (Lin *et al.*, 2014; Peng *et al.*, 2015). The porous nature of LIG, unlike LSG, can be observed both at the surface and also in the cross-sectional images; with pore sizes in the region of 1-20 μm which appear to form an interconnecting porous network throughout the material. Laser-scribed graphene demonstrated a roughened surface, offering increased surface area, however pores were only visible within cross sectional views potentially limiting access for electrochemical reactions to occur (Figure 2-2).

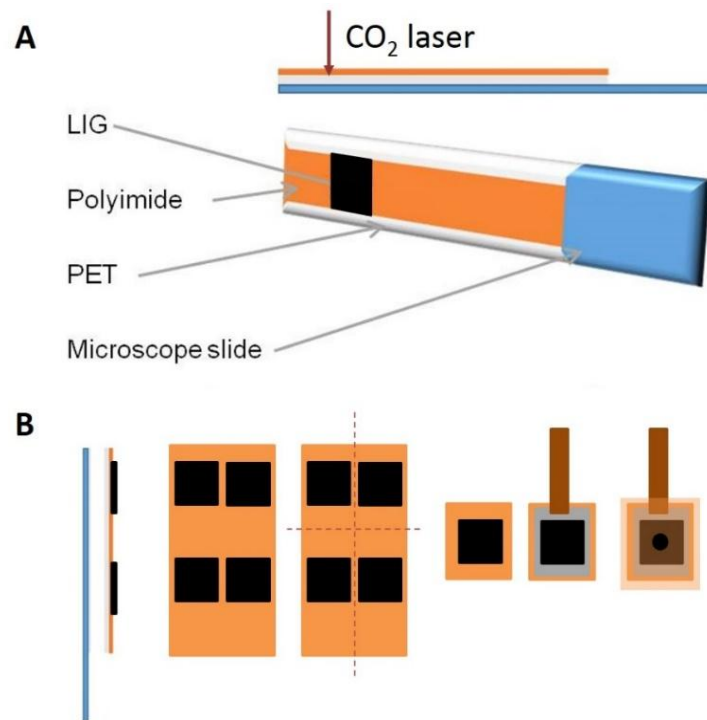


**Figure 3-2** Process of manufacturing LIG electrodes

A glass microscope slide was used to hold the PET substrate and Kapton<sup>®</sup> (Polyimide) during CO<sub>2</sub> laser ablation of Kapton<sup>®</sup> into LIG. The LIG on the PET substrate was then removed from the glass slide and cut into individual 1 cm<sup>2</sup> LIG electrodes. A 3 mm diameter working electrode was then created with the use of conductive silver paint and copper tape, using Kapton<sup>®</sup> tape to passivate all but a 3 mm diameter area of the LIG.

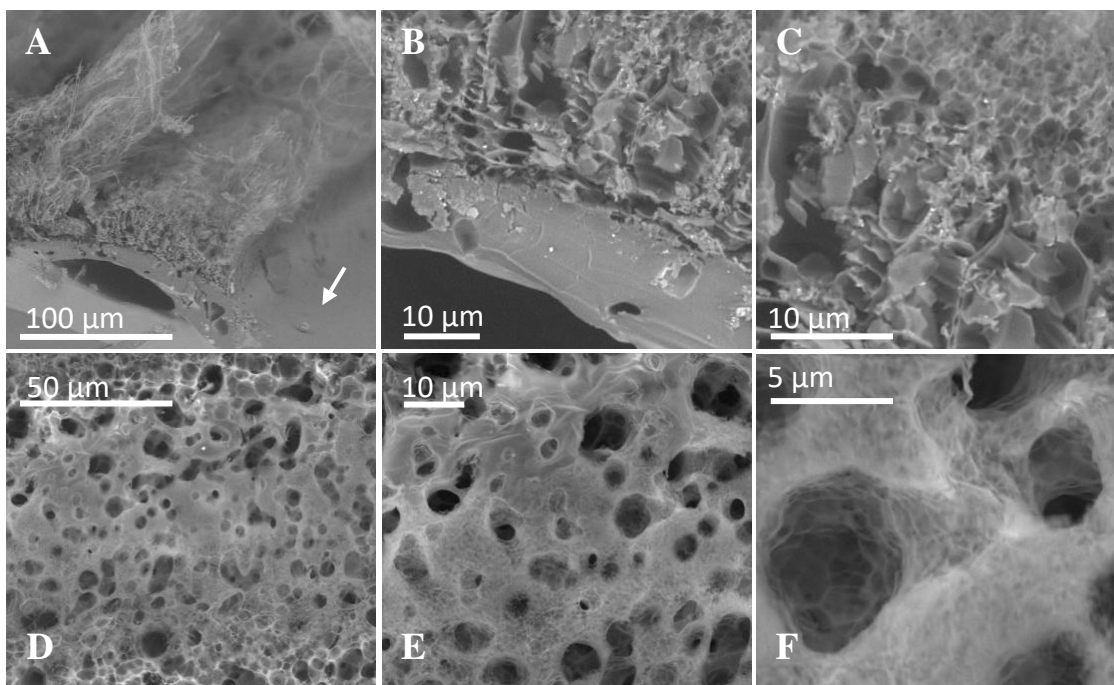


**Figure 3-3** Scanning electron microscope images of LIG cross-sections

(A-C) and top-views (D-F) demonstrating its porous nature as formed using 30% laser power. The arrow in (A) identifies an area of Kapton<sup>®</sup> that has not undergone CO<sub>2</sub> laser ablation to form LIG, showing the drastic transformation in structure.

Sheet resistance measurements were performed to confirm the change in state from a fully insulating Kapton<sup>®</sup> layer to a highly conductive LIG material and to confirm agreement with earlier work (Lin *et al.*, 2014). Sheet resistance was calculated using a four probe resistance measurement and found to be as low as  $23 \Omega \text{ sq}^{-1}$  for LIG, a measurement for Kapton<sup>®</sup> could not be performed due to its insulating properties. This result surpasses that of LSG at  $589 \Omega \text{ sq}^{-1}$  (Griffiths *et al.*, 2014) and is in good agreement with the  $15 \Omega \text{ sq}^{-1}$  reported in the original publication of this method for production of LIG (Lin *et al.*, 2014).

To further characterise the LIG material and in order to confirm its graphene like properties Raman spectroscopy was performed. Earlier work pre-dating that of the recent work from the Tour group (Lin *et al.*, 2014) had presented the use of lasers to carbonise Kapton<sup>®</sup>, these examples did not make claims of being able to produce materials with the exceptional qualities and characteristics of a graphene material, but instead had likened their materials to GCE (Wynn and Fountain, 1997), known to be suitable for electrochemistry but not performing with the superior capacity of EPPG. Tour demonstrated the power of the CO<sub>2</sub> laser to have an effect on the resultant material characteristics (Lin *et al.*, 2014) and so a range of power intensities from 12 W to 17 W were used to create samples of LIG from Kapton<sup>®</sup> by means of altering the 40 W power of the CO<sub>2</sub> laser from 30 % to 42.5 %. These power intensities varied from those used in the original paper, using the 40 W CO<sub>2</sub> laser instrument model LS6040PRO with the Kapton<sup>®</sup> on PET and glass failed to consistently produce the change to LIG at lower powers and at powers above 17 W resulted in ablation of the LIG from the surface. This can be due to variations in power density introduced by varied spot size, z height and write speed as well as variation in the thickness of the Kapton<sup>®</sup> used. It was also noted that laser performance varied with extended use and could not be controlled as precisely as required for the purpose of creating reproducible sensors in its current format, as this was not its intended use.

The data shown in Figure 3-4 demonstrates graphene like properties for the LIG regardless of laser power intensity used within this range. The emergence of a 2D peak is exhibited in all kinds of sp<sup>2</sup> carbon materials (Gupta *et al.*, 2006; Pimenta *et al.*, 2007), and in the case of LSG it arises around  $2688 \text{ cm}^{-1}$  which is in agreement with the analysis of LSG which was confirmed to be a graphene like material (Strong *et al.*, 2012) and with work examining the Raman spectra of highly ordered pyrolytic graphite which has a 2D peak showing a split into a double peak at  $>2700 \text{ cm}^{-1}$  (Gupta *et al.*, 2006). This combined with the G-band is a Raman signature of graphitic sp<sup>2</sup> materials demonstrating a graphene

like material. The G-band arises from the stretching of the C-C bond in graphitic materials, and is common to all  $sp^2$  carbon systems and impurities or surface charges in the graphene can cause the G-peak to split in two, a G-peak ( $1583\text{ cm}^{-1}$ ) and D'-peak ( $1620\text{ cm}^{-1}$ ) (Pimenta *et al.*, 2007). This can be seen in the samples generated here in Figure 3-4. The ratio of the G:2D peak varies dependent upon laser intensity used, but in all cases is indicative of a few layer graphene structure (Gupta *et al.*, 2006) supported by the symmetry seen in the 2D peaks (Ferrari *et al.*, 2006). The significant size of the D peak is confirmation of high defect content as the D-mode is caused by disordered structure of graphene, yet its symmetry is indicative of graphene edge sites as opposed to graphite edge sites (Ferrari *et al.*, 2006) suggesting real potential as an electrochemical electrode in which surface defects, particularly oxygen groups are critical for optimal electrochemical performance. Previous literature has confirmed the presence of a C-N peak at approx.  $1380\text{ cm}^{-1}$  and C=O peak at approx.  $1790\text{ cm}^{-1}$  for polyimide (Ge *et al.*, 1998) and the loss of these peaks in the LIG samples suggests the loss of nitrogen and double bonded oxygen following the laser treatment.

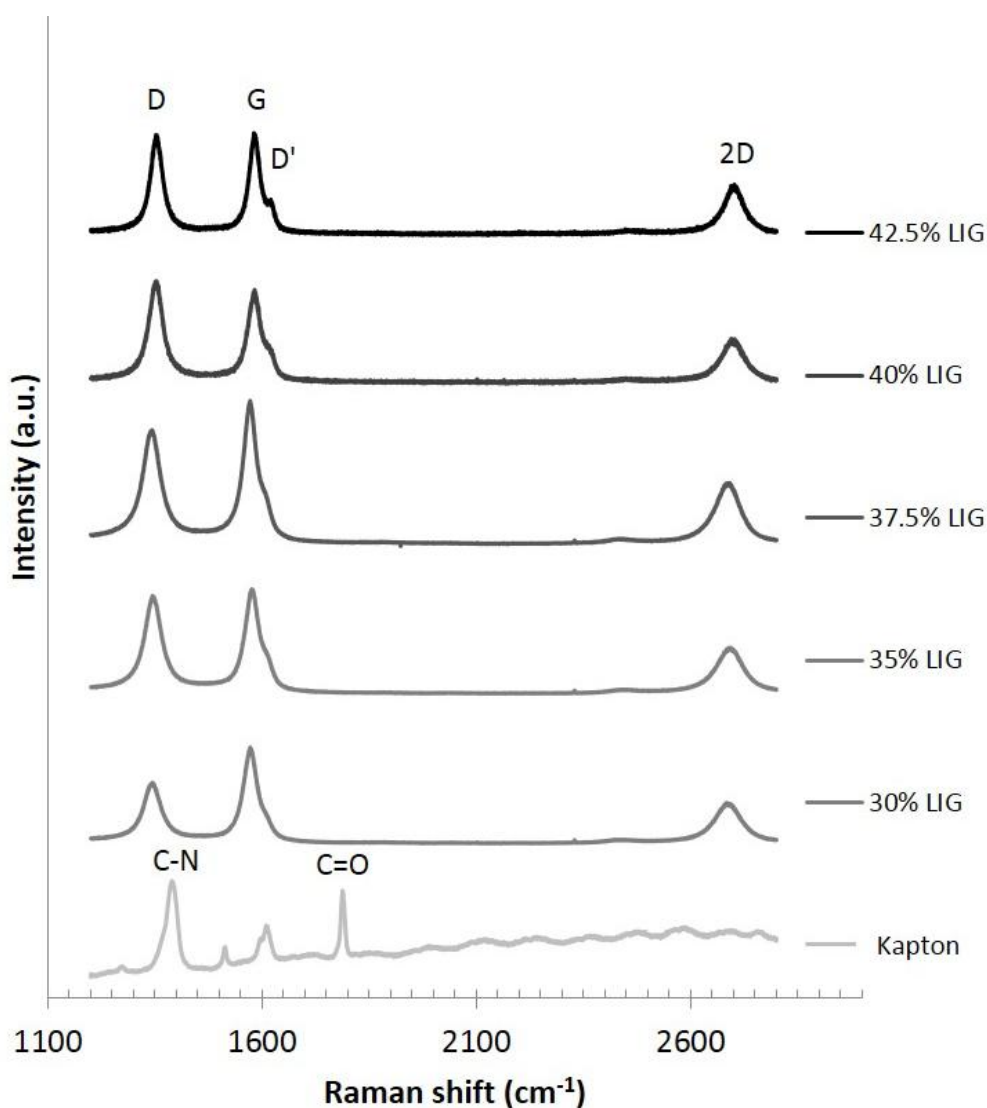


Figure 3-4 Raman analysis of Kapton<sup>®</sup> and LIG produced from varying CO<sub>2</sub> laser powers

From the peak ratios deduced by Raman spectroscopy, 12 W laser power (30% LIG) would appear to produce the best quality of graphene like material with a lower density of defects to the carbon structure. However this may not result in the optimal material for electrochemistry and so LIG samples prepared from the range of laser powers were investigated as part of this study with both potassium ferricyanide an inner- sphere redox probe and the outer-sphere redox probe 1,1'-ferrocene dimethanol (Results discussed later in this chapter).

Change in elemental composition of the Kapton<sup>®</sup> film following laser irradiation to form LIG was analysed with XPS. A full survey scan, as shown in Figure 3-5 demonstrates the reduced level of both oxygen and nitrogen in LIG compared with Kapton<sup>®</sup>, seen as a reduction in the O<sub>1s</sub> peak at around 540 eV and the N<sub>1s</sub> peak at approximately 400 eV. The

oxygen content reduced from 25% in Kapton<sup>®</sup> to 10% in LIG and the nitrogen was reduced to 0.3% in LIG compared with the 1.5% found in Kapton<sup>®</sup> this is in agreement with the Raman data as shown in Figure 3-4.

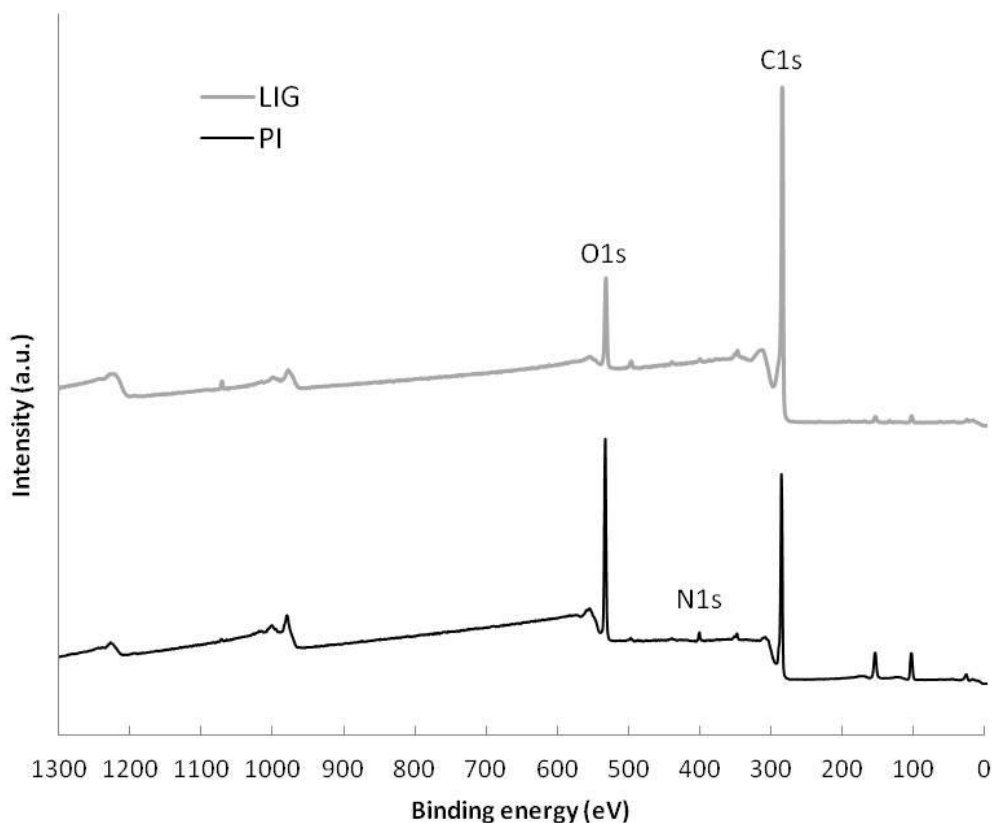


Figure 3-5 Survey scan XPS spectra of Kapton<sup>®</sup> (PI) and laser-induced graphene (30%)

The high resolution spectra of the C<sub>1s</sub> peak for both Kapton<sup>®</sup> and LIG can be seen in Figure 3-6 and this data supports the earlier findings with a large increase in the sp<sup>2</sup> carbon peak at 284.3 eV and reduction in the ratio between this and the O-C=N peak at around 287 eV and the O-C=O peak at 289 eV, where they also show a small shift towards a lower binding energy following laser treatment (Lin *et al.*, 2014). This data also confirms a similarity in C/O ratios to the LSG material which had an oxygen content of 6.5% (Figure 2-3) which performed well in electrochemical studies, further promoting the study of LIG in electrochemical sensing.

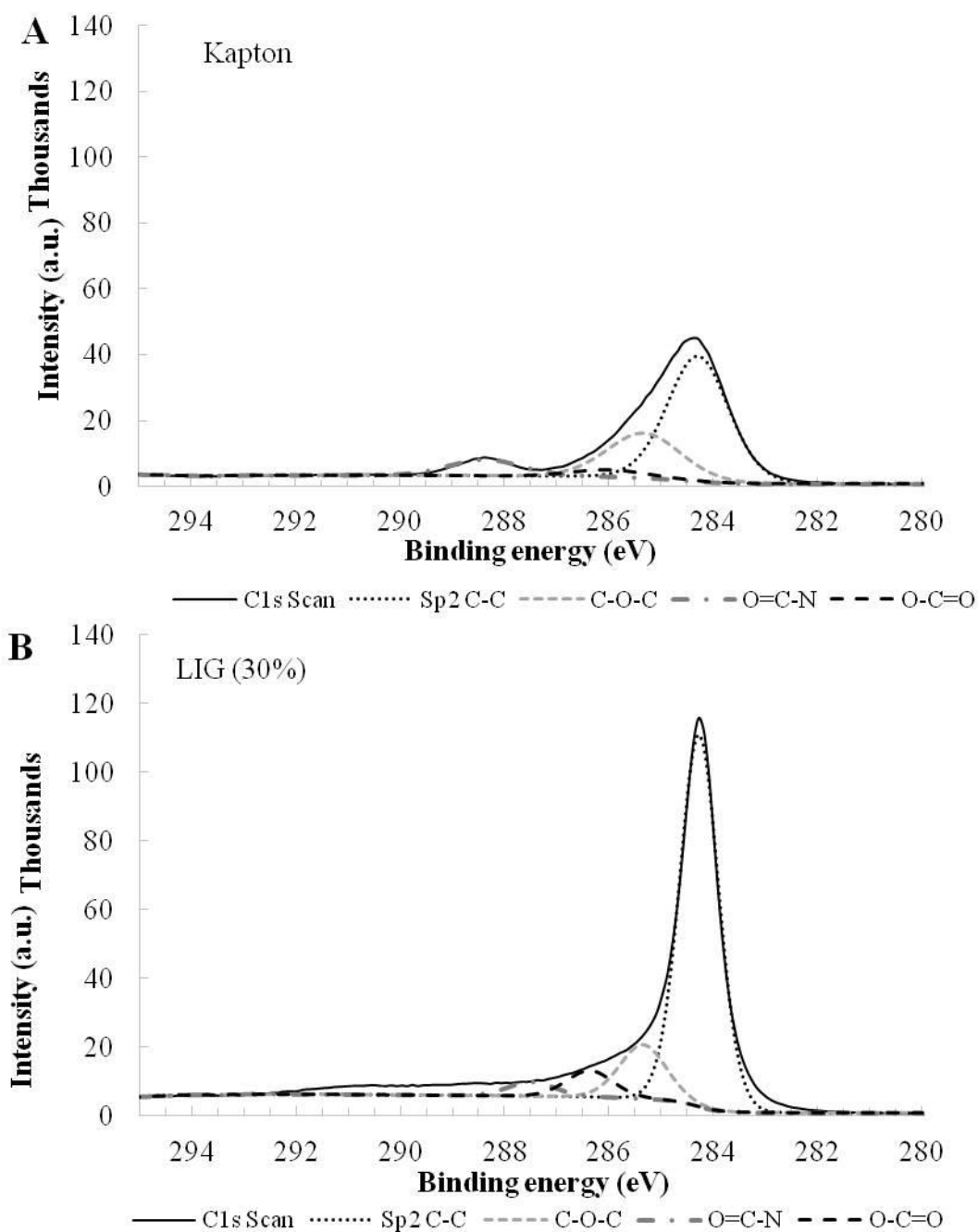


Figure 3-6 High resolution XPS spectra of the C1s peak with peak fitting of Kapton<sup>®</sup> (A) and LIG from 30% power (B).

### 3.3.2 Electrochemical Assessment of Laser-induced Graphene

An illustration of the electrode design is shown in Figure 2-4, in this case LSG is replaced with LIG as shown in Figure 3-2. The LIG electrodes were then assessed with the use of CV as described in the Methods section. A range of carbon based electrodes were again selected for comparison, all with 3 mm diameter. LIG electrodes were compared with EPPG, BPPG and LSG. Again EPPG was chosen as the 'gold standard' for comparison due to its excellent performance as a result of its high edge plane content and thus fast

heterogeneous electron transfer rate (Banks and Compton, 2006; Ji *et al.*, 2006). The BPPG electrode was chosen as it is known to perform poorly in comparison with EPPG in the case of inner-sphere redox species reliant upon surface oxygen groups for efficient electron transfer, due to its basal nature ensuring a lack of oxygen defects and edge plane sites for such electrochemical reactions to occur (Randviir *et al.*, 2012). As LSG had previously been shown to compare well with EPPG (Griffiths *et al.*, 2014), this was also included for comparison to determine which of these new materials would demonstrate the greatest potential as a simple to manufacture standalone graphene electrode. Comparison with GCE was also included with this work to determine whether the LIG would outperform this material to which earlier laser carbonised polymers had been likened (Wynn and Fountain, 1997).

Preliminary electrochemical studies demonstrated large variation between LIG electrodes and results hinted towards a porous electrode surface (Data not shown) supported by the SEM images in Figure 3-3 (Electrode porosity will be discussed in detail later in this chapter with supporting results). Thus a process of optimisation was performed to determine the optimal pre-incubation time for the LIG electrodes and the most favourable CO<sub>2</sub> laser intensity to be used. If an electrode surface is in fact porous to redox species then the effect of incubation time should be considered. This is likely to have an effect on whether the response is more reliant upon bulk diffusion or thin-layer diffusion, dependent upon the time taken for complete infiltration of the redox species into the electrodes porous network. To test this theory a 30% LIG electrode was placed into 1 mM 1,1'-ferrocene dimethanol (Figure 3-7) or 1 mM potassium ferricyanide (Figure 3-8) and CVs were performed at 0, 5, 10, 15, 20 and 25 minutes. The results (Mean of 3 electrodes +/- 1sd) are plotted as the relationship of time with peak currents and peak potential separation.

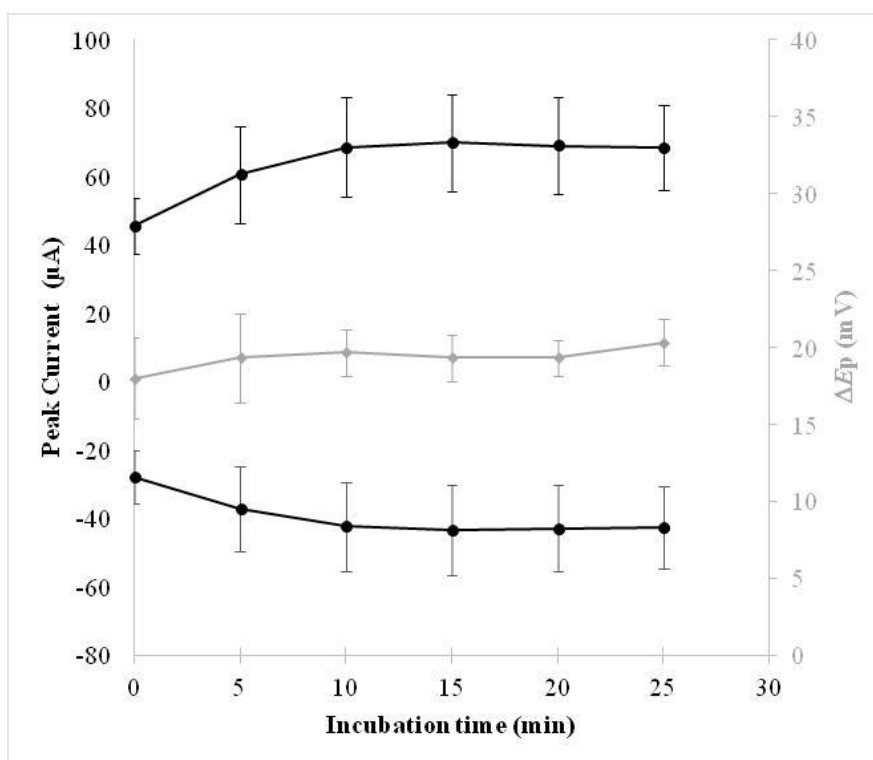


Figure 3-7 Effect of incubation time on electrochemical response of LIG electrodes in 1,1'-ferrocene dimethanol. Peak current and peak potential separation in 1 mM 1,1'-ferrocene dimethanol 1 M KCl are shown when using  $50 \text{ mV s}^{-1}$  scan rate and 30% LIG electrodes.

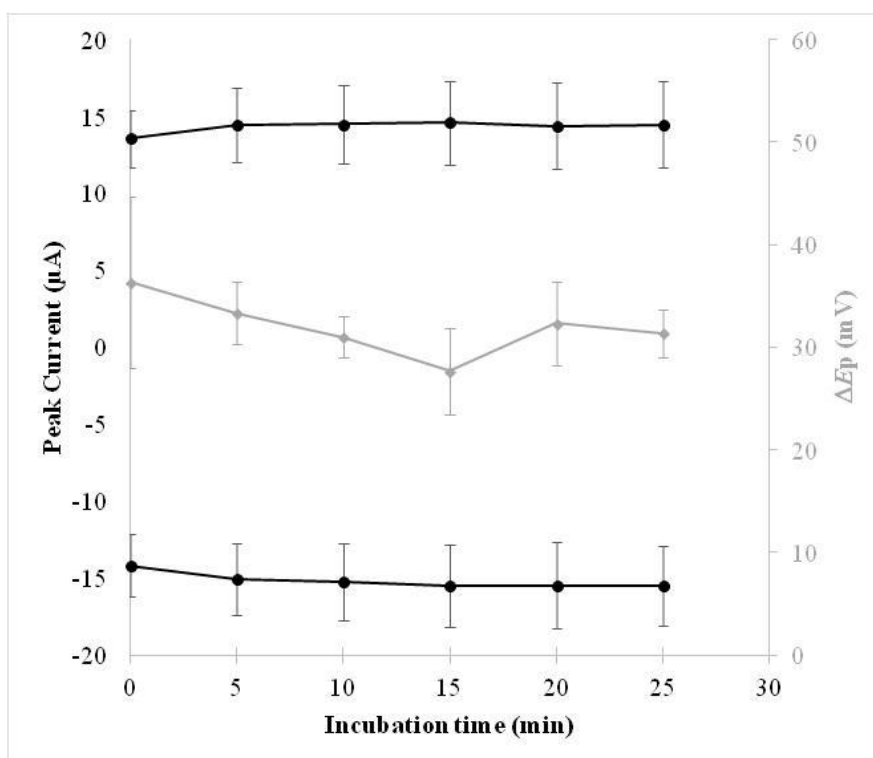


Figure 3-8 Effect of incubation time on electrochemical response of LIG electrodes in potassium ferricyanide. Peak current and peak potential separation in 1 mM potassium ferricyanide 1 M KCl are shown when using  $50 \text{ mV s}^{-1}$  scan rate and 30% LIG electrodes.

It can be seen in Figure 3-7 and Figure 3-8 that incubation time of the electrode does in fact have an effect on the electrochemical result with a general trend of increased peak current responses and reduced peak potential separation between 0 and 10 minutes, beyond 10 minutes incubation the resulting peak currents and peak potential separation remain relatively constant. This behaviour can be both a benefit and draw-back during the development of an electrochemical sensor with LIG. The response of such a sensor could be increased with an incubation period but this incubation period would need to be tightly controlled to ensure consistent results. All future experiments utilising LIG electrodes were performed following a 10 minute incubation of electrodes in the solution of interest.

The Tour group had previously demonstrated that the threshold laser power required for conversion to LIG was dependent upon the write speed of the CO<sub>2</sub> laser (Lin *et al.*, 2014). Also, that the laser power altered the LIG composition and the material expansion (Sheet thickness), sheet resistance and specific areal capacitance (Lin *et al.*, 2014). For LIG use in micro-supercapacitors the power resulting in the highest capacitance was selected as optimal for further investigation and development. However, in this study the importance was electrochemical behaviour with redox species. Thus the effect of laser power on the electrochemical properties of the LIG was investigated. Electrodes were made from samples of LIG created with the 40 W CO<sub>2</sub> laser intensity set at 30%, 35%, 37.5%, 40% and 42.5%. This range of CO<sub>2</sub> laser powers was chosen as using the CO<sub>2</sub> laser instrument at Newcastle with the Kapton<sup>®</sup> in the configuration shown in Figure 3-2 on a flexible substrate attached to a glass slide these covered the range from which a carbonisation process could routinely be observed by eye at 30 % to powers where routinely the intensity was too high causing a complete etching of the Kapton<sup>®</sup> from the substrate. The difference in power intensity used between the work here and that performed by (Lin *et al.*, 2014) may be due to a number of variables including the power density due to laser spot size, write speed, the Kapton<sup>®</sup> thickness and the substrate. The electrodes were first assessed by CV in 1,1'-ferrocene dimethanol across scan rates from 10-200 mV s<sup>-1</sup>, the resultant  $\Delta E_p$  values for each electrode across the scan rates can be seen in Figure 3-9. A general trend is observed with all electrodes, that is a decrease in  $\Delta E_p$  with increase in scan rate. This does not follow the trend observed with EPPG and LSG of an increase in  $\Delta E_p$  with increase in scan rate as the electrode kinetics fail to maintain maximum response to faster scan rates demonstrating quasi-reversible behaviour (Data not shown). The  $\Delta E_p$  values of less than 59 mV, the expected value of an ideal Nernstian one electron transfer diffusional process, is indicative of a 'thin layer' response (Barnes *et al.*, 2014). This is

most likely due to the entrapment of redox species within the porous structure of the LIG electrodes. The porosity due to size and distribution of the pores will alter the electrochemical response and can be tuned with adjustment of the laser intensity used to create the LIG. In the case of the  $\Delta E_p$  values for 1,1'-ferrocene dimethanol, electrodes produced with 30% laser intensity demonstrated the lowest peak separation with  $\Delta E_p$  values as low as 20 mV observed. The greatest  $\Delta E_p$  values of 55-58 mV were witnessed with electrodes produced with 35% to 42.5% laser intensity (Figure 3-9).

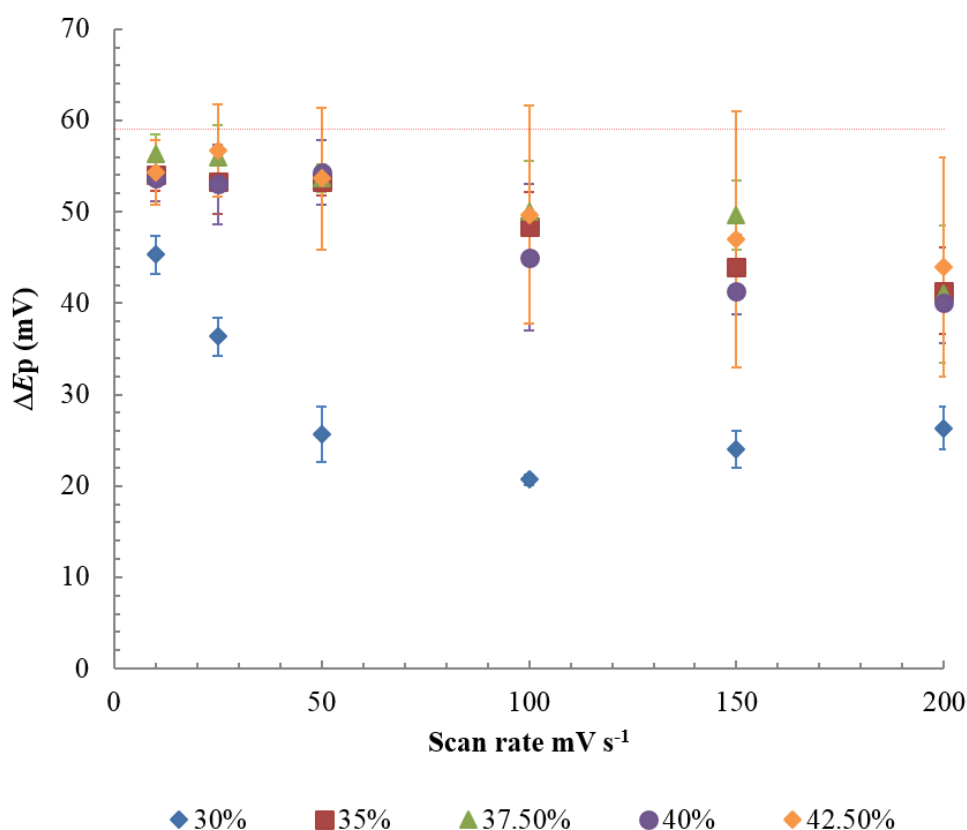


Figure 3-9 Peak potential separation in 1,1'-ferrocene dimethanol for LIG electrodes produced from various laser powers  
CV performed in 1 mM 1,1'-ferrocene dimethanol 1 M KCl with LIG obtained from Kapton<sup>®</sup> using different 40 W CO<sub>2</sub> laser intensities. Mean of 3 electrodes(+/- 1sd) shown and 59 mV Nernstian ideal response for a one electron transfer is marked with red line.

The peak current response with increasing scan rate was also scrutinised for these electrodes. The results can be seen in Figure 3-10 plotted as peak current against the square root of the scan rate, where a linear relationship would indicate a diffusional response at the electrodes. However we can see from these data that the LIG electrodes do not demonstrate a linear relationship between peak current and square root of the scan rate (Figure 3-11: Linear trend lines shown on individual graphs for clarity of all powers,

only oxidation current responses shown) with  $R^2$  values of 0.9405, 0.9654 (30% LIG), 0.9793, 0.9808 (35% LIG), 0.9291, 0.9838 (37.5% LIG), 0.9682, 0.9695 (40% LIG) and 0.9755, 0.9783 (42.5% LIG). The 30% laser intensity electrodes demonstrate the greatest peak currents of all of the electrodes tested. The same data are shown in Figure 3-12 plotted instead as current directly against the scan rate, here we see a more linear response particularly noticeable with 30% LIG electrodes than when plotted against the square root of the scan rate. Here  $R^2$  values of 0.9940, 0.9996 (30% LIG), 0.9988, 0.9986 (35% LIG), 0.8615, 0.9981 (37.5% LIG), 0.9983, 0.9996 (40% LIG) and 0.9988, 0.9994 (42.5% LIG) are achieved (Figure 3-13). This indicates that the electrochemical response, particularly of the 30% LIG electrodes is largely due to a thin-layer behaviour, rather than the diffusional response that was observed with EPPG and LSG (data not shown here) as seen in studies with porous electrodes created from CNT modified GCEs (Keeley and Lyons, 2009).

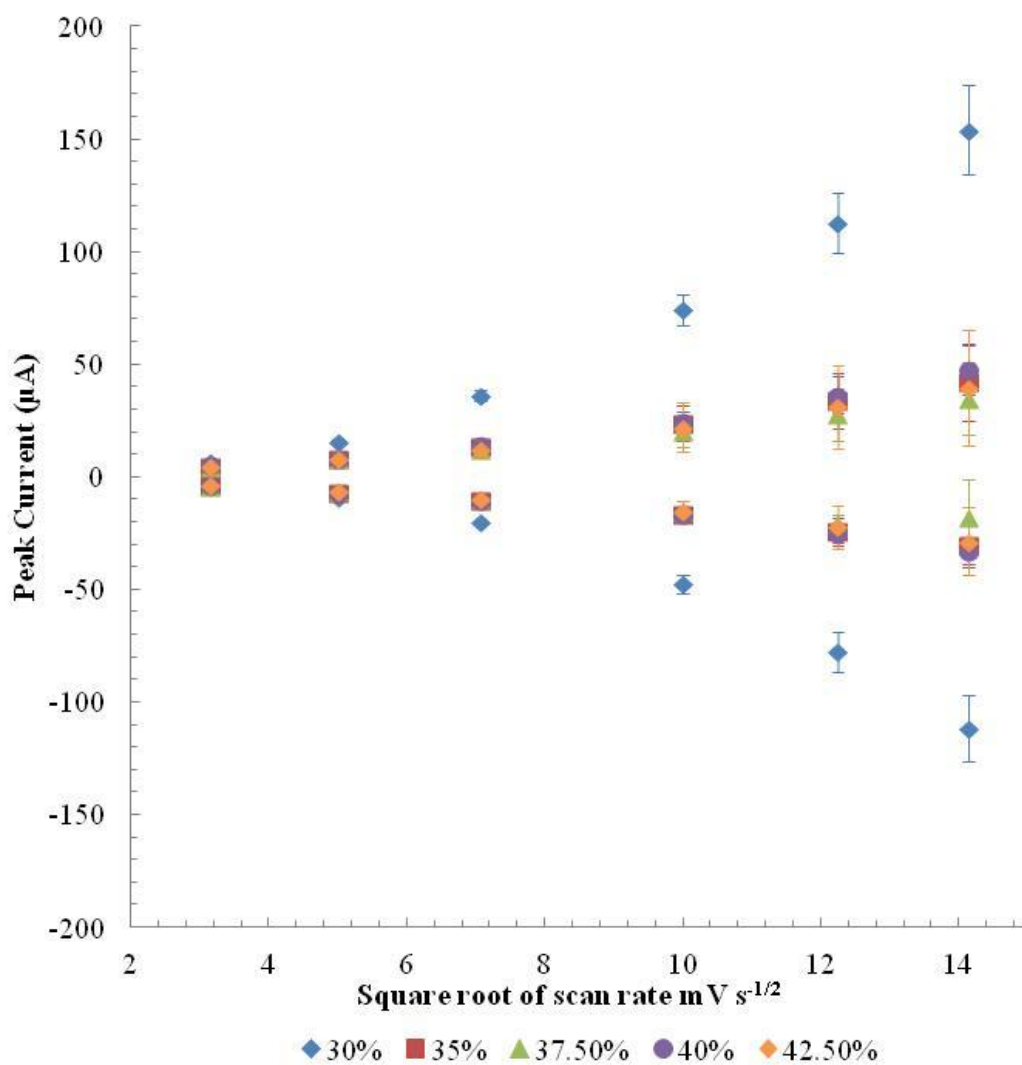


Figure 3-10 Peak current of various LIG samples in 1,1'-ferrocene dimethanol plotted against square root of scan rate  
 CV performed in 1 mM 1,1'-ferrocene dimethanol 1 M KCl with LIG obtained from Kapton<sup>®</sup> using different 40 W CO<sub>2</sub> laser intensities plotted against square root of scan rate. Mean +/- 1sd n=3.

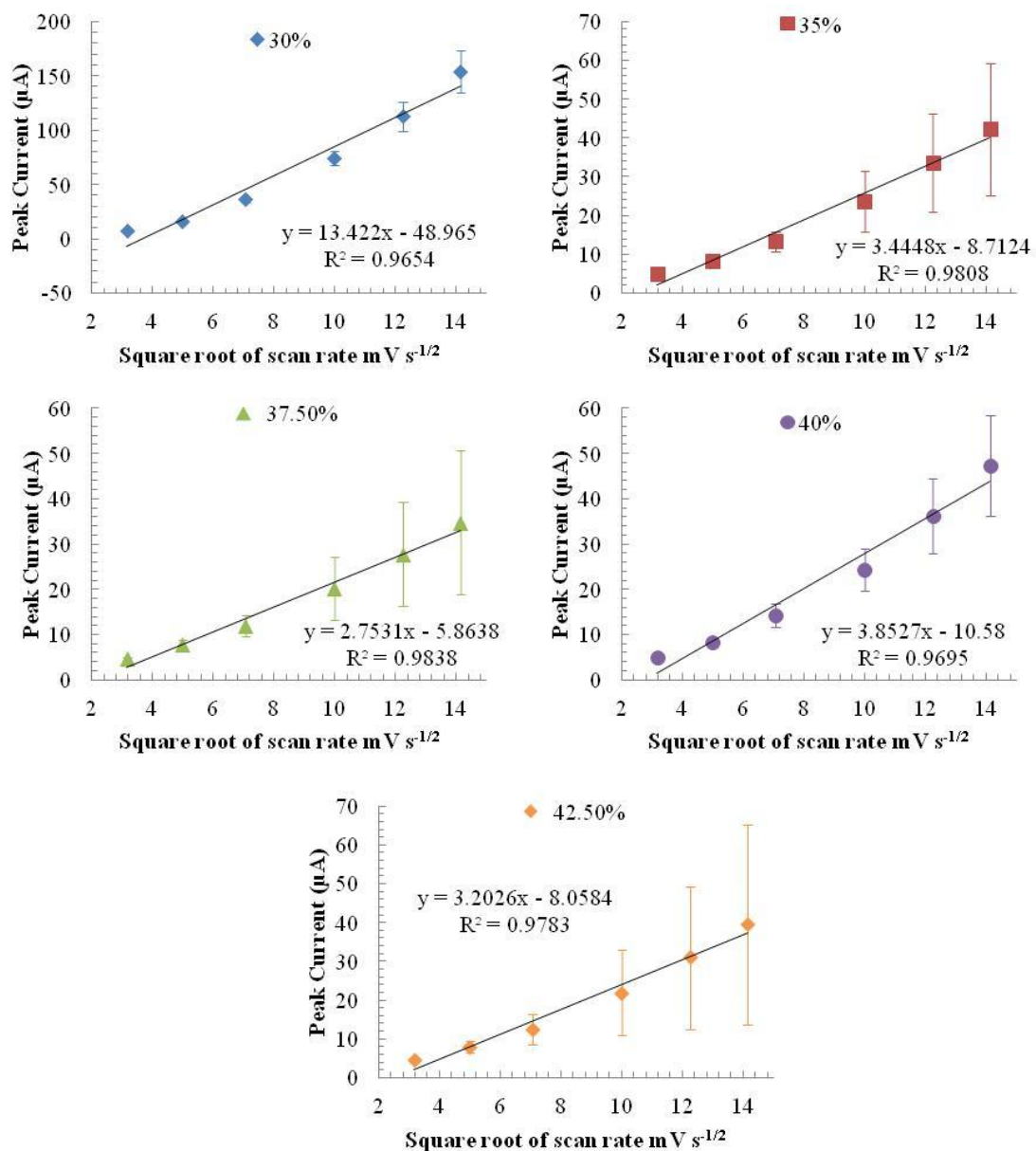


Figure 3-11 Linearity of peak oxidation current vs square root of scan rate for various LIG samples in 1,1'ferrocene dimethanol 1 mM 1,1' ferrocene dimethanol 1 M KCl with LIG obtained from Kapton<sup>®</sup> using different 40 W CO<sub>2</sub> laser intensities plotted against square root of scan rate. Mean +/- 1sd n=3 with linear trend line shown for each power intensity.

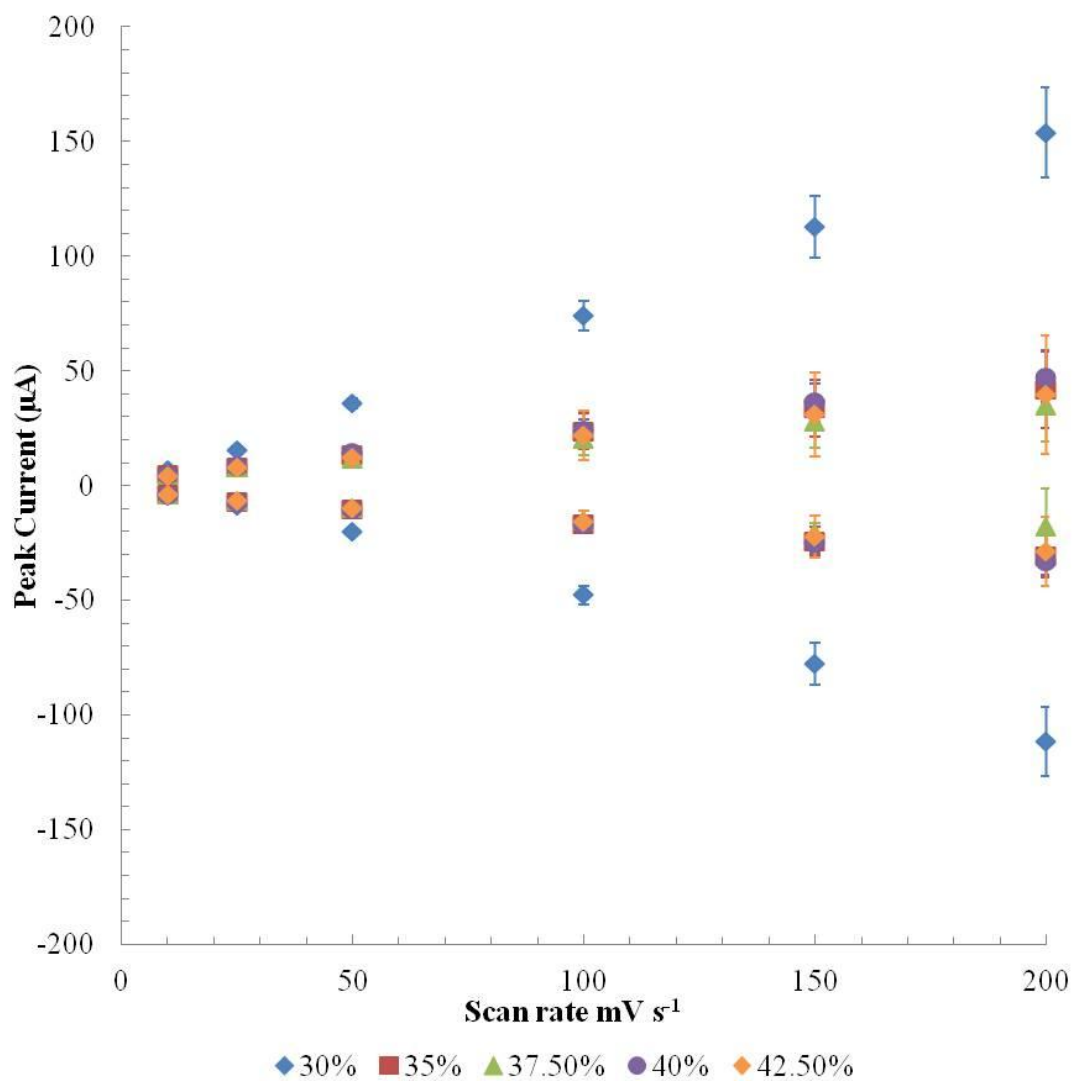


Figure 3-12 Peak current of various LIG samples in 1,1'-ferrocene dimethanol plotted against scan rate CV performed in 1 mM 1,1'-ferrocene dimethanol 1 M KCl with LIG obtained from Kapton<sup>®</sup> using different 40 W CO<sub>2</sub> laser intensities plotted against scan rate. Mean +/- 1sd n=3.

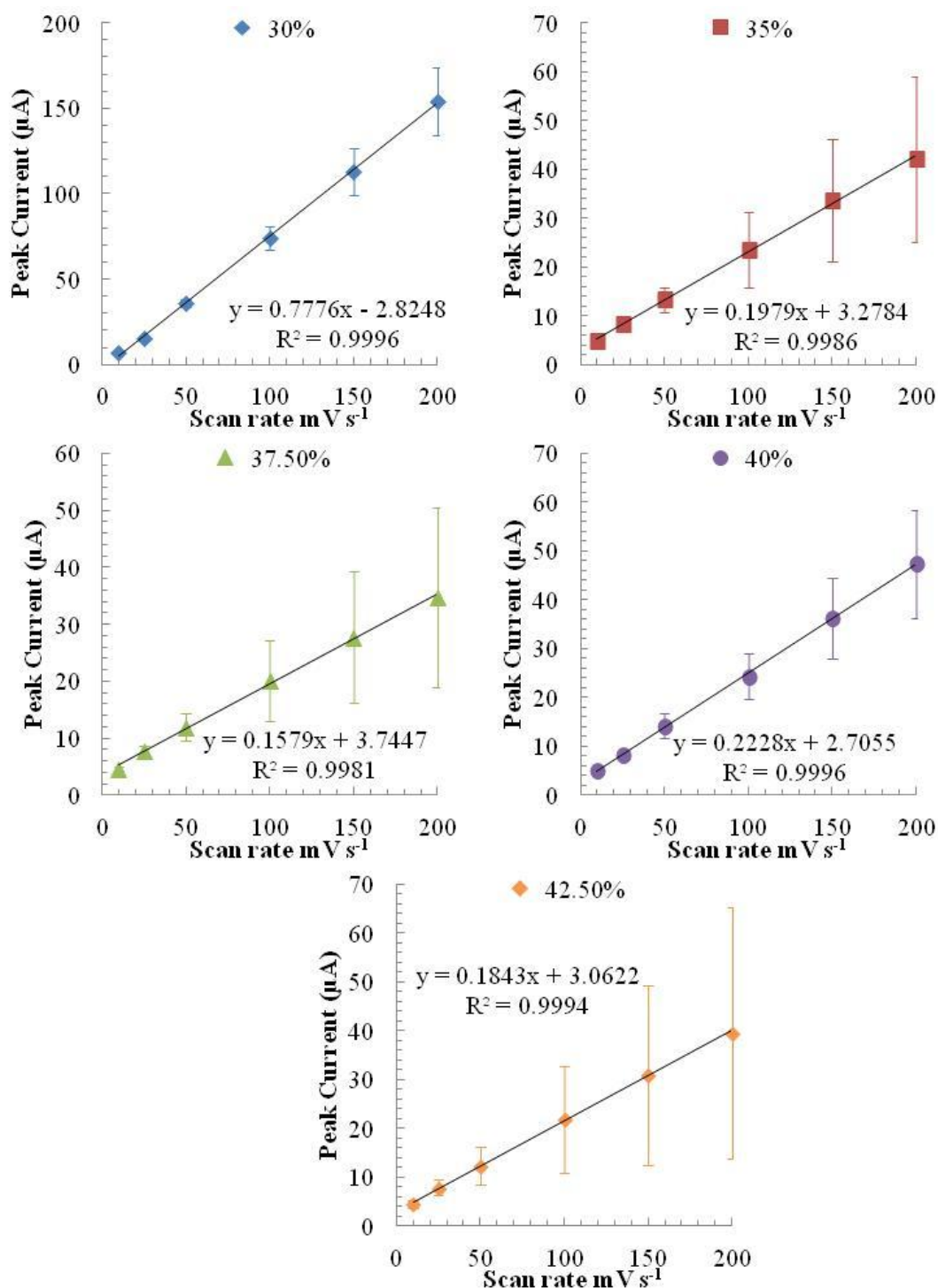


Figure 3-13 Linearity of peak oxidation current vs scan rate for various LIG samples in 1,1' ferrocene dimethanol 1 mM 1,1' ferrocene dimethanol 1 M KCl with LIG obtained from Kapton<sup>®</sup> using different 40 W CO<sub>2</sub> laser intensities plotted against scan rate. Mean +/- 1sd n=3 with linear trend line shown for each power intensity.

The electrodes produced from a range of laser intensities were then also assessed in the inner-sphere redox probe potassium ferricyanide in the same way. The peak separation data are shown in Figure 3-14 and again a general trend is observed in reduced peak separation with increased scan rate, which is indicative of thin layer behaviour rather than

the standard diffusion controlled reactions of standard planar electrodes such as EPPG and LSG. The electrodes produced from 40% and 42.5% laser intensity have the largest  $\Delta E_p$  values yet still appear to have a porous nature; but to a lesser degree than the 30% and 35% LIG electrodes, due to the heterogeneous nature of the pores it was not possible to accurately quantitate this variation in pore size. These results indicate that a fine line exists in which to produce LIG electrodes, a small change in  $\text{CO}_2$  laser intensity can result in a very different electrochemical response. This is not unexpected when comparing the physicochemical profiles of the LIG produced from various laser powers as the Raman profile of the 30% LIG showed a reduction in defects, with the 2D peak showing greater symmetry and appearing closer to  $2688\text{ cm}^{-1}$  than the LIG samples produced from greater laser intensities. It would appear from the electrochemical analysis that the pore structure is the key defining element in this alternative electrochemical thin layer response.

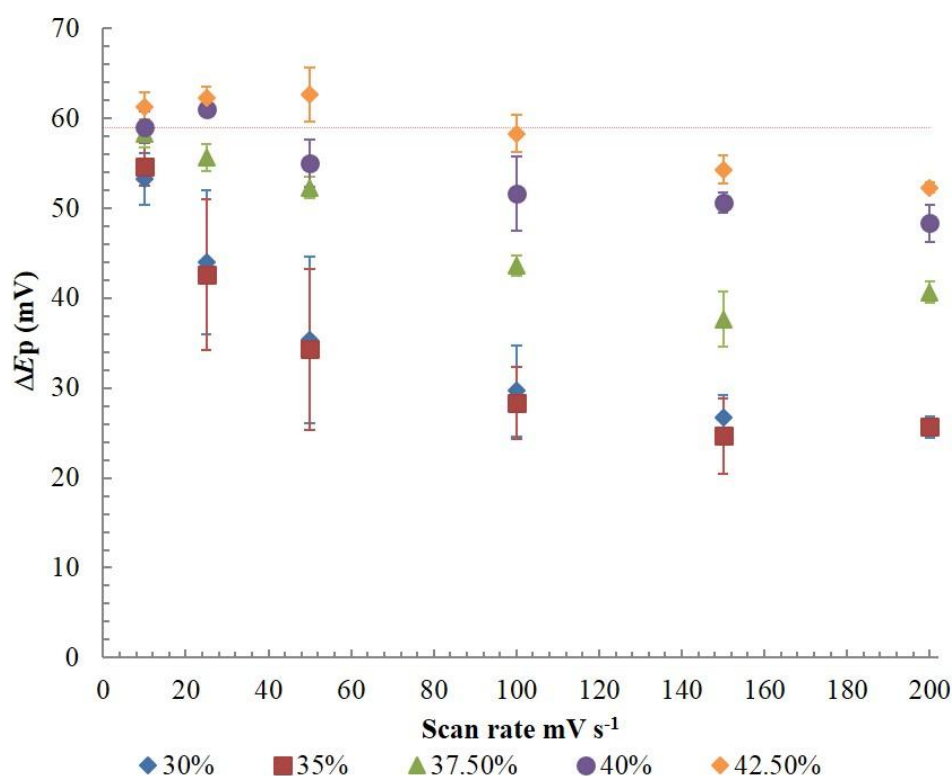


Figure 3-14 Peak potential separation in potassium ferricyanide for LIG electrodes produced from various laser powers  
CV performed in 1 mM potassium ferricyanide 1 M KCl with LIG obtained from Kapton<sup>®</sup> using different 40 W  $\text{CO}_2$  laser intensities. Mean of 3 electrodes (+/- 1sd) shown and 59 mV Nernstian ideal response for a one electron transfer is marked with red line.

In potassium ferricyanide the  $\Delta E_p$  values varied from 24 mV to 63 mV dependent upon scan rate and electrode used, still much reduced compared to the 59 mV Nernstian value,

particularly the 30% and 35% LIG electrodes. Further evidence that these electrodes are behaving in a manner not limited by the bulk diffusional response but instead by thin-layer diffusion. The current responses were much smaller in the potassium ferricyanide than in the 1,1'-ferrocene dimethanol as shown in Figure 3-10. Current against the square root of scan rate is shown in Figure 3-15 with  $R^2$  values of 0.9796, 0.9820 (30% LIG), 0.9806, 0.9817 (35% LIG), 0.9928, 0.9918 (37.5% LIG), 0.9958, 0.9990 (40% LIG) and 0.9981, 0.9984 (42.5% LIG) (Figure 3-16). This is followed by current against the scan rate in Figure 3-17 with  $R^2$  values of 0.9993, 0.9985 (30% LIG), 0.9990, 0.9982 (35% LIG), 0.9920, 0.9938 (37.5% LIG), 0.9878, 0.9792 (40% LIG) and 0.9836, 0.9831 (42.5% LIG) (Figure 3-16, Figure 3-18). These graphs provide yet further evidence of thin-layer behaviour of the 30% LIG compared with more standard diffusional behaviour with 37.5%, 40% and 42.5% LIG electrodes.

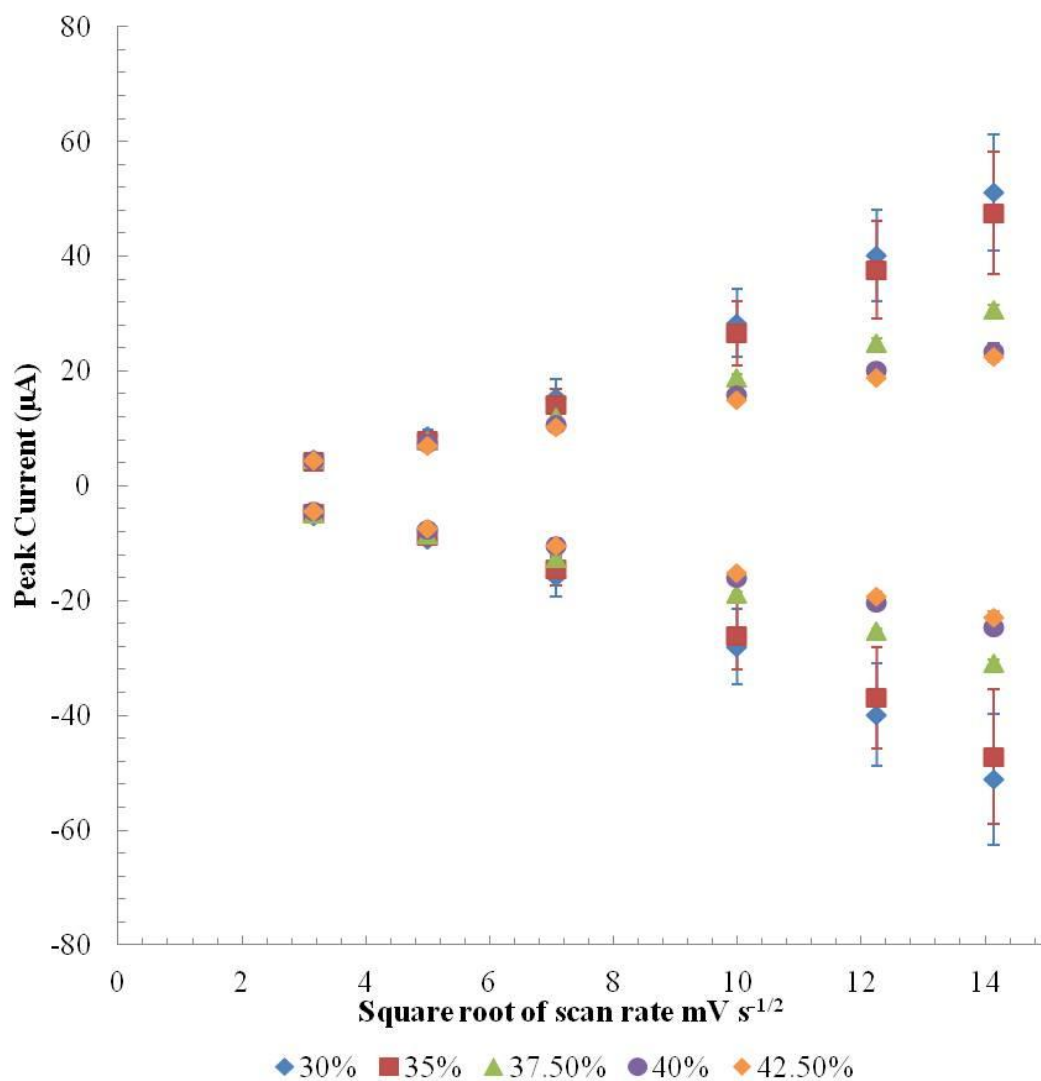


Figure 3-15 Peak current of various LIG samples in potassium ferricyanide plotted against square root of scan rate

CV performed in 1 mM potassium ferricyanide 1 M KCl with LIG obtained from Kapton<sup>®</sup> using different 40 W CO<sub>2</sub> laser intensities plotted against square root of scan rate. Mean +/- 1sd n=3.

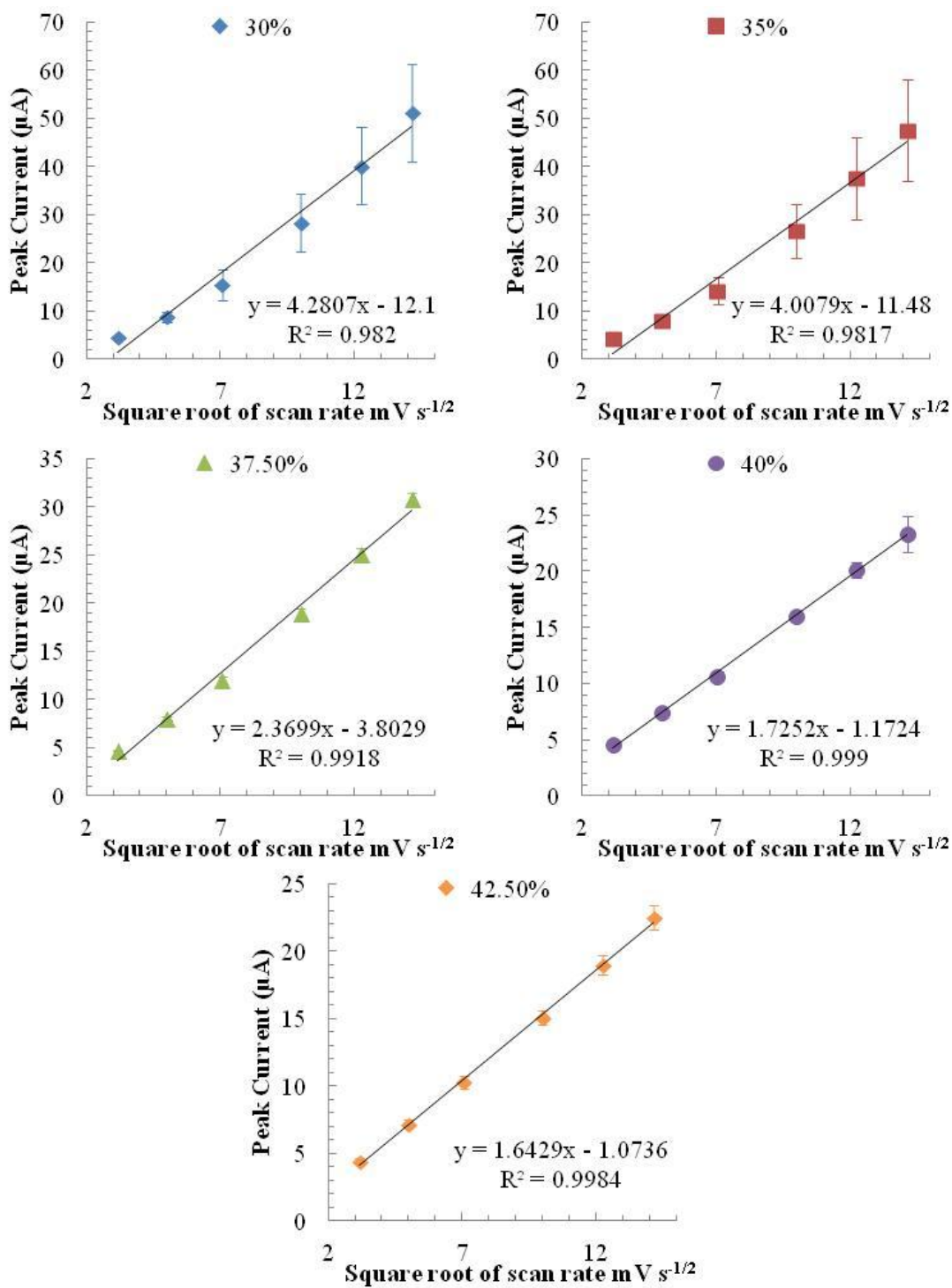


Figure 3-16 Linearity of peak oxidation current vs square root of scan rate for various LIG samples in potassium ferricyanide 1 mM potassium ferricyanide 1 M KCl with LIG obtained from Kapton<sup>®</sup> using different 40 W CO<sub>2</sub> laser intensities plotted against square root of scan rate. Mean +/- 1SD n=3 with linear trend line shown for each power intensity.

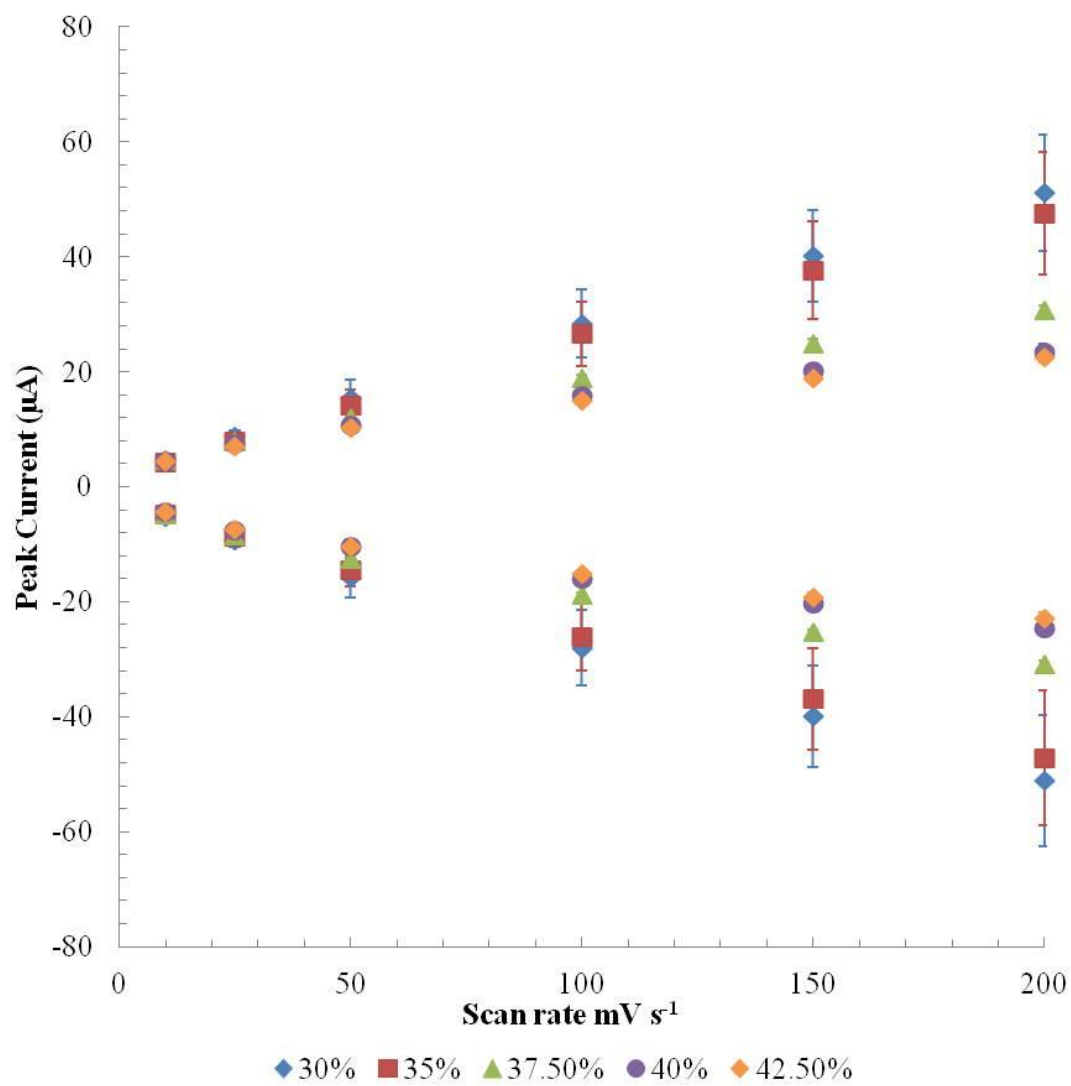


Figure 3-17 Peak current of various LIG samples in potassium ferricyanide plotted against scan rate CV performed in 1 mM potassium ferricyanide 1 M KCl with LIG obtained from Kapton<sup>®</sup> using different 40 W CO<sub>2</sub> laser intensities plotted against scan rate. Mean +/- 1SD n=3.

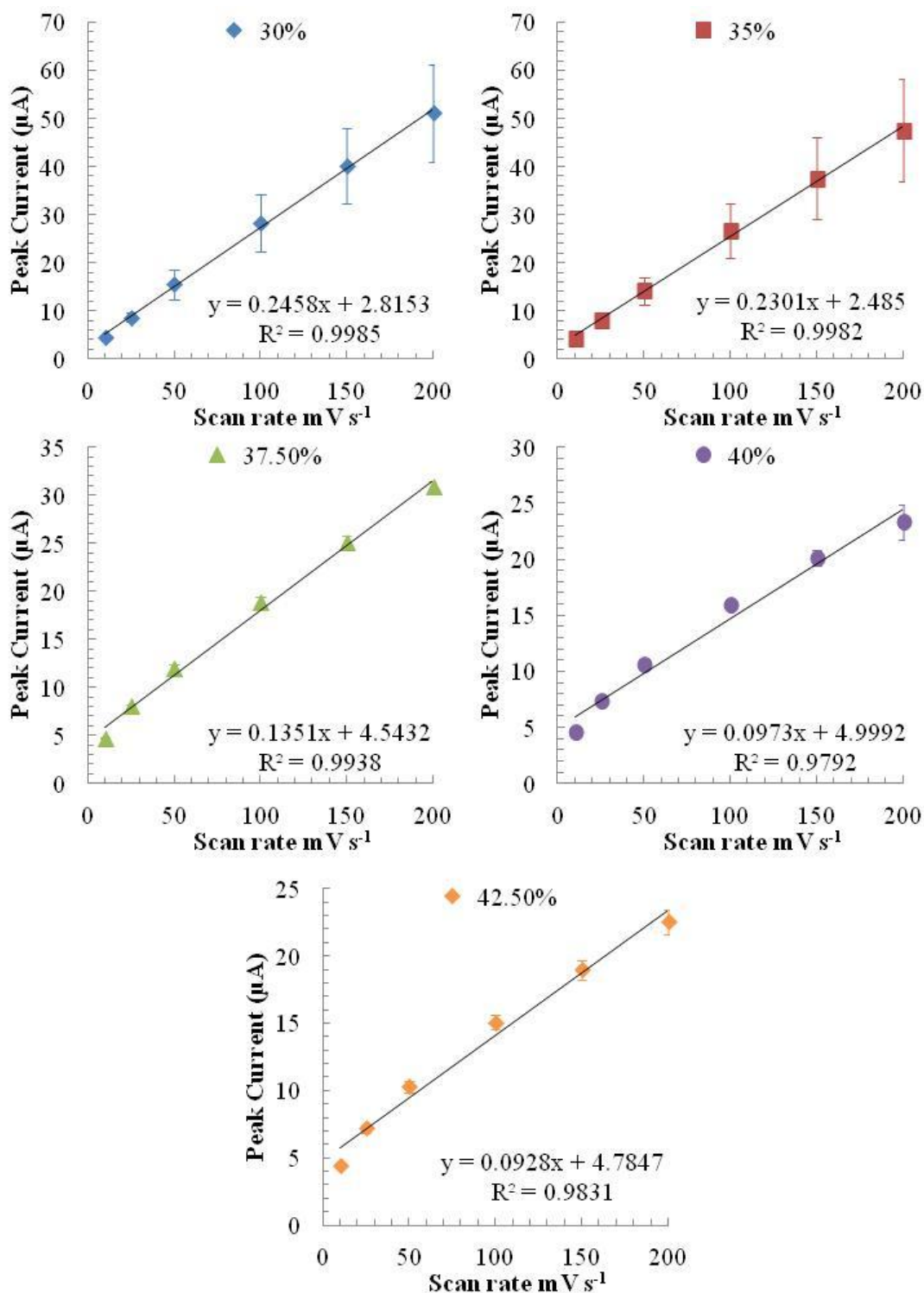


Figure 3-18 Linearity of peak oxidation current vs scan rate for various LIG samples in potassium ferricyanide 1 mM potassium ferricyanide 1 M KCl with LIG obtained from Kapton<sup>®</sup> using different 40 W CO<sub>2</sub> laser intensities plotted against scan rate. Mean +/- 1sd n=3 with linear trend line shown for each power intensity.

With the results of peak separation and peak current response in both inner- and outer-sphere redox species taken into consideration, it could be assumed that the 30% LIG electrodes were in fact behaving as porous electrodes. This must be taken into

consideration when attributing electrochemical behaviour to the electrode material as any responses are likely to be summative of thin-layer diffusion within the pores and bulk diffusion at the surface of the electrode. These results also demonstrate the fine line of electrode behaviour dependent upon CO<sub>2</sub> laser power used to create the LIG and how this must be strictly controlled to maximise precision.

Comparison with other carbon electrodes was then performed with LIG produced using 30 % of the 40 W CO<sub>2</sub> laser power and following a 10 minute pre-incubation of LIG electrodes in the redox solution. CVs were performed at 10 mV s<sup>-1</sup> scan rate in 1,1'-ferrocene dimethanol, an outer-sphere redox species, insensitive to the surface oxides of the electrodes. The resultant CV scans are shown in Figure 3-19, LIG demonstrated the greatest peak currents of the electrodes tested with BPPG displaying the smallest in 1,1'-ferrocene dimethanol. The peak potential separation was determined for each electrode and results are shown in Table 2-1.

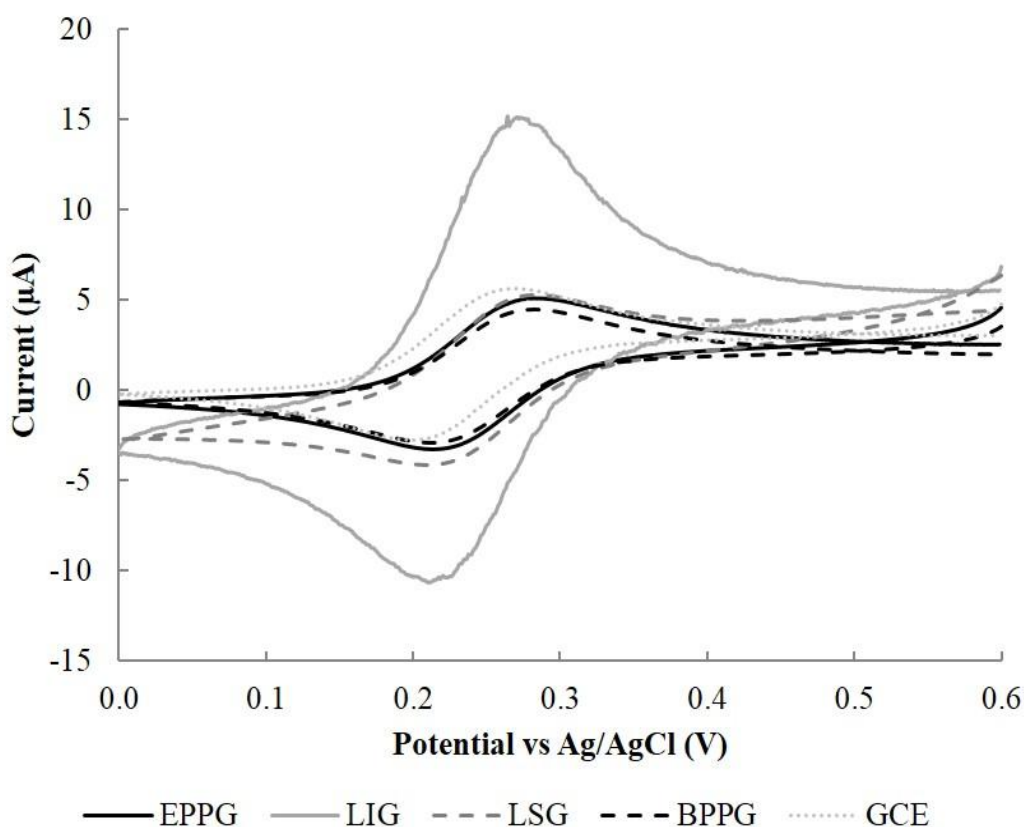


Figure 3-19 Comparing LIG CV profiles with EPPG, LSG, BPPG and GCE in 1,1'-ferrocene dimethanol Representative cyclic voltammograms of 1 mM 1,1'-ferrocene dimethanol in 1 M KCl at a scan rate of 10 mV s<sup>-1</sup> at unmodified 3 mm diameter EPPG, LIG, LSG, BPPG and GCE electrodes.

Table 3-1  $\Delta E_p$  values for selected electrode materials at  $10 \text{ mV s}^{-1}$

Electrode material	$\Delta E_p/\text{mV}$ in 1,1'-ferrocene dimethanol
EPPG	58
BPPG	59
GCE	59
LSG	54
LIG average (n=3)	45
RSD	4.6 %

In the case of 1,1'-ferrocene dimethanol the peak separation of the EPPG, BPPG and GCE were 58 mV, 59 mV and 59 mV respectively, corresponding well with the theoretical ideal of 59 mV for a one electron transfer Nernstian process. In comparison the LSG and LIG demonstrated values of 54 mV and 45 mV, below the theoretical Nernstian response of 59 mV for a one electron diffusion controlled response. Such values had been witnessed earlier with LSG and had been reasonably rationalised as within the experimental error, in part due to the large background capacitive current observed with LSG. However the LIG does not demonstrate such a large background capacitance, the electrochemical reaction with LIG electrodes contains components of both diffusional and thin-layer responses as evidenced by reduced peak potential separation values and linear relationships between peak current and scan rate (Figure 3-9 to Figure 3-17). Peak potential separation values of less than 59 mV are reported in the literature, and can be due to adsorption of the reactant to the electrode surface (Wopschall and Shain, 1967), use of electroactive thin films (Strycharz *et al.*, 2011) or due to entrapment of the reactant for example within a porous electrode (Punckt *et al.*, 2010; Punckt *et al.*, 2013). The results of peak potential separation in potassium ferricyanide were somewhat different (Figure 3-20 and Table 3-2), with both EPPG and BPPG performing poorly with a  $\Delta E_p$  of 85 mV and 176 mV respectively compared with 59 mV and 53 mV for LSG and LIG, although now understanding the porous structure of LIG this cannot be solely attributed to faster heterogeneous electron transfer rates at the LIG surface. GCE performed well compared with EPPG and BPPG achieving a  $\Delta E_p$  of 66 mV, but cannot compete with the outstanding electrochemical performance of LSG and LIG. Figure 3-20 shows the cyclic voltammograms for the electrodes in potassium ferricyanide, where it can be seen that LIG also has greater peak current density than the EPPG, GCE and BPPG. This enhanced performance of graphene materials can be ascribed to an optimal O:C ratio combined with the porosity factor of these electrodes resulting in an increased electrochemically active

surface area and a mixture of thin-layer and diffusional behaviour. Such excellent performance of the LIG electrodes is important due to the ease of manufacture and the suitability for affordable disposable sensors, not possible with the pyrolytic graphite materials.

With the results of peak separation and peak current response in both inner- and outer-sphere redox species taken into consideration, it could be assumed that the LIG electrodes were in fact behaving as a truly porous electrode. This must be taken into consideration when attributing electrochemical behaviour to the electrode material as any responses are likely to be summative of thin-layer diffusion within the pores and bulk diffusion at the surface of the electrode.

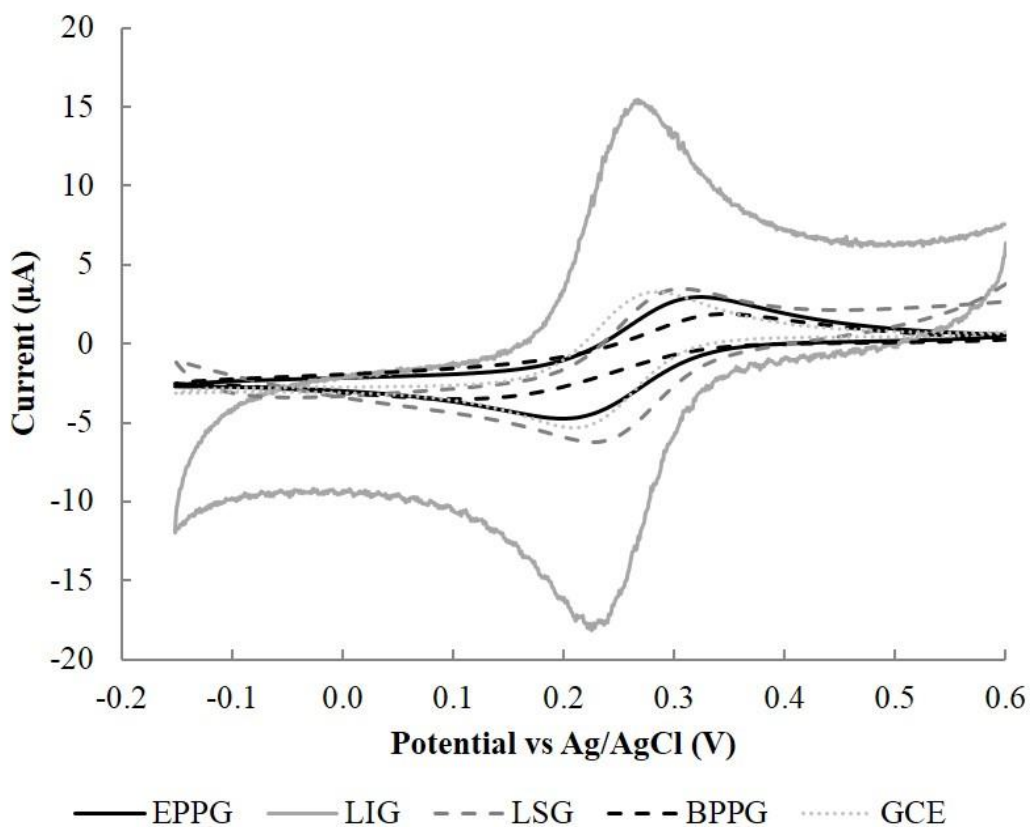


Figure 3-20 Comparing LIG CV profiles with EPPG, LSG, BPPG and GCE in potassium ferricyanide. Representative cyclic voltammograms of 1 mM potassium ferricyanide in 1 M KCl at a scan rate of  $10 \text{ mV s}^{-1}$  at unmodified 3 mm diameter EPPG, LIG, LSG, BPPG and GCE electrodes.

Table 3-2  $\Delta E_p$  values for selected electrode materials at  $10 \text{ mV s}^{-1}$

Electrode material	$\Delta E_p/\text{mV}$ in potassium ferricyanide
EPPG	85
BPPG	176
GCE	66
LSG	59
LIG average (n=3)	53
RSD	5.4 %

CV studies were performed with varying concentrations of 1,1'-ferrocene dimethanol and potassium ferricyanide from 0.1 mM to 10 mM, the results of which can be observed in Figure 3-21 and Figure 3-22. What can be seen is that with potassium ferricyanide (Figure 3-22) the CV scans appear similar to those with EPPG and LSG (Data not shown here) with a smooth, symmetrical, 1:1 oxidation and reduction peak indicative of a fully reversible reaction. However with 1,1'-ferrocene dimethanol (Figure 3-21) the peaks appear to split into two; the sum of the diffusional and thin-layer response occurring at slightly different potentials. It is also observed that the forward reaction peak has a much greater current response than the reverse reaction resulting in a peak ratio closer to 2:1 (Figure 3-21) which may indicate quasi-reversibility of the 1,1'-ferrocene dimethanol redox reaction with LIG electrodes.

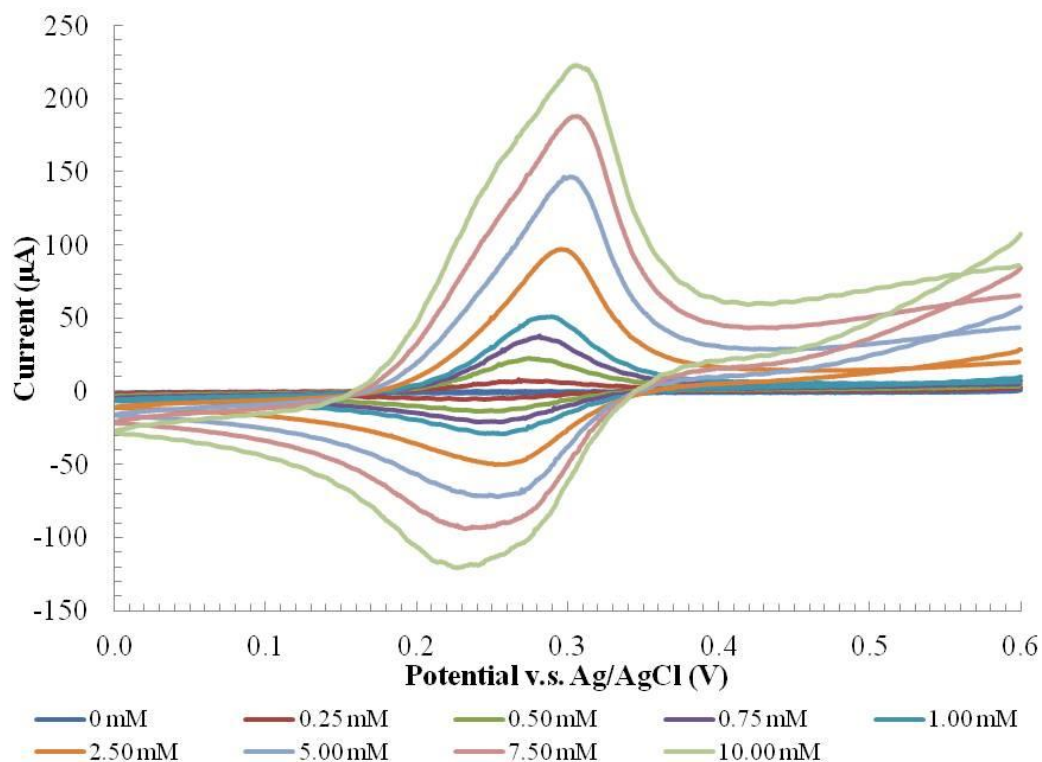


Figure 3-21 Concentration dependent CV profiles of 30 % LIG in 1,1'-ferrocene dimethanol  
CV scans of 30 % LIG in various concentrations of 1,1'-ferrocene dimethanol from 0 mM to 10 mM (Scan rate  $50 \text{ mV s}^{-1}$ )

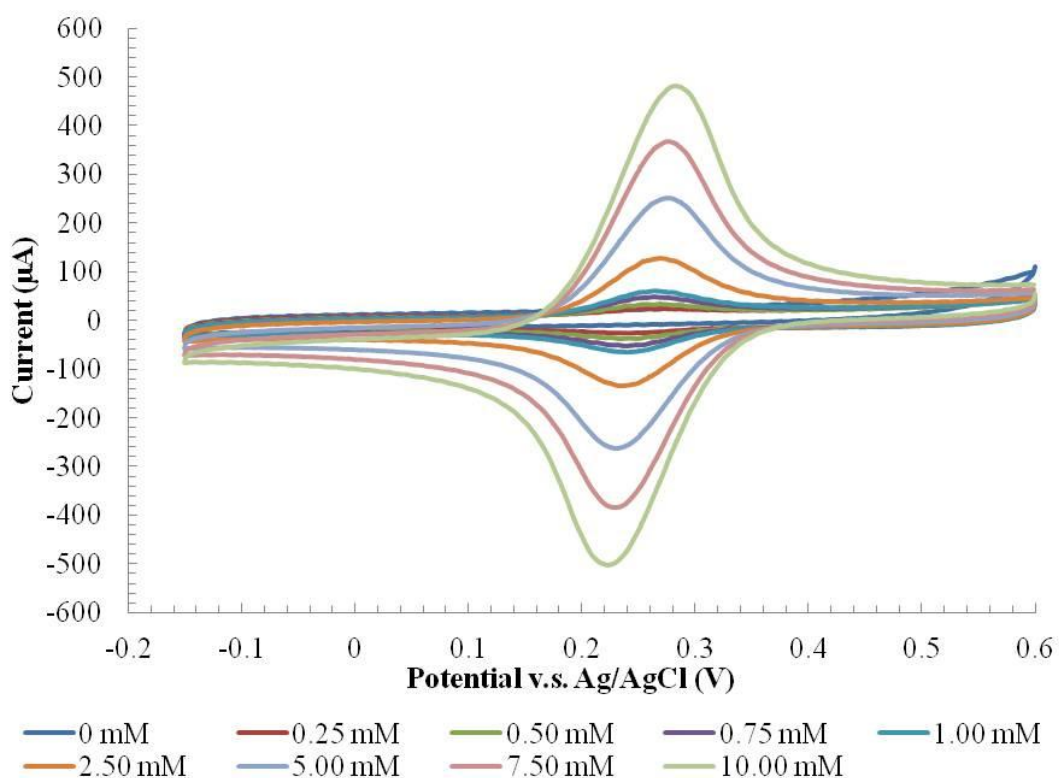
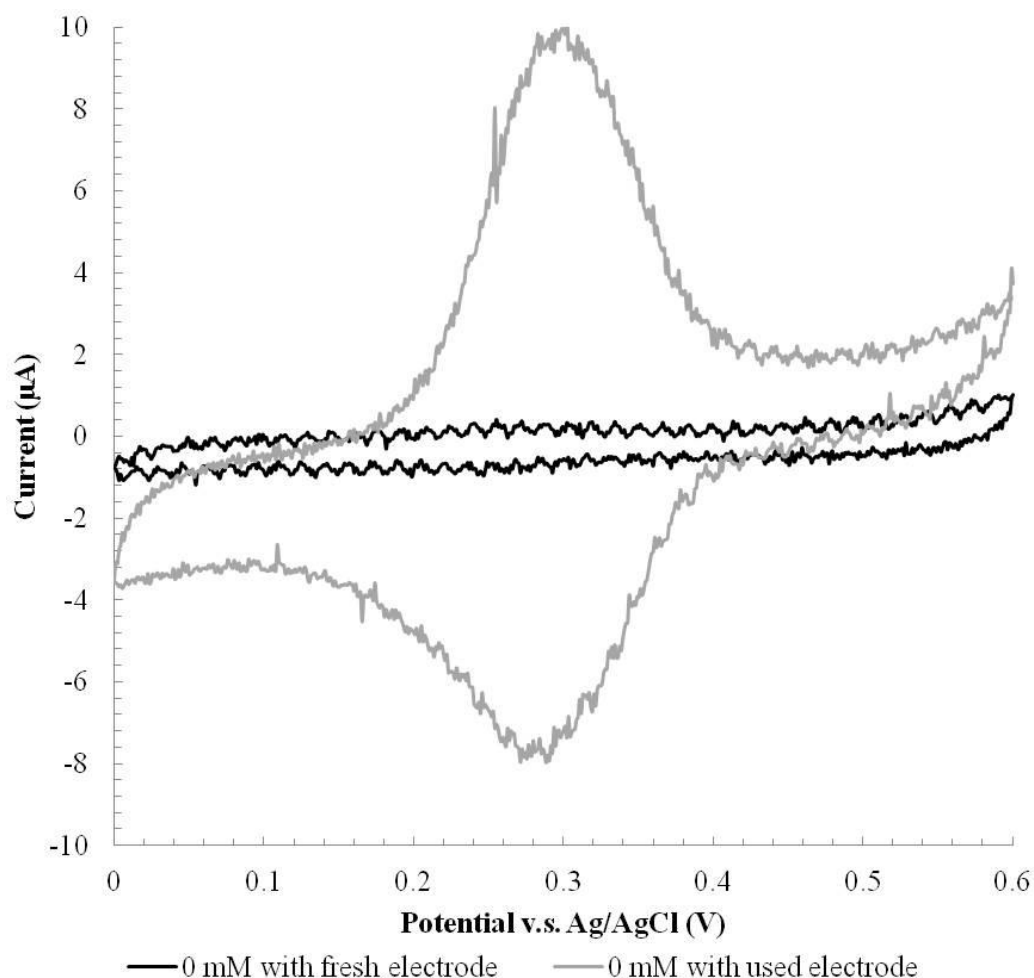


Figure 3-22 Concentration dependent CV profiles of 30 % LIG in potassium ferricyanide  
CV scans of 30% LIG in various concentrations of potassium ferricyanide from 0 mM to 10 mM (Scan rate  $50 \text{ mV s}^{-1}$ )

A final test was performed to confirm the porous nature of the LIG electrodes and that the redox species were entering the pores and behaving in a thin-layer manner. A 30% LIG electrode was placed in 1 M KCl electrolyte with 0 mM 1,1'-ferrocene dimethanol, a CV scan was performed to confirm the background capacitive current. The CV scan was then performed with the same electrode in 1 M KCl electrolyte containing 1 mM 1,1'-ferrocene dimethanol, the electrode was then rinsed under a flow of dH<sub>2</sub>O for 60 seconds and returned to the 1 M KCl electrolyte with 0 mM 1,1'-ferrocene dimethanol and a further CV scan performed after 5 minutes. The results of the scans in supporting electrolyte can be seen in Figure 3-23 where each CV shown was carried out in 1 M KCl. The initial CV performed with a new electrode can be seen to have a low background current response with no distinguishable peaks confirming that no redox reactions are occurring at the electrode within the scan window. However when the electrode is assessed following immersion and testing in 1 M KCl containing 1,1'-ferrocene dimethanol, despite electrode cleaning with a flow of dH<sub>2</sub>O, an oxidation and reduction peak can be observed with a peak separation of only 18 mV suggesting that the redox species is in fact trapped within the pores and behaving as would a redox species that was chemically linked to the surface following thin-layer behaviour and under no diffusional control (Barnes *et al.*, 2014). The results have shown that the LIG electrodes are porous in nature and that this can result in both reduced peak separation potentials and increased current responses for redox couples, this may confer advantages in sensing of biologically relevant molecules such as NADH which has a non-reversible process, where use of LIG electrodes may reduce the over-potential conferring an electrocatalytic effect (Punckt *et al.*, 2013).



*Figure 3-23 Entrapment of redox species in close proximity to the electrode surface within the pores of LIG shown by CV profiles*

*Cyclic voltammograms were used to confirm the entrapment of redox species in close proximity to the electrode surface within the pores of the electrode. 30% LIG electrodes are used with a scan rate of  $50 \text{ mV s}^{-1}$  in  $1 \text{ M KCl}$  supporting electrolyte.*

### 3.4 Conclusions

Electrochemical performance of standalone LIG electrodes has been systematically investigated against EPPG and LSG electrodes previously shown to have excellent electrochemical behaviour. Interestingly the LIG has shown electrochemical responses that could be said to be enhanced compared with LSG and EPPG due to its porous structure, confirmed by SEM and electrochemical studies, allowing a summative response of thin-film and diffusional redox behaviour. Following laser reduction the material is similar in composition to the LSG with high  $\text{sp}^2$  carbon content and low levels of oxygen functionalities remaining, allowing for efficient electron shuttling between the electrode and inner-sphere redox species. The simple method of producing LIG from Kapton<sup>®</sup> by  $\text{CO}_2$  laser ablation offers an opportunity to develop sensitive, cost effective disposable electrochemical sensors suited to clinical and environmental monitoring. Care must be

taken to optimise and control the laser intensity used to create the electrodes and also in the optimisation of sample delivery and measurement to enhance signals and precision of results. It has been shown here that a small variation in laser intensity used can significantly alter both physicochemical and electrochemical properties of the resultant material. Similar work performed recently by another group would appear to add to this belief, as they have used the same techniques to create what they refer to as laser scribed graphene from Kapton<sup>®</sup> and CO<sub>2</sub> laser irradiation (Nayak *et al.*, 2016). They have also characterised the material properties by Raman and SEM, with results supporting the work reported here. However, where their results and conclusions vary is in the electrochemical characterisation. Using ferricyanide as their inner-sphere mediator and alternatively ruthenium hexamine as an outer-sphere mediator they have calculated  $\Delta E_p$  values of their laser scribed graphene to be lesser than those for EPPG but that remain > 59 mV, thus have not observed the thin-layer response reported in this work. This may be due to this 'optimal' level of laser intensity required to create material that demonstrates such thin layer behaviour, they also do not according to the reportings observe any variation in CV profile with continuous cycling and extended periods of electrode incubation in electrolyte solution. Even with these differences in findings, the physicochemical characterisations compare well and both sets of data support the LIG having superior electrochemical performance to EPPG. With a manufacturing process similar to laser-scribed graphene (Griffiths *et al.*, 2014), this material could also be amenable to large scale mass manufacture of disposable planar three electrode systems with an electrodeposited Ag/AgCl pseudo-reference electrode.

### 3.5 References

- Banks, C.E. and Compton, R.G. (2005) 'Edge Plane Pyrolytic Graphite Electrodes in Electroanalysis: An Overview', *Analytical Sciences*, 21(11), pp. 1263-1268.
- Banks, C.E. and Compton, R.G. (2006) 'New electrodes for old: from carbon nanotubes to edge plane pyrolytic graphite', *Analyst*, 131(1), pp. 15-21.
- Barnes, E.O., Chen, X., Li, P. and Compton, R.G. (2014) 'Voltammetry at porous electrodes: A theoretical study', *Journal of Electroanalytical Chemistry*, 720–721(0), pp. 92-100.
- Brannon, J.H., Lankard, J.R., Baise, A.I., Burns, F. and Kaufman, J. (1985) 'Excimer laser etching of polyimide', *Journal of Applied Physics*, 58(5), pp. 2036-2043.
- Chang, S.C., Rawson, K. and McNeil, C.J. (2002) 'Disposable tyrosinase-peroxidase bi-enzyme sensor for amperometric detection of phenols', *Biosensors and Bioelectronics*, 17(11–12), pp. 1015-1023.
- Culková, E., Švorc, L., Tomčík, P., Durdiak, J., Rievaj, M., Bustin, D., Brescher, R. and Lokaj, J. (2013) 'Boron-doped diamond electrode as sensitive and selective green electroanalytical tool for heavy metals environmental monitoring: Zinc detection in rubber industry waste', *Polish Journal of Environmental Studies*, 22(5), pp. 1317-1323.
- Díaz Toro, P.C., Arévalo, F.J., Zon, M.A. and Fernández, H. (2015) 'Studies of the electrochemical behavior of moniliformin mycotoxin and its sensitive determination at pretreated glassy carbon electrodes in a non-aqueous medium', *Journal of Electroanalytical Chemistry*, 738, pp. 40-46.
- Dyer, P.E. and Sidhu, J. (1985) 'Excimer laser ablation and thermal coupling efficiency to polymer films', *Journal of Applied Physics*, 57(4), pp. 1420-1422.
- El-Kady, M.F., Strong, V., Dubin, S. and Kaner, R.B. (2012) 'Laser Scribing of High-Performance and Flexible Graphene-Based Electrochemical Capacitors', *Science*, 335(6074), pp. 1326-1330.
- Ferrari, A.C., Meyer, J.C., Scardaci, V., Casiraghi, C., Lazzeri, M., Mauri, F., Piscanec, S., Jiang, D., Novoselov, K.S., Roth, S. and Geim, A.K. (2006) 'Raman Spectrum of Graphene and Graphene Layers', *Physical Review Letters*, 97(18), p. 187401.
- Ge, J.J., Xue, G., Li, F., McCreight, K.W., Wang, S.-Y., Harris, F.W., Cheng, S.Z.D., Zhuang, X., Hong, S.-C. and Shen, Y.R. (1998) 'Surface studies of polyimide thin films via surface-enhanced Raman scattering and second harmonic generation', *Macromolecular Rapid Communications*, 19(12), pp. 619-623.
- Gorodetsky, G., Kazyaka, T.G., Melcher, R.L. and Srinivasan, R. (1985) 'Calorimetric and acoustic study of ultraviolet laser ablation of polymers', *Applied Physics Letters*, 46(9), pp. 828-830.
- Griffiths, K., Dale, C., Hedley, J., Kowal, M.D., Kaner, R.B. and Keegan, N. (2014) 'Laser-scribed graphene presents an opportunity to print a new generation of disposable electrochemical sensors', *Nanoscale*, 6(22), pp. 13613-13622.
- Gupta, A., Chen, G., Joshi, P., Tadigadapa, S. and Eklund (2006) 'Raman Scattering from High-Frequency Phonons in Supported n-Graphene Layer Films', *Nano Letters*, 6(12), pp. 2667-2673.
- Gutierrez, F., Comba, F.N., Gasnier, A., Gutierrez, A., Galicia, L., Parrado, C., Rubianes, M.D. and Rivas, G.A. (2014) 'Graphene paste electrode: Analytical applications for the quantification of dopamine, phenolic compounds and ethanol', *Electroanalysis*, 26(8), pp. 1694-1701.
- Ingram, J.M., Greb, M., Nicholson, J.A. and Fountain Iii, A.W. (2003) 'Polymeric humidity sensor based on laser carbonized polyimide substrate', *Sensors and Actuators B: Chemical*, 96(1–2), pp. 283-289.

- Ji, X., Banks, C.E., Crossley, A. and Compton, R.G. (2006) 'Oxygenated Edge Plane Sites Slow the Electron Transfer of the Ferro-/Ferricyanide Redox Couple at Graphite Electrodes', *ChemPhysChem*, 7(6), pp. 1337-1344.
- Keeley, G.P. and Lyons, M.E.G. (2009) 'The effects of thin layer diffusion at glassy carbon electrodes modified with porous films of single-walled carbon nanotubes', *International Journal of Electrochemical Science*, 4(6), pp. 794-809.
- Koren, G. and Yeh, J.T.C. (1984) 'Emission spectra, surface quality, and mechanism of excimer laser etching of polyimide films', *Applied Physics Letters*, 44(12), pp. 1112-1114.
- Kutluay, A. and Aslanoglu, M. (2013) 'Modification of electrodes using conductive porous layers to confer selectivity for the voltammetric detection of paracetamol in the presence of ascorbic acid, dopamine and uric acid', *Sensors and Actuators, B: Chemical*, 185, pp. 398-404.
- Lim, C.S., Chua, C.K. and Pumera, M. (2014) 'Detection of biomarkers with graphene nanoplatelets and nanoribbons', *Analyst*, 139(5), pp. 1072-1080.
- Lin, J., Peng, Z., Liu, Y., Ruiz-Zepeda, F., Ye, R., Samuel, E.L.G., Yacaman, M.J., Yakobson, B.I. and Tour, J.M. (2014) 'Laser-induced porous graphene films from commercial polymers', *Nat Commun*, 5.
- Nayak, P., Kurra, N., Xia, C. and Alshareef, H.N. (2016) 'Highly Efficient Laser Scribed Graphene Electrodes for On-Chip Electrochemical Sensing Applications', *Advanced Electronic Materials*, pp. n/a-n/a.
- Peng, Z., Lin, J., Ye, R., Samuel, E.L.G. and Tour, J.M. (2015) 'Flexible and Stackable Laser-Induced Graphene Supercapacitors', *ACS Applied Materials & Interfaces*, 7(5), pp. 3414-3419.
- Pimenta, M.A., Dresselhaus, G., Dresselhaus, M.S., Cancado, L.G., Jorio, A. and Saito, R. (2007) 'Studying disorder in graphite-based systems by Raman spectroscopy', *Physical Chemistry Chemical Physics*, 9(11), pp. 1276-1290.
- Ping, J., Wu, J., Wang, Y. and Ying, Y. (2012) 'Simultaneous determination of ascorbic acid, dopamine and uric acid using high-performance screen-printed graphene electrode', *Biosensors and Bioelectronics*, 34(1), pp. 70-76.
- Punckt, C., Pope, M.A. and Aksay, I.A. (2013) 'On the Electrochemical Response of Porous Functionalized Graphene Electrodes', *The Journal of Physical Chemistry C*, 117(31), pp. 16076-16086.
- Punckt, C., Pope, M.A. and Aksay, I.A. (2014) 'High Selectivity of Porous Graphene Electrodes Solely Due to Transport and Pore Depletion Effects', *The Journal of Physical Chemistry C*, 118(39), pp. 22635-22642.
- Punckt, C., Pope, M.A., Liu, J., Lin, Y. and Aksay, I.A. (2010) 'Electrochemical performance of graphene as effected by electrode porosity and graphene functionalization', *Electroanalysis*, 22(23), pp. 2834-2841.
- Randviir, E.P., Brownson, D.A.C., Gomez-Mingot, M., Kampouris, D.K., Iniesta, J. and Banks, C.E. (2012) 'Electrochemistry of Q-Graphene', *Nanoscale*, 4(20), pp. 6470-6480.
- Salinas-Torres, D., Huerta, F., Montilla, F. and Morallón, E. (2011) 'Study on electroactive and electrocatalytic surfaces of single walled carbon nanotube-modified electrodes', *Electrochimica Acta*, 56(5), pp. 2464-2470.
- Smits, F.M. (1958) 'Measurement of Sheet Resistivities with the Four-Point Probe', *Bell System Technical Journal*, 37(3), pp. 711-718.
- Srinivasan, R. (1986) 'Ablation of polymers and biological tissue by ultraviolet lasers', *Science*, 234(4776), pp. 559-565.

- Srinivasan, R., Hall, R.R. and Allbee, D.C. (1993) 'Generation of electrically conducting features in polyimide (Kapton<sup>TM</sup>) films with continuous wave, ultraviolet laser radiation', *Applied Physics Letters*, 63(24), pp. 3382-3383.
- Strong, V., Dubin, S., El-Kady, M.F., Lech, A., Wang, Y., Weiller, B.H. and Kaner, R.B. (2012) 'Patterning and Electronic Tuning of Laser Scribed Graphene for Flexible All-Carbon Devices', *American Chemical Society Nano*, 6(2), pp. 1395-1403.
- Strycharz, S.M., Malanoski, A.P., Snider, R.M., Yi, H., Lovley, D.R. and Tender, L.M. (2011) 'Application of cyclic voltammetry to investigate enhanced catalytic current generation by biofilm-modified anodes of *Geobacter sulfurreducens* strain DL1 vs. variant strain KN400', *Energy & Environmental Science*, 4(3), pp. 896-913.
- Tehrani, F. and Bavarian, B. (2016) 'Facile and scalable disposable sensor based on laser engraved graphene for electrochemical detection of glucose', *Scientific Reports*, 6, p. 27975.
- Wang, C., Du, J., Wang, H., Zou, C.e., Jiang, F., Yang, P. and Du, Y. (2014) 'A facile electrochemical sensor based on reduced graphene oxide and Au nanoplates modified glassy carbon electrode for simultaneous detection of ascorbic acid, dopamine and uric acid', *Sensors and Actuators B: Chemical*, 204(0), pp. 302-309.
- Wopschall, R.H. and Shain, I. (1967) 'Effects of adsorption of electroactive species in stationary electrode polarography', *Analytical Chemistry*, 39(13), pp. 1514-1527.
- Wynn, G.H. and Fountain, A.W. (1997) 'Development and Characterization of Electrochemical Devices Using Ultraviolet Laser Induced Carbonization of Polyimide Films', *Journal of The Electrochemical Society*, 144(11), pp. 3769-3772.

## Chapter 4. Electrochemical Detection of Biologically Relevant Molecules

### 4.1 Introduction

Electrochemistry is a useful tool in the detection of biological molecules such as dopamine (DA), ascorbic acid (AA) and uric acid (UA). dopamine (4-(2-aminoethyl)benzene-1,2-diol) is found throughout the body, it is both an important neurotransmitter and a hormone that plays a crucial role in renal, insulin and immune control. Within the brain it is implicated in motor control and reward pathways. However DA cannot cross the blood brain barrier, its synthesis and function as a neurotransmitter in the brain and hormonal chemical messenger at peripheral sites are independent of one another. Abnormal DA biochemistry levels can be indicative of Parkinson's disease (Calabresi *et al.*, 2009), schizophrenia (Howes *et al.*, 2012) and Huntington's disease (Esmaeilzadeh *et al.*, 2011). Routine use of DA testing in clinical biochemistry for such diseases is not yet fully appreciated, however an ability to determine levels within the body is essential to further understanding its role and action in such disease states. Dopamine levels are useful in clinical evaluation of catecholamine-secreting tumours where raised levels of DA in the urine can be used for both diagnosis and monitoring progression (Maclagan, 2013). Dopamine is a catecholamine and a phenethylamine, closely related to melanins (Fedorow *et al.*, 2005). In cells it is synthesised from L-DOPA, a precursor that is capable of crossing the blood-brain barrier (Hashimoto *et al.*, 2005) which itself is converted from the amino acid tyrosine (Figure 4-1). Dopamine is highly stable and water soluble at neutral to acidic pH levels however in basic conditions it becomes deprotonated, less soluble and particularly reactive thus being capable of spontaneous oxidation and formation of polydopamine (Lyngé *et al.*, 2011).

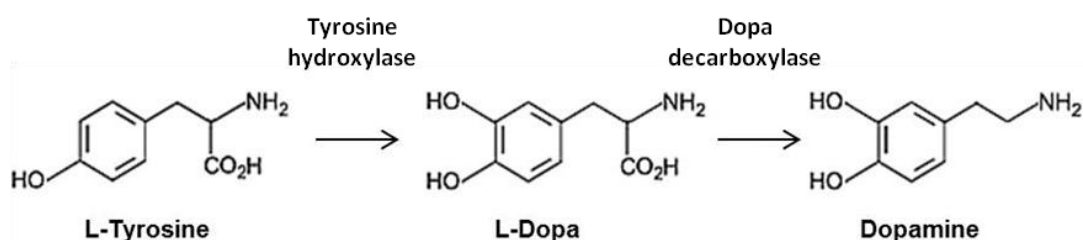


Figure 4-1 Synthesis of dopamine from tyrosine.

Ascorbic acid, also known as vitamin C is an essential nutrient for the maintenance of connective tissues and bones (van B. Robertson, 1961; Simon and Hudes, 2001), it has important antioxidant properties; being a reducing agent, scavenging free radicals (Tariq, 2007) and also functioning as a coenzyme in metabolic pathways (Sealock and Goodland, 1951). Lack of AA can lead to the condition scurvy and having sufficient levels is believed to improve immunity and play a role in cancer prevention. Ascorbic acid must be taken in from the diet, citrus fruit and vegetables contain high levels (Szeto *et al.*, 2002), it is neither created nor stored by the body, and excess is passed in the urine (Davies *et al.*, 1992). As AA is available from many foods and often taken as a supplement it is possible to find it in urine samples at a wide range of concentrations, and concentrations can greatly exceed those of urine metabolites of clinical significance, thus having potential to cause interference in urine testing for analytes such as dopamine and glucose. The interferent effect can be due to its effect on the pH of the urine and in the case of electrochemical testing due to potential overlapping of peak potentials with other analytes. Another metabolite worthy of investigation when considering electrochemical analysis of urine samples is UA, which is excreted in the urine as an end product of purine metabolism. Uric acid is associated with diabetes (Dehghan *et al.*, 2008; Johnson *et al.*, 2013) and high concentrations can lead to gout (Magnus-Levy, 1910; Seegmiller *et al.*, 1962; Martinon *et al.*, 2006) and kidney stones (Taylor *et al.*, 2005). This is due to the chemical nature of UA which forms crystals at biological pH, deposits of these crystals lead to pain and blockages. On the other hand, low levels of UA can also be indicative of disease, as an association has been suggested between low levels of UA and multiple sclerosis (Sotgiu *et al.*, 2002; Marcus and Jacques De, 2006). Finally nicotinamide adenine dinucleotide (NADH) was selected as a fourth electro-active biological molecule for study. NADH is a co-enzyme involved in many metabolic redox reactions within cells involving dehydrogenase enzymes and thus is important for numerous functions throughout the body. Unfortunately oxidation of NADH at standard electrodes requires a large potential, typically +0.6 V and above and its oxidation product causes fouling of the electrodes. Direct oxidation of NADH has therefore been relatively unsuccessful with low sensitivity achieved, however use of carbon based nanomaterials has shown some promise in reducing the over-potential required (Musameh *et al.*, 2002; Arvinte *et al.*, 2007; Zhang *et al.*, 2011). Detection of these analytes has been reported using a variety of techniques including HPLC (Zhao *et al.*, 2011), chemiluminescence (Liu *et al.*, 2014b), capillary electrophoresis (Zhao *et al.*, 2008) and electrochemistry. The electrochemical redox reactions of DA, AA, UA and NADH can be seen in Figure 4-2.

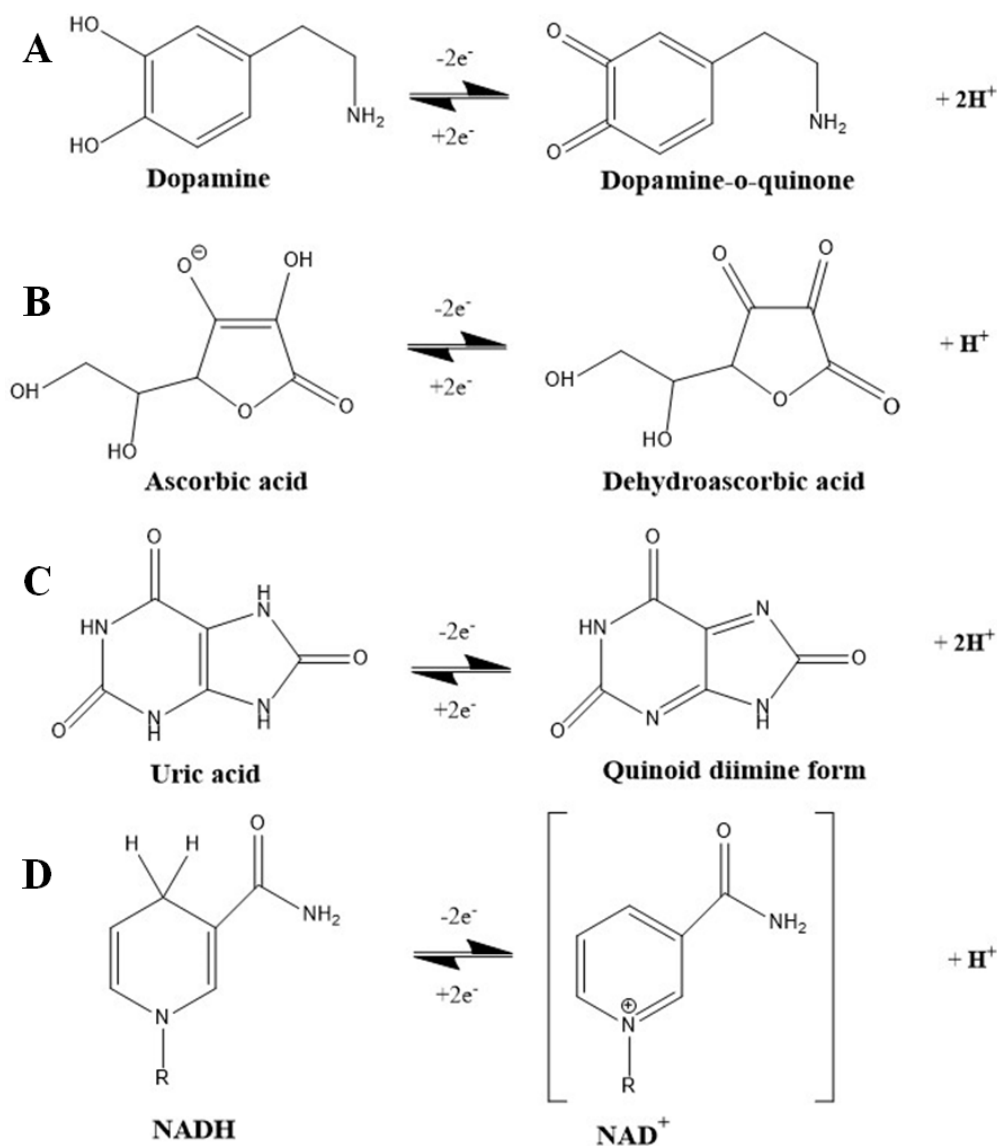


Figure 4-2 Electrochemical redox reactions for (A) dopamine, (B) ascorbic acid, (C) uric acid and (D) NADH

Electrochemical detection of course offers a low cost method with high sensitivity and ease of integration into point of need sensor systems however detection of these analytes can be problematic. The quasi-reversible nature of the electrochemical reaction of DA (Liu *et al.*, 2014a), its low concentration compared with known interferences and fouling of conventional electrode surfaces has resulted in a large body of research into various means of reducing these problems. Oxidation products of AA are also known to adsorb to electrode surfaces. The use of alternative electrode materials including conductive layers (Kutluay and Aslanoglu, 2013; Pakapongpan *et al.*, 2014), nanoparticles (Kaur *et al.*, 2013; Wang *et al.*, 2013), redox mediators (Kumar *et al.*, 2008; Tang *et al.*, 2008) and self-assembled films (Retna Raj and Ohsaka, 2003; Raouf *et al.*, 2010) have been investigated as a means to producing a viable electrochemical DA sensor. Improvements have been

made but often at the cost of introducing drawbacks such as expensive and costly manufacturing processes.

The analytes also oxidise at similar potentials when using standard conventional electrode materials. Carbon materials have been investigated for use in electrochemical analysis of urine samples and have been shown to separate the peak potential of AA from that of DA, with more recent work focussed around the use of graphene. Many graphene formats have been considered including pristine graphene (Qi *et al.*, 2015), graphene paste electrodes (Gutierrez *et al.*, 2014), graphene modified GCE (Han *et al.*, 2010; Gao *et al.*, 2013; Tang *et al.*, 2014), screen printed electrodes containing graphene (Ping *et al.*, 2012), 3D graphene foams (Xiao *et al.*, 2014), the use of dopants (Feng *et al.*, 2015) and nanoparticles including metal and carbon nanotubes (Li *et al.*, 2012; Jiang and Du, 2014; Wang *et al.*, 2015) particularly in the case of rGO which offers an excellent support for modification due to its residual oxygen functional groups. Here we investigate the use of LSG and LIG as electrode materials for detection of DA, AA, UA and NADH and for distinguishing peak potentials of DA, AA and UA using Differential Pulse Voltammetry (DPV) for simultaneous detection. It was postulated that the rapid electron transfer rate, optimal C:O ratio and unique surface morphologies of these materials could result in improved detection limits and specificity due to increased current densities, peak potential separation and narrow symmetrical peak responses.

## **4.2 Experimental**

### **4.2.1 Materials**

All chemicals were of analytical grade and purchased from Sigma-Aldrich (Dorset) unless otherwise stated including the  $\beta$ -nicotinamide adenine dinucleotide, reduced dipotassium salt, dopamine hydrochloride, uric acid and L-ascorbic acid. The graphite powder was sourced from Bay carbon Inc (Michigan). Polyethylene terephthalate (PET, Niceday Guilbert) was used as a flexible substrate for GO deposition. The Lightscribe DVDs were Verbatim 43643 16x DVD-R Lightscribe enabled, the DVD drive a LG GP08LU11 8x External DVDRW and these were used in conjunction with standard Hewlett Packard Lightscribe software. Spraymount, Kapton<sup>®</sup> tape, conductive copper tape and adhesive silver paint used in creating LSG and LIG electrodes were sourced from RS components (Northants). A standard 50 mM pH 7.0 PBS solution was used containing 137 mM NaCl and 2.7 mM KCl as supporting electrolyte unless otherwise stated.

Electrochemical measurements were performed using an Autolab electrochemical workstation (Ecochemie) and general purpose electrochemical system software. Experiments were performed with a standard three electrode configuration with a Ag/AgCl reference electrode (BASi, West Lafayette, USA) and a platinum counter electrode of 3mm diameter (BASi, West Lafayette, USA), using a 3 mm diameter LSG, LIG, EPPG or GCE (both EPPG and GCE from IJ Cambria Scientific Ltd, Llanelli) working electrode as specified.

#### **4.2.2 Manufacture of Electrodes**

Laser-scribed graphene electrodes were prepared from GO produced via a modified Hummers method (Hummers and Offeman, 1958; Tung *et al.*, 2009). A GO solution was then prepared where 0.05 g GO was suspended in 16 ml dH<sub>2</sub>O and sonicated at 55 °C for 90 minutes. A light-scribe DVD was covered with PET using spraymount to hold in place. The GO solution was then drop cast onto the PET coated DVD immediately following sonication and allowed to dry overnight at room temperature. Once dry, the GO coated disc was placed into a light-scribe enabled drive and laser reduced to form LSG on a flexible PET substrate. This could then be utilised as an electrode. Conductive silver paint was used to connect copper tape to the LSG film for ease of use with the Autolab system and Kapton<sup>®</sup> tape was utilised to passivate the surface leaving only a 3mm diameter LSG window to act as the electrode working area as detailed in previous work (Griffiths *et al.*, 2014).

Laser-induced graphene electrodes were prepared as described in chapter 3 where Kapton<sup>®</sup> tape was transformed into LIG utilising a CO<sub>2</sub> laser (Figure 3-2). The electrodes were then constructed in the same manner as LSG electrodes using LIG material in place of LSG.

#### **4.2.3 Electrode Material Characterisation**

Nexus at nanoLAB (Newcastle University) performed XPS measurements of the samples of GO and LSG. Full spectrum surveys were analysed as well as the C<sub>1s</sub> and O<sub>1s</sub> peaks at 284 eV and 532 eV respectively in order to confirm the absence of contaminants and the level of reduction following laser irradiation. CasaXPS was used to analyse the data and to confer the bond composition of the GO and LSG using peak fitting.

#### **4.2.4 Electrochemistry**

Initial electrochemical analysis of DA, UA, AA and NADH was performed using CV. Scans were performed in PBS at a scan rate of 10 mV s<sup>-1</sup> with 5 mM analyte and the potential was ramped between +1.0 V and -0.2 V with a 1 mV step potential. Each scan was

performed four times and the first result discarded to allow for electrode equilibration, scans shown here represent the mean of three scans. The CV performance of LSG, LIG, GCE and EPPG electrodes in DA, UA, AA and NADH were compared, where all electrodes had a 3mm diameter electrode surface. Edge plane pyrolytic graphite was selected for comparison as it is widely regarded as the gold standard of carbon electrodes.

Differential pulse voltammetry was used as a more sensitive technique than CV for the simultaneous detection of 1 mM DA, AA and UA in PBS with both LSG and EPPG electrodes. The parameters used were 0.05 s modulation time, 0.5 s interval time, initial potential of -0.2 V, end potential 0.7 V, step potential 0.005 V and modulation amplitude at 0.025 V. Baseline corrections were performed using a moving average peak width of 0.01. Following the initial experiment to confirm whether LSG electrodes could distinguish three peaks for DA, AA and UA further experiments were performed to confirm dose dependent responses for each of these biologically relevant molecules and compared to the result when using an EPPG electrode. A calibration curve was produced from triplicate measurements for DA within the clinically relevant range of 0-10  $\mu$ M in PBS using LSG and this was then repeated in the presence of 0.5 mM AA and 0.1 mM UA.

## **4.3 Results and discussion**

### **4.3.1 Characterisation of Electrode Materials**

Electrode materials have been thoroughly characterised and the results presented in earlier chapters (LSG: Chapter 2, LIG: Chapter 3), however a new batch of GO was manufactured in house following a modified Hummers method (Hummers and Offeman, 1958; Tung *et al.*, 2009) including extensive wash procedures ensuring low levels of contaminants. Metal impurities within carbon based electrodes can significantly affect the electrochemical behaviour, adding summative electrocatalytic effects thus thorough washing was critical (Merisalu *et al.*, 2010; Sánchez Arribas *et al.*, 2013). The quality and composition of the new GO was confirmed by XPS and electrochemical measurements. First the GO was deposited onto a flexible PET substrate and using lightscribe technology the GO was thermally reduced by the lightscribe laser to produce laser-scribed graphene (El-Kady *et al.*, 2012; Strong *et al.*, 2012; Griffiths *et al.*, 2014), a material that was earlier shown to have an expanded structure with increased surface area, larger numbers of edge sites and greater conductivity compared with the precursor GO film. The XPS data shown in Figure 4-3 confirms the reduction of GO to LSG with an oxygen content of 56.5% reduced to only 3.9% following the lightscribe laser reduction process. Peak fitting to the C<sub>1s</sub> peak also demonstrates the high sp<sub>2</sub> content in the LSG sample, confirming the

graphene bond configuration has been achieved, further supported by a  $\pi$  satellite  $C=C^*$  resonance at approx. 292 eV that can be observed when analysing this samples  $C_{1s}$  peak.

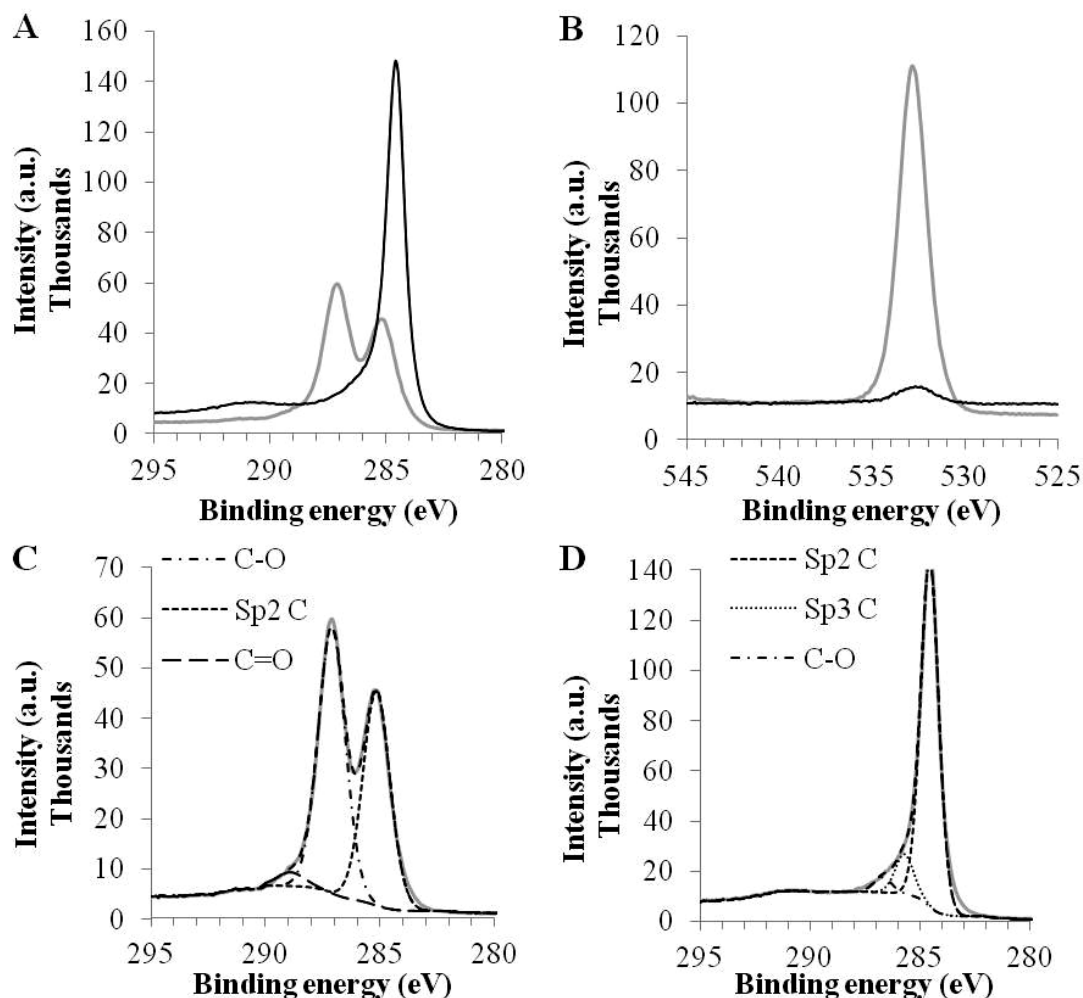


Figure 4-3 X-ray photoelectron spectroscopy of GO and LSG  $C_{1s}$  (A) and  $O_{1s}$  (B) peak of GO (grey) and LSG (Black). Further analysis of the  $C_{1s}$  peak of GO (C) and LSG (D), demonstrates a reduction in oxygen content from 56.5% to 3.9% following laser reduction.

#### 4.3.2 Electrochemical Detection of Biologically Relevant Molecules

Both LSG and LIG electrodes have previously been shown to outperform EPPG and single layer CVD graphene electrodes using standard inner- and outer-sphere redox species such as 1,1'-ferrocene dimethanol and potassium ferricyanide. However it is important to consider their use in the detection of biologically relevant molecules in order to further evidence their use as clinically relevant electrochemical sensors and point of care testing platforms. Here the ability of the new graphene materials to detect DA, UA, AA and NADH via cyclic voltammetry has been compared with standard EPPG and GCE electrodes. The results in Figure 4-4 demonstrate that LSG and LIG both have potential to out-perform not only GCE but also EPPG for this purpose. The oxidation potential of the four analytes

tested occurred at lower potentials at LSG and LIG electrodes compared with EPPG and in the case of DA, UA and AA the oxidation peak current response was greater with LSG electrodes. With DA both LSG and LIG perform well against EPPG with peak potentials of +0.376 V, +0.221 V and +0.830 V respectively. The greatest current response is observed with LIG followed by LSG, thus both graphene materials tested may prove effective for DA detection. In the case of UA detection by CV, LIG and LSG electrodes show much sharper oxidation peak than the EPPG and at a much lowered potential at +0.361 V (LIG) and +0.362 V (LSG) opposed to +0.629 V for EPPG. In this case again the current response was greatest with LIG with LSG also performing well, demonstrating a current response double that of EPPG. The sharpest oxidation peak and the lowest potential in the detection of AA was achieved with LIG, the current peaked at +0.002 V, lower than the LSG at +0.221 V and EPPG at +0.583 V, however it showed the lowest peak current. Finally detection potentials for NADH were reduced with both LIG (+0.340 V) and LSG (+0.487 V) compared with EPPG at +0.733 V, though peak current response was not improved. Compared with EPPG, LSG and LIG demonstrated a similar current response. The GCE performed poorly with all four analytes demonstrating no discernible peaks within the scan windows.

Further investigation of DA, UA and AA individually with DPV demonstrated the outstanding ability of LSG compared with EPPG electrodes. The LSG electrodes are shown as a representative example that improvements in the electrochemical response can be engendered by refining the electrochemical technique and utilising DPV analysis of electrode materials whilst the LIG electrode manufacture and use was being further optimised. Dose dependent current responses were of greater magnitude for all tested analytes with LSG than with EPPG and a reduced oxidation potential was observed with UA and AA. The DA response with LSG was at a similar potential as EPPG but its peak was not only much greater but also more symmetrical. The potential of AA was reduced from +0.332 V with EPPG to -0.049 V with LSG and for UA from +0.396 V to +0.274 V (Figure 4-5) thus having greater potential for simultaneous detection of these analytes with LSG than with EPPG. It can be seen that with both EPPG and LSG peak shape and peak potential can change with increasing analyte concentration, this is most likely due to the experimental design where electrodes were not cleaned between measurements in order to control the process between EPPG and LSG as LSG electrodes cannot be physically re-generated in the same manner as EPPG electrodes. It would be envisaged that future commercial LSG electrodes in clinical diagnostics would be single use, evading the

cleaning issue. The minimal peak shift observed due to the experimental design did not hinder our evaluation of the electrode performance, as demonstrated herein.

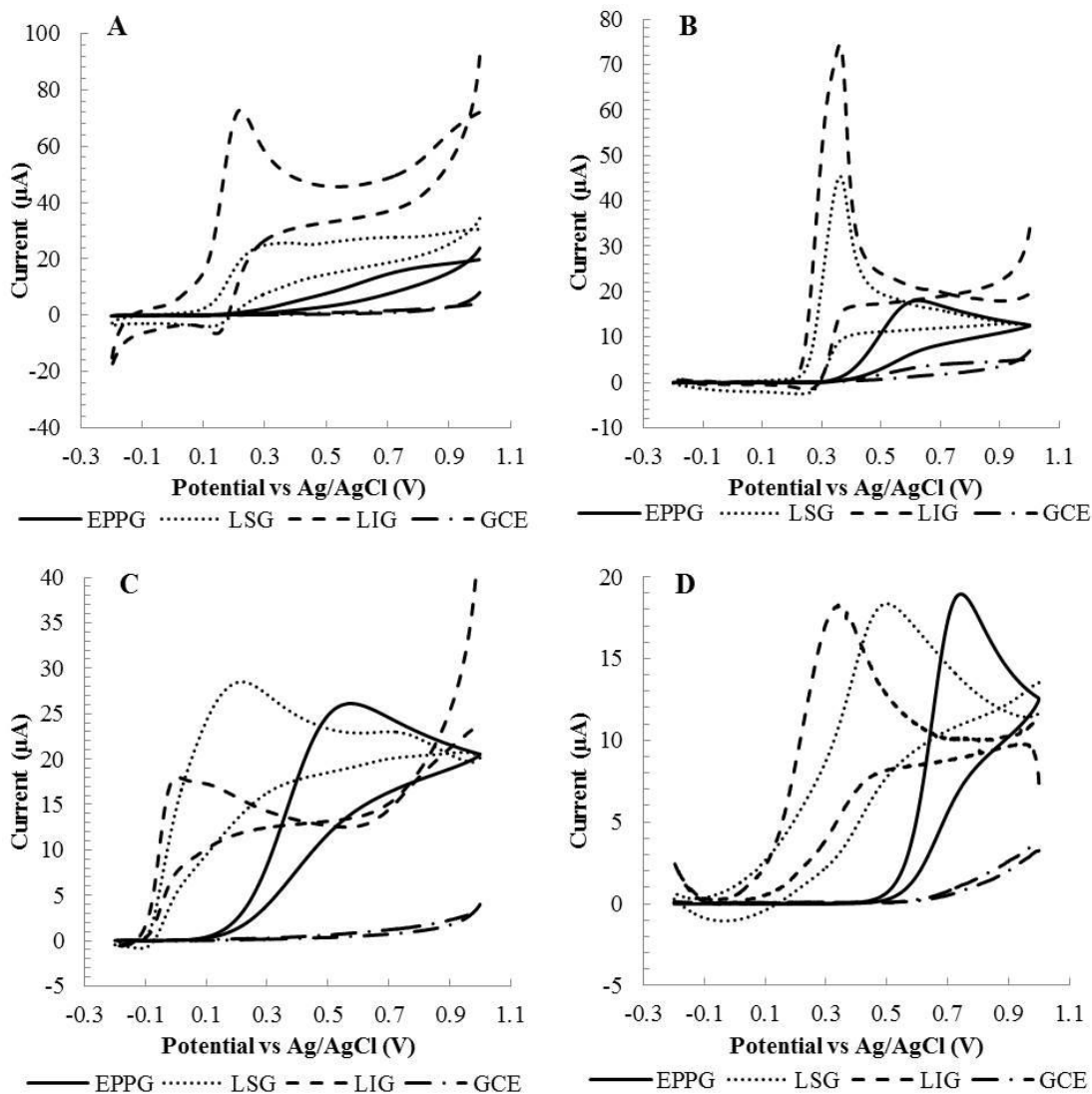


Figure 4-4 Cyclic voltammograms of electrodes in electroactive analytes A) 5 mM dopamine, B) 5 mM uric acid, C) 5 mM ascorbic acid and D) 5 mM NADH at EPPG, LSG, LIG and GCE electrodes at a scan rate of  $10 \text{ mV s}^{-1}$ .

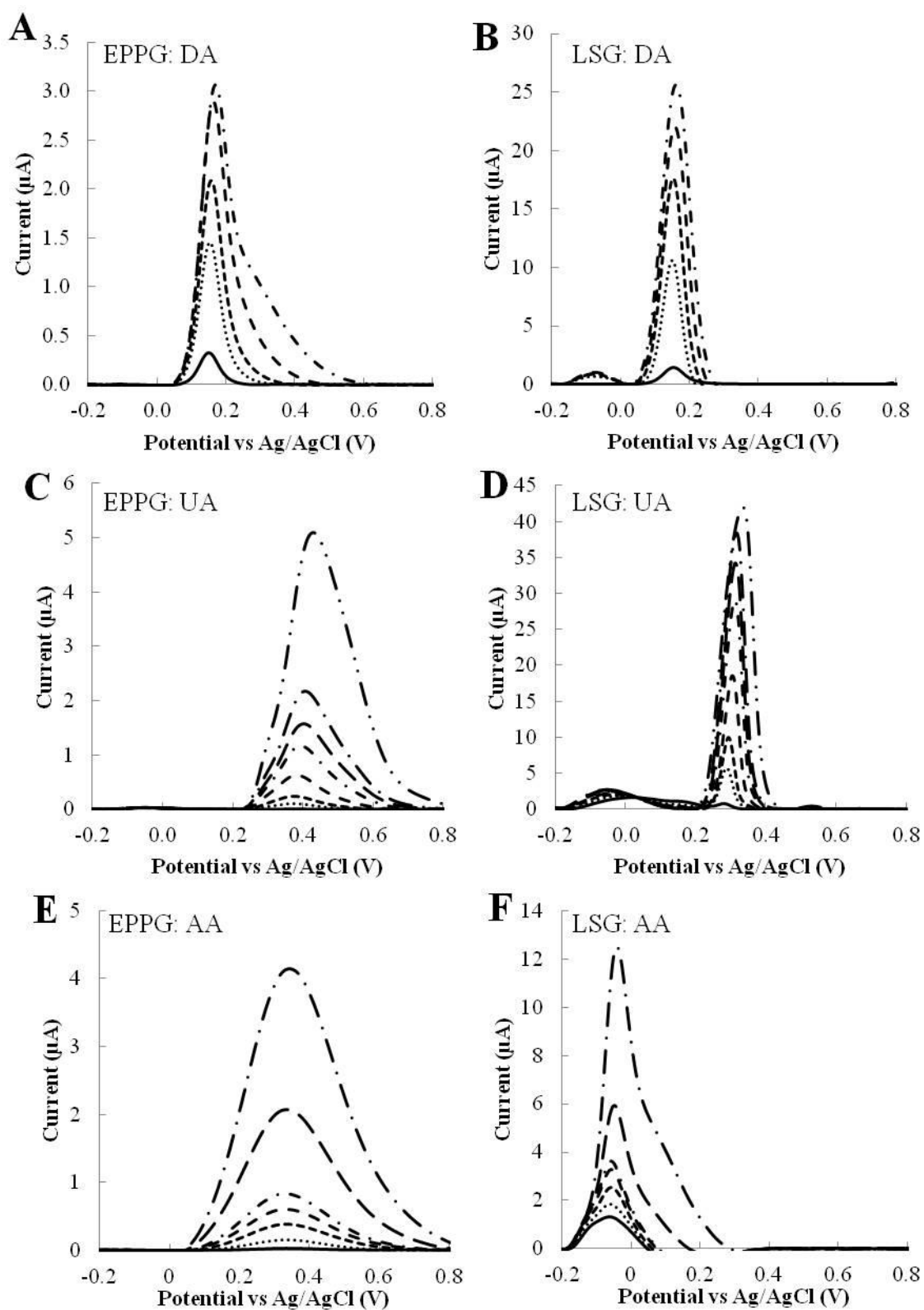


Figure 4-5 Differential Pulse Voltammetry profiles of various analytes with EPPG and LSG electrodes dopamine (A,B) at 10, 50, 100, 250 and 500  $\mu\text{M}$ , (C,D) uric acid at 10, 50, 100, 250, 500, 750, 1000 and 2500  $\mu\text{M}$  and (E,F) ascorbic acid at 0.1, 0.25, 0.5, 0.75, 1.0, 2.5 and 5 mM with EPPG (A,C,E) and LSG (B,D,F) electrodes.

### 4.3.3 Simultaneous Detection of Dopamine, Ascorbic Acid and Uric Acid

It can be seen from the CV results in Figure 4-4 that the peak potentials for the three analytes DA, AA and UA are likely to overlap even in the case of the LSG electrodes. To detect all three simultaneously in a solution would not be possible using the CV technique. However, DPV offering improved sensitivity for individual detection of DA, UA and AA and increased peak separation as seen in Figure 4-5 could also be used for simultaneous detection of multiple analytes. Differential pulse voltammetry profiles for EPPG, GCE, LSG, and LIG electrodes in a solution containing 50  $\mu\text{M}$  dopamine, 100  $\mu\text{M}$  uric acid and 500  $\mu\text{M}$  ascorbic acid in PBS are shown in Figure 4-6. It can be seen that even using this technique the EPPG, the 'gold standard' of carbon electrodes cannot distinguish three peaks relating to the analytes in solution, with only two peaks consistently detected at -0.16 V and 0.42 V. The GCE also only detects two peaks at -0.08 V and 0.15 V. Use of LSG electrodes begins to differentiate the three peaks but with some overlap at 0.03 V, 0.16 V and 0.29 V. The greatest performance in terms of peak separation and peak current response is achieved with the LIG electrodes with peaks detected at -0.02 V, 0.14 V and 0.28 V. This can be attributed to the porous nature creating an increased surface area for current response and thin film diffusional behaviour giving altered peak potentials allowing for distinction of various analytes of interest. The effects of electrode morphology have often been overlooked when analysing electrochemical performance of carbon based electrodes whose functions have been improved with the addition of e.g. graphene layers to underlying electrodes and enhancements have generally been ascribed to the catalytic behaviour of the added materials. Yet, a small number of groups in the field have begun to acknowledge the power of electrode morphology. It has been demonstrated that an increased depth of porous layer can reduce the  $\Delta E_p$ , whilst increasing the peak current and capacitive background, but only up to a critical point in which the  $\Delta E_p$  will begin to increase again as it becomes more difficult for electrons and ions to travel through the structure (Punckt *et al.*, 2013). The scan rate will also influence whether the thin film or diffusional behaviour becomes more dominant and at higher scan rates the electrode performance will be more similar to that of a corresponding flat surfaced electrode (Punckt *et al.*, 2013). In a similar manner to depth of the porous structure pore size will have an impact, as pores become smaller, thin layer behaviour will take precedent until the pores become so small that they in fact hinder diffusive transport into the pore. These effects of pore size and depth of porous structure have a twofold effect in terms of detection of multiple analytes from solution in that it has potential to reduce over potentials and increase the current response with greatly increased surface

area (Punckt *et al.*, 2013). The recent publication showing similar work with CO<sub>2</sub> laser reduced Kapton<sup>®</sup> also demonstrated simultaneous detection of DA, AA and UA with an apparent larger separation of peaks by DPV (Nayak *et al.*, 2016), although these were each tested at 1 mM as opposed to 50 μM dopamine, 100 μM uric acid and 500 μM ascorbic acid shown here and larger concentrations of analyte can cause a small shift in the peak positions which may be due to limitations in electrode response and also changes in solution pH caused by addition of various analytes at high levels and at varied ratios.

It should be noted that the DPV profile shown for LSG in Fig 4-6 represents the typical behaviour observed with the electrodes, however some electrodes demonstrated peak currents 10 times this example, which can only be attributed to the variation in pore size, accessible surface area and edge defects/oxygen content variation observed upon small changes in laser power when creating these electrodes with a CO<sub>2</sub> laser engraver not built for this purpose which appears to require a very narrow tolerance.

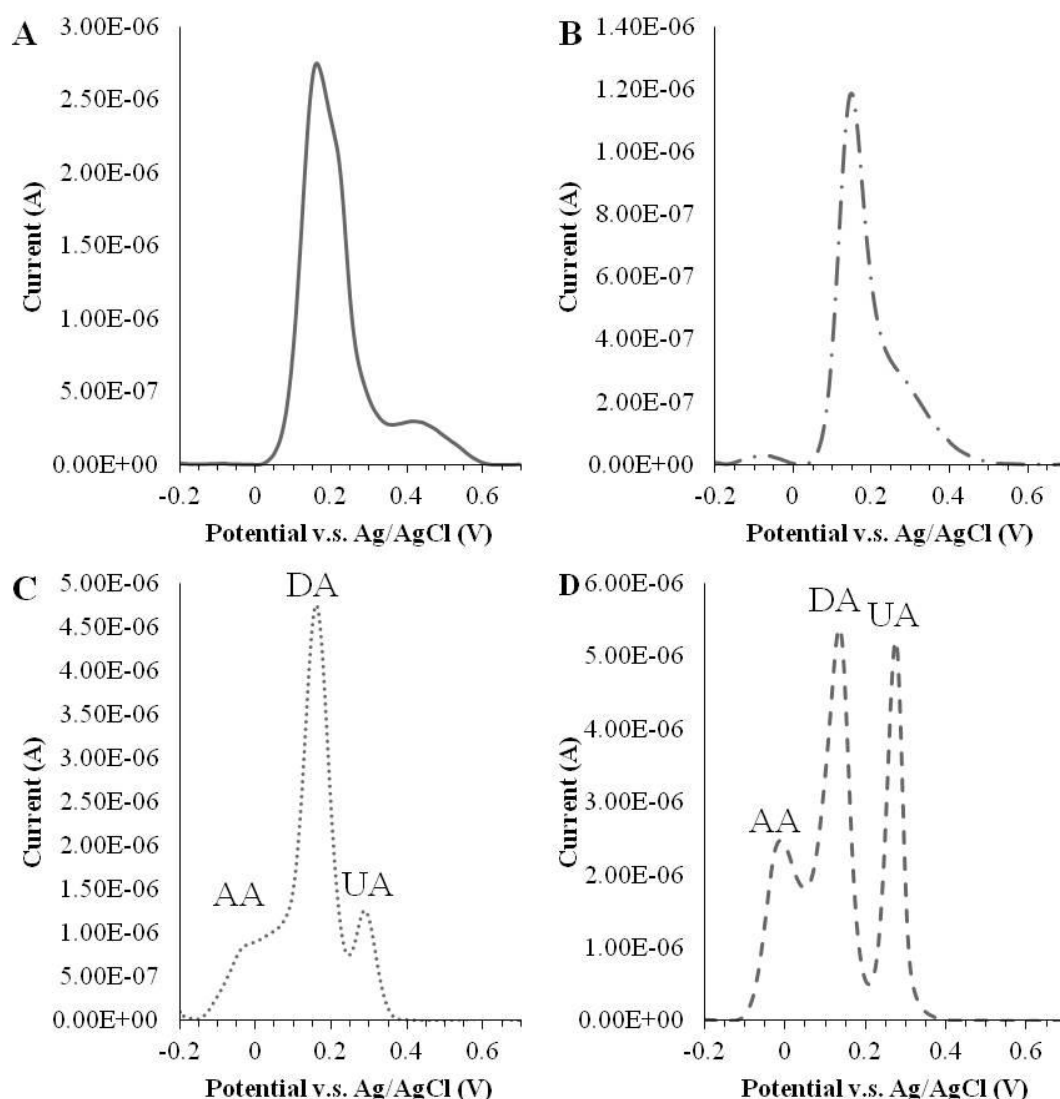


Figure 4-6 Differential Pulse Voltammograms of solution containing multiple analytes at various electrodes. The solution contained 50  $\mu\text{M}$  dopamine, 100  $\mu\text{M}$  uric acid and 500  $\mu\text{M}$  ascorbic acid in PBS at (A) EPPG, (B) GCE, (C) LSG and (D) LIG electrodes.

The use of LSG and LIG electrodes for the detection of DA was tested further; to produce a dose response curve and to assess interference from UA and AA, analytes known to cause interference in the detection of DA when using conventional electrodes (Safavi *et al.*, 2006; Zheng *et al.*, 2009; Alwarappan *et al.*, 2010). The concentrations of interferents were chosen in line with existing literature (Ping *et al.*, 2012; Li *et al.*, 2013; Jiang and Du, 2014; Liu *et al.*, 2014c; Tang *et al.*, 2014; Yang *et al.*, 2014). The DPV profiles for DA detection at 1, 2, 4, 6, 8 and 10  $\mu\text{M}$  in 50 mM PBS were compared with those in 50 mM PBS, 0.5 mM AA, 0.1 mM UA. The DA peak current appeared at +0.132 V and was unchanged regardless of the presence or absence of 0.5 mM AA and 0.1 mM UA. This is most likely due to the improved peak separation observed with LSG when using the DPV techniques compared to EPPG electrodes. The improved electrode performance can be

attributed to the optimal oxygen to carbon ratio of the LSG for electrochemistry and its excellent heterogeneous electron transfer rate as demonstrated in earlier work (Griffiths *et al.*, 2014). The calibration curves comparing the peak current at 0.132 V for DA detection at concentrations from 1-10  $\mu\text{M}$  when alone in PBS or with the addition of 0.5 mM AA and 0.1 mM UA can be seen in Figure 4-7 for both LSG and LIG electrodes. It can be seen that a linear dose response is achieved across this range, which is of importance to clinical detection of DA in urine samples. LSG electrodes provide a more linear response with  $R^2$  values of 0.995 in absence and presence of interferents than LIG electrodes with  $R^2$  values of 0.987 in PBS and 0.973 in a solution containing interferents. LSG results are less effected by the presence of interferents than the LIG electrodes (at the concentrations tested here). No interference effect is observed with the detection of DA when using LSG electrodes with DPV thus placing LSG in good stead as a clinically relevant electrochemical sensor. The limit of detection (LoD) was determined from the slope of the calibration curves and 3 SD, in PBS this was calculated as 0.33  $\mu\text{M}$  and in the presence of 0.5 mM AA and 0.1 mM UA was determined to be similar at 0.17  $\mu\text{M}$  with LIG faring better at 0.103  $\mu\text{M}$ . The measurement of DA in PBS revealed a sensitivity of 202  $\text{nA } \mu\text{M}^{-1}$  for the LSG electrode compared with 228  $\text{nA } \mu\text{M}^{-1}$  in the presence of 0.5 mM AA 0.1 mM UA and again was similar with the LIG electrodes tested at 200  $\text{nA } \mu\text{M}^{-1}$  and 277  $\text{nA } \mu\text{M}^{-1}$  respectively across the linear dopamine concentration range of 0-10  $\mu\text{M}$ . Dopamine response was tested beyond 10  $\mu\text{M}$  to 50  $\mu\text{M}$ , a dose response was observed but did not remain linear. It should be noted that this data was collected before the optimal method of LIG production and electrochemical testing had been determined as per results described in Chapter 3 and so with further testing and development may in fact far out-perform the LSG. Similar work reported recently, using the same electrode material has demonstrated a linear response to DA across the range of 0.5-32.5  $\mu\text{M}$  which was improved with the addition of platinum nanoparticles (Pt NPs) at the electrode surface to increase the current response and assay range to 0.5-56  $\mu\text{M}$  (Nayak *et al.*, 2016).

The results using LSG and LIG electrodes were compared with examples from recent literature of graphene/GO based electrodes for detection of DA using the DPV technique (Table 4-1). These examples taken from a range of journals across the period of 2010-2015 demonstrate an overwhelming use of graphene/GO in electrochemical detection, yet most often as a modification to an underlying electrode, as opposed to standalone electrodes as is detailed here with LSG.

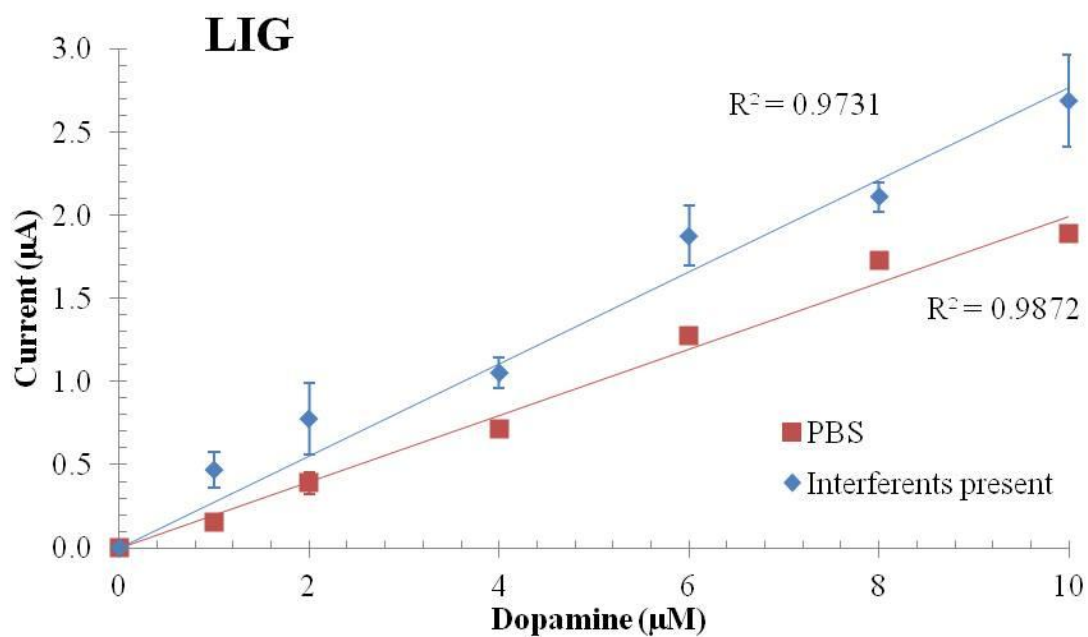
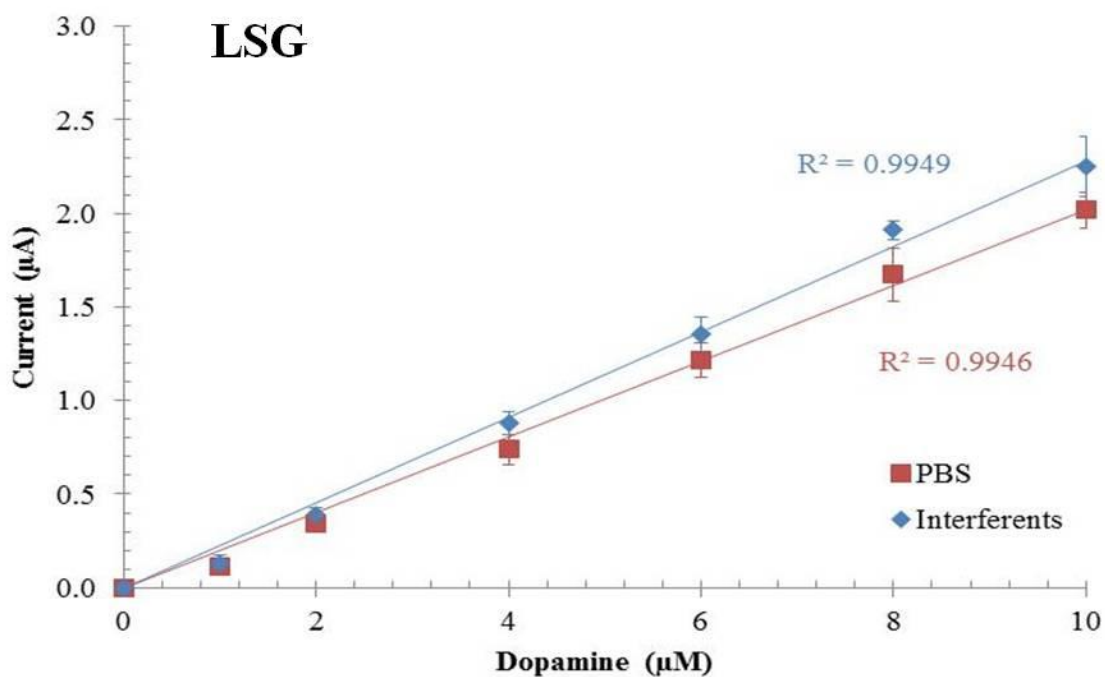


Figure 4-7 Dopamine calibration curves with LSG and LIG electrodes  
 Taken from the DPV current response at +0.132 V vs Ag/AgCl with LSG (top) and LIG electrodes (Bottom) in PBS and in PBS plus interferents (0.5 mM AA and 0.1 mM UA). (Mean of n=3 and 1 sd error bars shown).

Table 4-1 Analytical parameters for dopamine detection by DPV

Reference	Material	Potential (V)	Linear range ( $\mu\text{M}$ )	Limit of detection ( $\mu\text{M}$ )	Conditions
(Han <i>et al.</i> , 2010)	Chitosan-Graphene-GCE	+0.185	1-24	1.00	50 mM PBS pH 7.0 0.1 mM AA and 0.02 mM UA
(Gao <i>et al.</i> , 2013)	GO/GCE	+0.420	1-15	0.27	0.04 M B-R buffer pH 5.0 0.1 mM AA
(Bao <i>et al.</i> , 2011)	GO-Polyaniline-GCE	+0.195	1-14	0.50	50 mM PBS pH 7.4 0.1 mM AA and 0.01 mM UA
(Zou <i>et al.</i> , 2015)	Haemin-GO-GCE	a	0.5-40	0.17	B-R buffer pH 6.0 0.02 mM AA and 0.02 mM UA
(Ping <i>et al.</i> , 2012)	Screen printed graphene	+0.150	20-140	0.12	100 mM PBS pH 7.0 0.04 mM AA and 0.03 mM UA
(Du <i>et al.</i> , 2014)	Graphene flower modified carbon fibre electrode	+0.160	1.36-125.69	1.36	100 mM PBS pH 7.0 AA range 0.07-2.30 mM UA range 3.98-371 $\mu\text{M}$
(Jiang and Du, 2014)	AuPd-rGO-GCE	+0.186	0.1-90	0.022	100 mM PBS pH 7.0 0.4 mM AA and 0.08 mM UA
(Wang <i>et al.</i> , 2015)	rGO-PAMAM-MWCNT-AuNps	+0.320	10-320	3.3	100 mM PBS pH 4.0 0.2 mM AA and 6 $\mu\text{M}$ UA
(Feng <i>et al.</i> , 2015)	3D N-doped graphene	+0.130	3-100	0.001	100 mM PBS pH 7.0 No interferences tested
(Nayak <i>et al.</i> , 2016)	CO <sub>2</sub> laser induced graphene from Kapton <sup>®</sup> + Pt NPs	a	0.5-56	0.07	100 mM PBS pH 7.0 30 $\mu\text{M}$ AA and 4 $\mu\text{M}$ UA
This work	<b>LSG</b>	+0.132	1-10	0.17	50 mM PBS pH 7.0 0.5 mM AA and 0.1 mM UA
This work	<b>LIG</b>	+0.132	1-10	0.103	50 mM PBS pH 7.0 No interferences

a: Not reported

B-R: Britton-Robinson

AuNPs: Gold nanoparticles

PAMAM: poly(amido-amine)

MWCNT: multi-walled carbon nanotubes

Of the examples presented in Table 4-1, only the electrodes reported here and by Nayak *et al.*, Ping *et al.* and Feng *et al.* can be considered standalone electrodes however the 3D N-doped graphene appear to require a complex manufacturing process (Feng *et al.*, 2015), so that in simple terms only the screen printed graphene electrodes (Ping *et al.*, 2012) are truly comparable with LSG (Griffiths *et al.*, 2014) and LIG (this work and (Nayak *et al.*, 2016)) in ease of manufacture. The reported LoD of 0.12  $\mu\text{M}$  for screen printed graphene compares well with 0.17  $\mu\text{M}$  and 0.103  $\mu\text{M}$  of the work described here with LSG and LIG respectively and with the 0.07  $\mu\text{M}$  reported with LSG Pt NPs (Nayak *et al.*, 2016). The LoD is only apparently improved by the 3D N-doped graphene that has a reported LoD of 0.001  $\mu\text{M}$  yet this appears to rely on a large extrapolation from their quoted linear range of 3-100  $\mu\text{M}$  (Feng *et al.*, 2015). However with both LSG and LIG the demonstrated linear range is extended lower than with either the 3D N-doped graphene or the screen printed graphene electrodes, to 1  $\mu\text{M}$  as opposed to 3  $\mu\text{M}$  and 20  $\mu\text{M}$  respectively. In terms of lower linear range the electrodes presented here and the LIG Pt NPs (Nayak *et al.*, 2016) are only out-performed by the AuPd-rGO-GCE (Jiang and Du, 2014) and Haemin-GO-GCE (Zou *et al.*, 2015) which both rely on underlying glassy carbon electrodes with further addition of catalytic entities making manufacture much more complex and less amenable to disposable point of need sensors. The peak potential for DA detection is lowest in the case of the 3D N-doped graphene electrodes at +0.130 V but is very closely followed by LSG and LIG both at +0.132 V, a reduction in over-potential that cannot be matched by the other electrodes compared here. Thus LSG and LIG perform exceptionally well in detection of DA compared with graphene/GO composites and standalone 3D N-doped graphene and screen printed graphene electrodes in terms of DA peak potential, linear range and LoD even in the presence of relatively high levels of AA and UA, analytes known to have potential for interference in electrochemical detection of DA. The LoD of DA detection with LSG at 0.17  $\mu\text{M}$  (3.2  $\text{ng ml}^{-1}$ ) and LIG at 0.103  $\mu\text{M}$  (1.9  $\text{ng ml}^{-1}$ ) also compares favourably with commercialised ELISA kits eg Genway Biotech Ltd have a dopamine ELISA kit with LoD in urine of 5  $\text{ng ml}^{-1}$  (GenWay, 2006). Thus both LSG and LIG electrodes offer a true solution for point of need electrochemical detection of dopamine and the lack of interference from AA and UA may also prove suitable for simultaneous detection of multiple analytes of interest.

#### 4.4 Conclusions

Both LSG and LIG electrodes offer a competitive alternative to the many examples in the current literature of graphene based electrodes for electrochemical detection of biological molecules. These materials are simpler to manufacture and thus more amenable to point of need sensors than single layer graphene or graphene modified GCE yet also perform well in terms of sensitivity and specificity. The results reported here with a direct comparison to EPPG the 'gold standard' of carbon electrodes also demonstrate the outstanding ability of LSG and LIG in the reduction of over-potentials and increased current densities for detection of the analytes DA, UA, AA and NADH. The small variation in composition of the LSG and LIG along with their distinct surface morphologies gives rise to variations in performance with the tested analytes, with LIG demonstrating improved peak separation between the UA, DA and AA and largely increased current response to the AA and UA. LIG proved more successful in simultaneous detection of AA, DA and UA with an ability to separate peak potentials and produce sharp peak current responses. Yet LSG gave improved current responses to DA than the EPPG and GCE. LSG whilst showing similar response to DA as LSG had a subdued response to the AA and UA peaks, resulting in the LSG electrode being less affected by the presence of interferents AA (0.5 mM) and UA (0.1 mM) when detecting much lower levels of DA (0-10  $\mu$ M). This suggests that the LSG has a favoured response to the positively charged DA over AA and UA that are neutral and negatively charged at physiological pH. Both LIG and LSG offer potential but require further optimisation of laser reduction methods used and may have potential for further improvement with the addition of metal nanoparticles (Nayak *et al.*, 2016) to confer catalytic activity or addition of enzymes and redox mediators to aid detection of specific analytes. Preliminary experiments were performed to this effect but insufficient data was collected to report. However copper, silver and platinum nanoparticles could simply be electrochemically deposited onto the LSG and LIG electrodes with the platinum nanoparticles appearing to demonstrate far greater current responses to NADH and hydrogen peroxide detection than the bare electrodes. This is an avenue that would be investigated in greater detail provided further time and funds were available to move the development of the sensors from theoretically good electrochemical sensors to proven electrochemical biosensors.

## 4.5 References

- Alwarappan, S., Liu, G. and Li, C. (2010) 'Simultaneous detection of dopamine, ascorbic acid, and uric acid at electrochemically pretreated carbon nanotube biosensors', *Nanomedicine: Nanotechnology, Biology and Medicine*, 6(1), pp. 52-57.
- Arvinte, A., Valentini, F., Radoi, A., Arduini, F., Tamburri, E., Rotariu, L., Palleschi, G. and Bala, C. (2007) 'The NADH Electrochemical Detection Performed at Carbon Nanofibers Modified Glassy Carbon Electrode', *Electroanalysis*, 19(14), pp. 1455-1459.
- Bao, Y., Song, J., Mao, Y., Han, D., Yang, F., Niu, L. and Ivaska, A. (2011) 'Graphene Oxide-Templated Polyaniline Microsheets toward Simultaneous Electrochemical Determination of AA/DA/UA', *Electroanalysis*, 23(4), pp. 878-884.
- Calabresi, P., Mercuri, N.B. and Di Filippo, M. (2009) *Synaptic plasticity, dopamine and Parkinson's disease: one step ahead*.
- Vitamin C: Its Chemistry and Biochemistry. (Reihe: Royal Society of Chemistry Paperbacks.)* (1992).
- Dehghan, A., van Hoek, M., Sijbrands, E.J.G., Hofman, A. and Witteman, J.C.M. (2008) 'High Serum Uric Acid as a Novel Risk Factor for Type 2 Diabetes', *Diabetes Care*, 31(2), pp. 361-362.
- Du, J., Yue, R., Ren, F., Yao, Z., Jiang, F., Yang, P. and Du, Y. (2014) 'Novel graphene flowers modified carbon fibers for simultaneous determination of ascorbic acid, dopamine and uric acid', *Biosensors and Bioelectronics*, 53(0), pp. 220-224.
- El-Kady, M.F., Strong, V., Dubin, S. and Kaner, R.B. (2012) 'Laser Scribing of High-Performance and Flexible Graphene-Based Electrochemical Capacitors', *Science*, 335(6074), pp. 1326-1330.
- Esmaeilzadeh, M., Farde, L., Karlsson, P., Varrone, A., Halldin, C., Waters, S. and Tedroff, J. (2011) 'Extrasynaptic dopamine D2 receptor binding in Huntington's disease', *Human Brain Mapping*, 32(10), pp. 1626-1636.
- Fedorow, H., Tribl, F., Halliday, G., Gerlach, M., Riederer, P. and Double, K.L. (2005) 'Neuromelanin in human dopamine neurons: Comparison with peripheral melanins and relevance to Parkinson's disease', *Progress in Neurobiology*, 75(2), pp. 109-124.
- Feng, X., Zhang, Y., Zhou, J., Li, Y., Chen, S., Zhang, L., Ma, Y., Wang, L. and Yan, X. (2015) 'Three-dimensional nitrogen-doped graphene as an ultrasensitive electrochemical sensor for the detection of dopamine', *Nanoscale*, 7(6), pp. 2427-2432.
- Gao, F., Cai, X., Wang, X., Gao, C., Liu, S., Gao, F. and Wang, Q. (2013) 'Highly sensitive and selective detection of dopamine in the presence of ascorbic acid at graphene oxide modified electrode', *Sensors and Actuators B: Chemical*, 186(0), pp. 380-387.
- GenWay, G.B.I. (2006) 'Dopamine ELISA Instructions For Use 40-371-25013' Version 1 / 2006-08-29 Inc, G.B.
- Griffiths, K., Dale, C., Hedley, J., Kowal, M.D., Kaner, R.B. and Keegan, N. (2014) 'Laser-scribed graphene presents an opportunity to print a new generation of disposable electrochemical sensors', *Nanoscale*, 6(22), pp. 13613-13622.
- Gutierrez, F., Comba, F.N., Gasnier, A., Gutierrez, A., Galicia, L., Parrado, C., Rubianes, M.D. and Rivas, G.A. (2014) 'Graphene Paste Electrode: Analytical Applications for the Quantification of Dopamine, Phenolic Compounds and Ethanol', *Electroanalysis*, 26(8), pp. 1694-1701.

- Han, D., Han, T., Shan, C., Ivaska, A. and Niu, L. (2010) 'Simultaneous Determination of Ascorbic Acid, Dopamine and Uric Acid with Chitosan-Graphene Modified Electrode', *Electroanalysis*, 22(17-18), pp. 2001-2008.
- Hashimoto, W., Kitayama, S., Kumagai, K., Morioka, N., Morita, K. and Dohi, T. (2005) 'Transport of dopamine and levodopa and their interaction in COS-7 cells heterologously expressing monoamine neurotransmitter transporters and in monoaminergic cell lines PC12 and SK-N-SH', *Life Sciences*, 76(14), pp. 1603-1612.
- Howes, O.D., Kambeitz, J., Kim, E., Stahl, D., Slifstein, M., Abi-Dargham, A. and Kapur, S. (2012) 'The Nature of Dopamine Dysfunction in Schizophrenia and What This Means for Treatment', *Archives of General Psychiatry*, 69(8), pp. 776-786.
- Hummers, W.S. and Offeman, R.E. (1958) 'Preparation of Graphitic Oxide', *Journal of the American Chemical Society*, 80(6), pp. 1339-1339.
- Jiang, J. and Du, X. (2014) 'Sensitive electrochemical sensors for simultaneous determination of ascorbic acid, dopamine, and uric acid based on Au@Pd-reduced graphene oxide nanocomposites', *Nanoscale*, 6(19), pp. 11303-11309.
- Johnson, R.J., Nakagawa, T., Sanchez-Lozada, L.G., Shafiu, M., Sundaram, S., Le, M., Ishimoto, T., Sautin, Y.Y. and Lanaspá, M.A. (2013) 'Sugar, Uric Acid, and the Etiology of Diabetes and Obesity', *Diabetes*, 62(10), pp. 3307-3315.
- Kaur, B., Pandiyan, T., Satpati, B. and Srivastava, R. (2013) 'Simultaneous and sensitive determination of ascorbic acid, dopamine, uric acid, and tryptophan with silver nanoparticles-decorated reduced graphene oxide modified electrode', *Colloids and Surfaces B: Biointerfaces*, 111(0), pp. 97-106.
- Kumar, S.A., Lo, P.-H. and Chen, S.-M. (2008) 'Electrochemical selective determination of ascorbic acid at redox active polymer modified electrode derived from direct blue 71', *Biosensors and Bioelectronics*, 24(4), pp. 518-523.
- Kutluay, A. and Aslanoglu, M. (2013) 'Modification of electrodes using conductive porous layers to confer selectivity for the voltammetric detection of paracetamol in the presence of ascorbic acid, dopamine and uric acid', *Sensors and Actuators B: Chemical*, 185(0), pp. 398-404.
- Li, S.-J., Deng, D.-H., Shi, Q. and Liu, S.-R. (2012) 'Electrochemical synthesis of a graphene sheet and gold nanoparticle-based nanocomposite, and its application to amperometric sensing of dopamine', *Microchimica Acta*, 177(3-4), pp. 325-331.
- Li, S.-J., He, J.-Z., Zhang, M.-J., Zhang, R.-X., Lv, X.-L., Li, S.-H. and Pang, H. (2013) 'Electrochemical detection of dopamine using water-soluble sulfonated graphene', *Electrochimica Acta*, 102, pp. 58-65.
- Liu, C.-Y., Liu, Z.-Y., Peng, R. and Zhong, Z.-C. (2014a) 'Quasireversible Process of Dopamine on Copper-Nickel Hydroxide Composite/Nitrogen Doped Graphene/Nafion Modified GCE and Its Electrochemical Application', *Journal of analytical methods in chemistry*, 2014, pp. 724538-724538.
- Liu, S., Zhang, X., Yu, Y. and Zou, G. (2014b) 'A Monochromatic Electrochemiluminescence Sensing Strategy for Dopamine with Dual-Stabilizers-Capped CdSe Quantum Dots as Emitters', *Analytical Chemistry*, 86(5), pp. 2784-2788.
- Liu, X., Wei, S., Chen, S., Yuan, D. and Zhang, W. (2014c) 'Graphene-Multiwall Carbon Nanotube-Gold Nanocluster Composites Modified Electrode for the Simultaneous Determination of Ascorbic Acid, Dopamine, and Uric Acid', *Applied Biochemistry and Biotechnology*, 173(7), pp. 1717-1726.

- Lynge, M.E., van der Westen, R., Postma, A. and Stadler, B. (2011) 'Polydopamine-a nature-inspired polymer coating for biomedical science', *Nanoscale*, 3(12), pp. 4916-4928.
- Maclagan, K. (2013) 'Dopamine (plasma, urine)', *Association for Clinical Biochemistry*, pp.1-4.
- Magnus-Levy, A. (1910) 'URIC ACID IN GOUT', *The American Journal of the Medical Sciences*, 140(5), pp. 625-643.
- Marcus, K. and Jacques De, K. (2006) 'Uric acid in multiple sclerosis', *Neurological Research*, 28(3), pp. 316-319.
- Martinon, F., Petrilli, V., Mayor, A., Tardivel, A. and Tschopp, J. (2006) 'Gout-associated uric acid crystals activate the NALP3 inflammasome', *Nature*, 440(7081), pp. 237-241.
- Merisalu, M., Kruusma, J. and Banks, C., E., (2010) 'Metallic impurity free carbon nanotube paste electrodes', *Electrochemistry Communications*, 12(1), pp. 144-147.
- Musameh, M., Wang, J., Merkoci, A. and Lin, Y. (2002) 'Low-potential stable NADH detection at carbon-nanotube-modified glassy carbon electrodes', *Electrochemistry Communications*, 4(10), pp. 743-746.
- Nayak, P., Kurra, N., Xia, C. and Alshareef, H.N. (2016) 'Highly Efficient Laser Scribed Graphene Electrodes for On-Chip Electrochemical Sensing Applications', *Advanced Electronic Materials*.
- Pakapongpan, S., Mensing, J.P., Phokharatkul, D., Lomas, T. and Tuantranont, A. (2014) 'Highly selective electrochemical sensor for ascorbic acid based on a novel hybrid graphene-copper phthalocyanine-polyaniline nanocomposites', *Electrochimica Acta*, 133(0), pp. 294-301.
- Ping, J., Wu, J., Wang, Y. and Ying, Y. (2012) 'Simultaneous determination of ascorbic acid, dopamine and uric acid using high-performance screen-printed graphene electrode', *Biosensors and Bioelectronics*, 34(1), pp. 70-76.
- Punckt, C., Pope, M.A. and Aksay, I.A. (2013) 'On the Electrochemical Response of Porous Functionalized Graphene Electrodes', *The Journal of Physical Chemistry C*, 117(31), pp. 16076-16086.
- Qi, S., Zhao, B., Tang, H. and Jiang, X. (2015) 'Determination of ascorbic acid, dopamine, and uric acid by a novel electrochemical sensor based on pristine graphene', *Electrochimica Acta*, 161(0), pp. 395-402.
- Raooof, J., Kiani, A., Ojani, R., Valiollahi, R. and Rashid-Nadimi, S. (2010) 'Simultaneous voltammetric determination of ascorbic acid and dopamine at the surface of electrodes modified with self-assembled gold nanoparticle films', *Journal of Solid State Electrochemistry*, 14(7), pp. 1171-1176.
- Retna Raj, C. and Ohsaka, T. (2003) 'Voltammetric detection of uric acid in the presence of ascorbic acid at a gold electrode modified with a self-assembled monolayer of heteroaromatic thiol', *Journal of Electroanalytical Chemistry*, 540(0), pp. 69-77.
- Safavi, A., Maleki, N., Moradlou, O. and Tajabadi, F. (2006) 'Simultaneous determination of dopamine, ascorbic acid, and uric acid using carbon ionic liquid electrode', *Analytical biochemistry*, 359(2), pp. 224-229.
- Sánchez Arribas, A., Moreno, M., Martínez-Fernández, M., Bermejo, E., Zapardiel, A. and Chicharro, M. (2013) 'Effect of edge plane sites, oxygenated species and metallic impurities upon the electroactivity of carbon nanotube-modified electrodes toward hydrazine', *Sensors and Actuators B: Chemical*, 182, pp. 31-39.

- Sealock, R.R. and Goodland, R.L. (1951) 'Ascorbic Acid, a Coenzyme in Tyrosine Oxidation', *Science*, 114(2972), pp. 645-646.
- Seegmiller, J.E., Grayzel, A.I., Howell, R.R. and Plato, C. (1962) 'THE RENAL EXCRETION OF URIC ACID IN GOUT', *Journal of Clinical Investigation*, 41(5), pp. 1094-1098.
- Simon, J.A. and Hudes, E.S. (2001) 'Relation of Ascorbic Acid to Bone Mineral Density and Self-reported Fractures among US Adults', *American Journal of Epidemiology*, 154(5), pp. 427-433.
- Sotgiu, S., Pugliatti, M., Sanna, A., Sotgiu, A., Fois, M.L., Arru, G. and Rosati, G. (2002) 'Serum uric acid and multiple sclerosis', *Neurological Sciences*, 23(4), pp. 183-188.
- Strong, V., Dubin, S., El-Kady, M.F., Lech, A., Wang, Y., Weiller, B.H. and Kaner, R.B. (2012) 'Patterning and Electronic Tuning of Laser Scribed Graphene for Flexible All-Carbon Devices', *ACS Nano*, 6(2), pp. 1395-1403.
- Szeto, Y.T., Tomlinson, B. and Benzie, I.F.F. (2002) 'Total antioxidant and ascorbic acid content of fresh fruits and vegetables: implications for dietary planning and food preservation', *British Journal of Nutrition*, 87(01), pp. 55-59.
- Tang, C.-F., Kumar, S.A. and Chen, S.-M. (2008) 'Zinc oxide/redox mediator composite films-based sensor for electrochemical detection of important biomolecules', *Analytical Biochemistry*, 380(2), pp. 174-183.
- Tang, J., Zhang, L., Liu, Y., Zhou, J., Han, G. and Tang, W. (2014) 'Gold Nanoparticles- $\beta$ -Cyclodextrin-Chitosan-Graphene Modified Glassy Carbon Electrode for Ultrasensitive Detection of Dopamine and Uric Acid', *Electroanalysis*, 26(9), pp. 2057-2064.
- Tariq, S. (2007) 'Role of Ascorbic Acid in Scavenging Free Radicals and Lead Toxicity from Biosystems', *Molecular Biotechnology*, 37(1), pp. 62-65.
- Taylor, E.N., Stampfer, M.J. and Curhan, G.C. (2005) 'Obesity, weight gain, and the risk of kidney stones', *The Journal of the American Medical Association*, 293(4), pp. 455-462.
- Tung, V.C., Allen, M.J., Yang, Y. and Kaner, R.B. (2009) 'High-throughput solution processing of large-scale graphene', *Nature Nanotechnology*, 4(1), pp. 25-29.
- van B. Robertson, W. (1961) 'THE BIOCHEMICAL ROLE OF ASCORBIC ACID IN CONNECTIVE TISSUE\*', *Annals of the New York Academy of Sciences*, 92(1), pp. 159-167.
- Wang, S., Zhang, W., Zhong, X., Chai, Y. and Yuan, R. (2015) 'Simultaneous determination of dopamine, ascorbic acid and uric acid using a multi-walled carbon nanotube and reduced graphene oxide hybrid functionalized by PAMAM and Au nanoparticles', *Analytical Methods*, 7(4), pp. 1471-1477.
- Wang, Z.-h., Tang, J., Zhang, F.-f., Xia, J.-f., Sun, N., Shi, G.-y., Xia, Y.-z., Xia, L.-h. and Qin, L.-c. (2013) 'Elimination of Ascorbic Acid and Sensitive Detection of Uric Acid at the MnO<sub>2</sub> Nanorods /Graphene-based Modified Electrode', *International Journal of Electrochemical Science*, 8(7), pp. 9967-9976.
- Xiao, X., Miller, P.R., Narayan, R.J., Brozik, S.M., Wheeler, D.R., Brener, I., Wang, J., Burckel, D.B. and Polsky, R. (2014) 'Simultaneous Detection of Dopamine, Ascorbic Acid and Uric Acid at Lithographically-Defined 3D Graphene Electrodes', *Electroanalysis*, 26(1), pp. 52-56.
- Yang, L., Liu, D., Huang, J. and You, T. (2014) 'Simultaneous determination of dopamine, ascorbic acid and uric acid at electrochemically reduced graphene oxide modified electrode', *Sensors and Actuators B: Chemical*, 193, pp. 166-172.

Zhang, L., Li, Y., Zhang, L., Li, D., Karpuzov, D. and Long, Y. (2011) 'Electrocatalytic Oxidation of NADH on Graphene Oxide and Reduced Graphene Oxide Modified Screen-Printed Electrode', *International Journal of Electrochemical Science*, 6, pp. 819-829.

Zhao, H.-X., Mu, H., Bai, Y.-H., Yu, H. and Hu, Y.-M. (2011) 'A rapid method for the determination of dopamine in porcine muscle by pre-column derivatization and HPLC with fluorescence detection', *Journal of Pharmaceutical Analysis*, 1(3), pp. 208-212.

Zhao, S., Wang, J., Ye, F. and Liu, Y.-M. (2008) 'Determination of uric acid in human urine and serum by capillary electrophoresis with chemiluminescence detection', *Analytical Biochemistry*, 378(2), pp. 127-131.

Zheng, D., Ye, J., Zhou, L., Zhang, Y. and Yu, C. (2009) 'Simultaneous determination of dopamine, ascorbic acid and uric acid on ordered mesoporous carbon/Nafion composite film', *Journal of Electroanalytical Chemistry*, 625(1), pp. 82-87.

Zou, H.L., Li, B.L., Luo, H.Q. and Li, N.B. (2015) 'A novel electrochemical biosensor based on hemin functionalized graphene oxide sheets for simultaneous determination of ascorbic acid, dopamine and uric acid', *Sensors and Actuators B: Chemical*, 207, Part A(0), pp. 535-541.

## Chapter 5. General Conclusions and Future Work

### 5.1 Conclusions and Future Work

The project set out to use the highly conductive material graphene to develop a biosensor. Electrochemical sensing was identified as the most promising transduction method for this purpose but with the use of graphene like materials rather than the pristine graphene which brings with it great difficulty in manufacture and handling of a material consisting of a single atomic layer. The laser scribed graphene introduced to the field of supercapacitors by Kaners group in 2012 (El-Kady *et al.*, 2012; Strong *et al.*, 2012) was a clear contender. With excellent electrochemical behaviour in terms of energy storage and release evidenced it was envisaged that this material would also perform well as an electrode material for sensing. The laser reduction method utilising a readily available lightscribe drive made the material accessible to all, yet the production of high quality LSG electrodes requires the graphite oxide starting material to be free of metallic impurities that would otherwise interfere in the analysis of the materials electrochemical properties. This is achieved following a modified hummers method (Fowler *et al.*, 2009) and requires further development to become a safe and scalable process. However with the interest that these materials have attracted and the breadth of research in the graphene arena these methods are likely to evolve rapidly thus not being a limitation to the further development of LSG electrodes for commercialised sensing purposes. The study of LSG electrodes as electrochemical sensors presented in Chapter 2 has provided evidence that the LSG material is capable of outperforming EPPG the 'gold standard' of carbon electrodes with both inner and outer sphere redox couples. It was also demonstrated as a 'printable' planar three electrode system consisting of a silver pseudo-reference electrode and LSG working and counter electrodes, with no loss in performance compared with use of external counter and reference electrodes. Most interestingly, despite being unable to physically or electrochemically polish the electrode surface between each use, the LSG electrodes demonstrated very good reproducibility. Within this work it was also shown that single layer graphene performed poorly as an electrode, with response more similar to BPPG supporting a data reported in more extensive investigations in the literature (McCreery and McDermott, 2012; Punckt *et al.*, 2014).

The use of a graphene like material with low levels of oxygen content for enhance electrochemical behaviour produced from the reduction process utilising a laser was then taken a step further. Kapton<sup>®</sup>, a polyimide film consisting of carbon ring structures was

shown to be reduced with the use of a CO<sub>2</sub> laser engraver (Lin et al., 2014), again this was then investigated as an electrode material for its energy storage and release properties. This material, LIG offered a simple one step process to the manufacture of a graphene like electrode, it had low levels of oxygen and a high sp<sup>2</sup> carbon content similar to LSG as confirmed by XPS analysis and SEM showed the material to have a highly expanded heterogeneous porous structure. The laser writing process offers great flexibility in the electrode size and geometry and the laser intensity can be precisely honed to optimise the resultant material for its intended use. When probed electrochemically and compared with the LSG and EPPG electrodes in both the inner- and outer-sphere redox probes used throughout this body of work, unusual responses to CV were identified, where the  $\Delta E_p$  was significantly below the 59 mV Nernstian ideal response of a one electron transfer process. With further analysis and a review of the literature (Punckt *et al.*, 2010; Punckt *et al.*, 2013; Barnes *et al.*, 2014; Punckt *et al.*, 2014) it was found that the porous electrodes were allowing a thin layer electrochemical behaviour due to the entrapment of the redox probes within the electrodes pores, removing the diffusional limitation on the system. This can result in reduced over potentials- ideal for a diagnostic electrochemical sensor in biological matrices where a lower potential reduces the risk of interferences from common interferences such as ascorbic acid. The LIG offers a simple manufacturing process but care must be taken to fully understand the electrochemical behaviour at these porous electrodes. Future work should include a much larger study on the effect of laser intensity, write speed, focal distance and Kapton<sup>®</sup> film thickness on the pore size, distribution, layer expansion, oxygen content and Raman finger print and how these variations relate to electrochemical response. With a thorough understanding of these behaviours this material should be very well suited to large scale and affordable manufacture for the use in planar disposable biological sensors, particularly due to its ability to simultaneously detect redox substances often seen as interferences due to inability to identify individual peak positions with traditional carbon electrodes.

Preliminary data on the electrodeposition of metallic nanoparticles onto both the LSG and LIG electrodes was not reported at this juncture due to insufficient material to cover a coherent study. However the successful deposition of gold, silver, nickel and platinum was confirmed by SEM and energy dispersive x-ray spectroscopy as per the recently published study on use of LIG as an electrochemical sensor with the addition of platinum nanoparticles to enhance activity towards AA, UA and DA (Nayak *et al.*, 2016). The platinised electrodes in the preliminary work demonstrated excellent linear current

responses to hydrogen peroxide, important in many enzyme based electrochemical systems and also to the direct electrochemical detection of glucose using chronoamperometry. This is an area that would require further investigation to determine the optimal deposition time and size of the metallic nanoparticles on the LIG and LSG electrode surfaces. It is also possible to add layered metallic nanoparticles which may confer additional catalytic behaviours. Of course the ultimate aim would be to develop a sensor based around the electrochemistry of the laser induced graphene but in tandem with the use of an enzyme conferring specific activity and detection. Having a large proportion of edge sites and remnant oxygen functionalities will allow the immobilisation of such enzymes to the surface and if combined with the use of short conducting polymer anchors may further enhance the thin layer behaviours of the porous electrodes discussed within.

In conclusion, 'graphene like' materials have been identified as a more promising material than pristine graphene suitable for electrochemical sensing purposes. Two such materials have been investigated within this project, both reliant on the reduction of an underlying insulating substrate by laser irradiation to create an expanded conductive material with graphene like physicochemical and electrical properties. These materials, LSG and LIG are simple to manufacture and electrochemically outperform EPPG, the 'gold standard' of carbon electrodes, whilst also being amenable to mass manufacture of planar disposable three electrode systems for sensing purposes. Not only do they perform well in terms of rapid heterogeneous electron transfer and current outputs but also allow for the simultaneous detection of the analytes DA, AA and UA of which the standard carbon electrodes fail to distinguish. These preliminary studies stand these materials in good stead for further development and transfer to fully commercialised electrochemical sensors and renew the hopes for a growth in the use of biosensors outside of the dominant area of glucose sensing.

## 5.2 References

- Barnes, E.O., Chen, X., Li, P. and Compton, R.G. (2014) 'Voltammetry at porous electrodes: A theoretical study', *Journal of Electroanalytical Chemistry*, 720–721(0), pp. 92-100.
- El-Kady, M.F., Strong, V., Dubin, S. and Kaner, R.B. (2012) 'Laser Scribing of High-Performance and Flexible Graphene-Based Electrochemical Capacitors', *Science*, 335(6074), pp. 1326-1330.
- Fowler, J.D., Allen, M.J., Tung, V.C., Yang, Y., Kaner, R.B. and Weiller, B.H. (2009) 'Practical Chemical Sensors from Chemically Derived Graphene', *American Chemical Society Nano*, 3(2), pp. 301-306.
- Lin, J., Peng, Z., Liu, Y., Ruiz-Zepeda, F., Ye, R., Samuel, E.L.G., Yacaman, M.J., Yakobson, B.I. and Tour, J.M. (2014) 'Laser-induced porous graphene films from commercial polymers', *Nature Communications*, 5.
- McCreery, R.L. and McDermott, M.T. (2012) 'Comment on Electrochemical Kinetics at Ordered Graphite Electrodes', *Analytical Chemistry*, 84(5), pp. 2602-2605.
- Nayak, P., Kurra, N., Xia, C. and Alshareef, H.N. (2016) 'Highly Efficient Laser Scribed Graphene Electrodes for On-Chip Electrochemical Sensing Applications', *Advanced Electronic Materials*.
- Punckt, C., Pope, M.A. and Aksay, I.A. (2013) 'On the Electrochemical Response of Porous Functionalized Graphene Electrodes', *The Journal of Physical Chemistry C*, 117(31), pp. 16076-16086.
- Punckt, C., Pope, M.A. and Aksay, I.A. (2014) 'High Selectivity of Porous Graphene Electrodes Solely Due to Transport and Pore Depletion Effects', *The Journal of Physical Chemistry C*, 118(39), pp. 22635-22642.
- Punckt, C., Pope, M.A., Liu, J., Lin, Y. and Aksay, I.A. (2010) 'Electrochemical performance of graphene as effected by electrode porosity and graphene functionalization', *Electroanalysis*, 22(23), pp. 2834-2841.
- Strong, V., Dubin, S., El-Kady, M.F., Lech, A., Wang, Y., Weiller, B.H. and Kaner, R.B. (2012) 'Patterning and Electronic Tuning of Laser Scribed Graphene for Flexible All-Carbon Devices', *American Chemical Society Nano*, 6(2), pp. 1395-1403.